Contraintes sur l'habitabilité d'exoplanètes et exolunes telluriques baser sur une modélisation géophysique

Constraints on the habitability of Earth-like exoplanets and exomoons: insights from geophysical modelling

Lena Noack

Royal Observatory of Belgium
Avenue Circulaire 3
1180 Brussels
Belgium *

March 2016

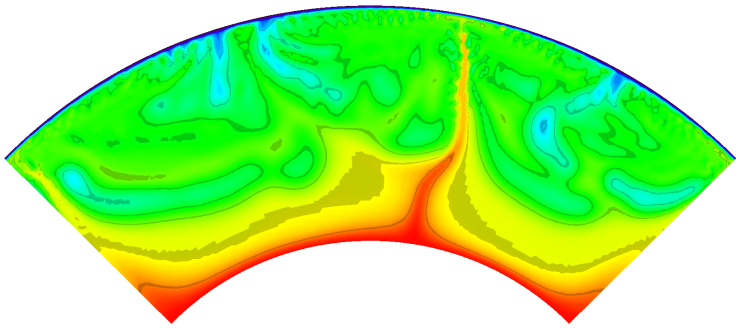

*L. Noack has been funded by the Interuniversity Attraction Poles Programme initiated by the Belgian Science Policy Office through the Planet Topers alliance.

Contraintes sur l'habitabilité d'exoplanètes et exolunes telluriques

L'humanité s'est toujours demandée d'où elle venait, et si la vie existait non seulement sur la Terre, mais ailleurs sur d'autres planètes. Pour trouver la vie en dehors de la Terre, la première question à se poser devrait plutôt être où la vie pourrait-elle survivre, en théorie. Les planètes, qui pourraient être en mesure d'accueillir la vie (même si elles ne sont pas habitées), sont appelées planètes habitables (voir la revue de Cockell et al., 2016). Au cours des dernières décennies – n'ayant jusqu'à présent pas réussi à trouver la vie extra-terrestre dans le système solaire – les scientifiques se sont plutôt tournés vers la recherche de planètes habitables extrasolaires. Comprendre ce qui rend une planète habitable et comment la vie sur une planète peut influer les caractéristiques observables des exoplanètes (les biosignatures, comme par exemple la composition d'atmosphère qui ne peuvent être expliquées par les seuls facteurs géochimiques), peut conduire à la détection future de la vie en dehors du système solaire. La vie est un concept qui n'est pas toujours très bien compris, même si les scientifiques tentent de percer le mystère de l'apparition de la vie et de son évolution sur la Terre. La vie pourrait prendre plusieurs formes différentes, que nous serions incapables de détecter. Les scientifiques se concentrent sur la recherche de la vie extraterrestre en se basant sur le seul exemple connu, la vie comme sur Terre, qui a besoin de l'existence d'eau liquide.

Lorsqu'on recherche la vie sur des planètes ou lunes (soit dans le système solaire et au-delà), il faut distinguer deux concepts d'habitabilité différents : la possibilité de la vie à la surface d'un corps et la possibilité de la vie dans le sous-sol.

Dans le système solaire, le premier concept peut être appliqué par exemple à la planète Mars, où de l'eau liquide a coulé sur la surface dans le passé, et où de l'eau salée peut exister localement même aujourd'hui (Haberle et al., 2001 ; Ojha et al., 2014). Actuellement, Mars ne peut pas avoir d'océan liquide à sa surface en raison d'une part du faible rayonnement solaire reçu (par rapport à la Terre) et d'autre part d'une atmosphère mince conduisant à des températures de surface inférieures à zéro. La zone des distances orbitales où le rayonnement solaire est suffisamment élevé pour permettre l'existence d'eau liquide à la surface (en supposant un effet de serre suffisamment efficace), est appelée la zone habitable (voir par exemple Kasting et al., 1993). La quantité de gaz à effet de serre, comme le dioxyde de carbone (CO_2), joue un rôle important pour la température de surface et, par conséquent, l'habitabilité d'une planète. La quantité de gaz à effet de serre dans l'atmosphère est en partie déterminée par le dégazage volcanique de l'intérieur.

Toutefois, la vie peut également exister sous la surface d'une planète ou d'une lune (voir par exemple la discussion dans Kereszturi et Noack, 2016). La possibilité de vie a souvent été envisagée pour certains corps glacés du système solaire, comme les lunes Europe ou Encelade à cause de l'existence d'océan interne ou de poche d'eau en dessous de leur surface glacée. Des missions spatiales sont actuellement prévues pour sonder la surface ou l'intérieur de ces lunes, et pour y trouver la preuve directe de vie (si elle existe). Pour les planètes et les lunes en dehors du système solaire, une telle approche est impossible, et nous devons nous appuyer sur les biosignatures observables dans les atmosphères (conduisant à des variations dans le spectre de celles-ci). Même si une atmosphère ne peut être exclue pour les corps glacés en dehors de la zone habitable, les candidats les plus probables pour lesquels la vie pourrait être détectée dans un avenir proche sont des planètes qui sont habitables à leur surface et principalement composées de roches et des métaux, c'est à dire des planètes comme la Terre (ou Mars, Vénus) dans la zone habitable. Même si ces planètes sont généralement dénommées telluriques ou semblables à la Terre, elles peuvent cependant être tout à fait différentes de la Terre dans leur composition (différents minéraux ou teneur en métal) et dans leur taille. Les premières exoplanètes telluriques qui ont été détectées sont plus grandes et plus massives que la Terre, et une nouvelle classe de planètes, les super-Terres, a été introduite. Avec l'augmentation de la précision des observations, de plus en plus de planètes de la taille de la Terre ont été détectées pendant ces dernières années, montrant cependant une large gamme de densité (et donc de composition).

La détection de plus de mille exoplanètes soulève la question de la façon dont nous pouvons mieux sélectionner, parmi les exoplanètes éventuellement habitables, celles qui seront observées par les missions de caractérisation de ces candidates (qui mesurera par exemple le spectre de l'atmosphère).

Ce manuscrit décrit une approche géophysique pour répondre à cette question en étudiant l'influence de l'intérieur d'une planète ou d'une lune sur son habitabilité possible, et en particulier l'influence liée au dégazage dû aux volcans et celle liée à l'existence de tectonique des plaques à long terme. Comme il est mentionné à la Section 1 de ce manuscrit, ces deux processus géophysiques ont une forte influence sur l'habitabilité de la surface d'une planète tellurique. Dans les sections suivantes, l'influence de la masse, de la taille et de la composition de la

planète sur les processus géophysiques de surface sont étudiés.

Nous avons utilisé des modèles de convection à deux dimensions pour calculer la fusion partielle et la quantité de CO_2 dégazé pour des planètes telluriques monoplaques à large couche stable en surface (stagnant-lid). L'évolution de l'atmosphère est étudiée en fonction de la structure interne (différentes tailles de noyau), de la composition du manteau (teneur en magnésium et en fer du manteau) et de la masse de la planète. En outre, nous avons étudié la probabilité d'avoir de la tectonique des plaques en fonction de la structure interne et de la masse, ainsi que son influence sur le dégazage volcanique.

Dans Noack et al. (2014), nous avons montré que pour des planètes telluriques monoplaques à large couche stable en surface, la taille relative du noyau de fer a un impact important sur la production de fusion partielle. Une variation de la structure interne modifie le gradient de pression et donc la température de fusion des roches silicatées avec la profondeur. En conséquence, pour les planètes avc un large noyau, le dégazage de l'intérieur est fortement réduit par rapport à une planète de même rayon, mais avec un petit noyau.

Des simulations plus récentes (pas encore publiées) montrent une tendance similaire pour les planètes avec une masse importante. Pour les planètes monoplaques les éruptions volcaniques sont fortement limitées si leur teneur en fer et/ou leur masse dépasse une valeur critique, conduisant à un effet de serre insuffisant. Dans ce cas, à la limite extérieure de la zone habitable classique, il n'est pas possible d'avoir de l'eau liquide à la surface et la limite extérieure de la zone habitable se déplace vers l'intérieur, ce qui donne une contrainte importante pour la sélection des exoplanètes habitables. La tectonique des plaques conduit toujours à une accumulation d'une atmosphère dense et donc à un effet de serre suffisant important (ainsi qu'un cycle de CO_2 efficace) pour réguler la composition de l'atmosphère sur des échelles de temps géologiques, comme le suggère Kasting et al. (1993).

Cependant, la tectonique des plaques pourrait ne pas être possible sur toutes les planètes telluriques. Mars et Vénus par exemple ne montrent pas de présence de tectonique des plaques à ce jour (mais une possible subduction de plaque est fortement débattue actuellement sur l'une de ces planètes). Dans Noack et Breuer (2014), nous montrons encore l'importance du rôle de la masse de la planète sur la possibilité d'initier la tectonique des plaques. En fonction de l'énergie disponible à l'intérieur après la formation de la planète, la tectonique des plaques peut être moins susceptible d'exister sur une super-Terre que sur une planète de masse terrestre. De plus, la structure interne (à savoir la taille du noyau) influe sur la probabilité d'avoir une tectonique des plaques (ainsi que la durée de la phase active de la tectonique des plaques) (Noack et al., 2014).

Les résultats combinés de mes études de ces deux dernières années et mentionnés ci-dessus (voir surtout Noack et al., 2014 ; Noack et Breuer, 2014, ainsi que des inédits présentés dans ce document) suggèrent que le bord extérieur de la zone habitable d'une étoile ne dépend pas seulement de la distance à l'étoile (ce qui est la définition classique, par exemple, Kasting et al., 1993), mais il est également limité par l'éventuel dégagement de gaz volcanique qui est influencé par l'intérieur de la planète. Ces éventuelles limitations géophysiques sur la zone habitable devraient être prises en considération dans la recherche de planètes telluriques habitables. Nous avons montré que le dégazage de CO_2 était insuffisant, et donc que la zone habitable était réduite, pour les planètes:

1. sans tectonique des plaques,
2. avec une grande masse, et/ou
3. avec une teneur élevée en fer.

Constraints on the habitability of Earth-like exoplanets and exomoons

Mankind has always wondered where it came from, and whether there is life not only on Earth, but also on other planets. To find life outside of Earth, the first question is where life could, in theory, survive. These planets, that could be able to host life (even if they may not be inhabited), are called habitable planets (see review Cockell et al., 2016). In the last decades – being so far unsuccessful in finding extra-terrestrial life in the solar system – the focus turned towards the goal of finding extra-solar habitable planets. Understanding what makes a planet habitable, and how life on a planet may influence the signatures we receive from the exoplanet (*biosignatures*, for example atmosphere compositions that cannot be explained by geochemical factors alone), can lead to future detection of life outside of the solar system.

Life is a concept that is still not very well understood, even though scientists get closer to unravel the mystery of how life originated and evolved on Earth. Life may take several different forms, some which we might be unable to detect. In search for extraterrestrial life, scientists therefore concentrate on Earth-like life, which needs liquid water to survive.

When searching for life on planets or moons (either in the solar system or beyond), we have to distinguish between two different habitability concepts: the possibility of life at the surface of a body and life in the subsurface.

In the solar system, the first concept can be applied for example to Mars, where in the past liquid water did flow on the surface, and where salty water may exist locally even today (Haberle et al., 2001; Ojha et al., 2014). Present-day Mars cannot have liquid oceans at the surface due to a small solar flux (compared to Earth) and its thin atmosphere leading to subzero surface temperatures. The region of orbital distances, where the solar flux is high enough to allow for liquid water at the surface (assuming a strong enough greenhouse effect), but not too high for water to boil away, is called the habitable zone (e.g. Kasting et al., 1993). Greenhouse gases, such as carbon dioxide (CO_2), play an important role for the surface temperature and, thus, the habitability of a planet. The amount of greenhouse gases in the atmosphere is in part determined by the volcanic outgassing from the interior.

Life, however, may also exist beneath the surface of a planet or moon (see for example discussion in Kereszturi and Noack, 2016). For some icy bodies of the solar system, like Europa or Enceladus, the possibility of life has often been discussed, because they contain liquid water underneath the ice shell (possibly in form of a global subsurface ocean). For these moons, missions are currently planned to probe the surface or interior and to find (if it exists) direct evidence of life. For planets and moons outside of the solar system, such an approach is impossible, and we have to rely on biosignatures in the atmospheres (observable in its spectrum), which can already be observed. Even though an atmosphere and thus the existence of biosignatures cannot be excluded for icy bodies outside of the habitable zone, the most likely candidates for which life can be detected in the near future are planets that are habitable at their surface, which means planets like Earth (or Mars, Venus) that are inside the habitable zone and that are mainly composed of rocks and metals. Even if these planets are typically named terrestrial or Earth-like, they may still be quite different to Earth in composition (different minerals or metal content) and size. The first terrestrial exoplanets that have been detected are larger and more-massive than Earth, and a new class of planets (super-Earths) was introduced. With more precise observations, more and more Earth-size planets have been detected in the recent years, as well, showing a wide range of densities (and hence compositions).

The detection of already more than thousand exoplanets raises the question on how we can best select the golden candidates of possibly habitable exoplanets, that will be observed by follow-up missions (measuring for example the spectrum of the atmosphere).

This manuscript describes a geophysical approach to answer this question by investigating the influence of the interior of a planet or moon on the possible surface habitability of terrestrial planets, especially the ability of long-term volcanic outgassing and plate tectonics. As is discussed in Section 1, both geophysical surface processes have a strong influence on the possible surface habitability of a terrestrial planet. In the succeeding sections, the influence of the planet mass, size and composition on the geophysical surface processes are investigated.

Two-dimensional convection models are used to calculate partial melting and the amount of CO_2 outgassed for Earth-sized stagnant-lid planets. The evolution of a secondary atmosphere is investigated depending on the interior structure (different core sizes), mantle composition (magnesium and iron content of the mantle) and mass of a planet. Furthermore the likelihood for plate tectonics depending on the interior structure and mass are investigated as well as its influence on volcanic outgassing.

In Noack et al. (2014) it is shown that for stagnant-lid planets the relative size of the iron core has a large

impact on the production of partial melt. A variation in the interior structure changes the pressure gradient and thereby the melting temperature of silicate rocks with depth. As a consequence, for planets with a large core, outgassing from the interior is strongly reduced in comparison to a planet with the same radius but a small core.

More recent simulations (not yet published) show a similar trend for the planet mass. One-plate planets may suffer strong volcanic limitations if their mass and/or iron content exceeds a critical value, leading to an insufficient greenhouse effect. In that case, at the outer boundary of the classical habitable zone, liquid water is not possible at the surface and the outer boundary of the habitable zone moves inward, setting an important constraint for the possible surface habitability of these planets.

Plate tectonics always leads to the build-up of a dense-enough atmosphere leading to a strong greenhouse effect (as well as an efficient CO_2-cycle to regulate the atmosphere composition on geological timescales as suggested in Kasting et al. (1993). However, plate tectonics may not be possible on all terrestrial planets. Mars and Venus for example don't show present day plate tectonics (and it is strongly debated if plate subduction ever occurred on either of these planets). In Noack and Breuer (2014) it is discussed that the planet mass plays an important role for the possibility to initiate plate tectonics. Depending on the energy available in the interior after planet formation, plate tectonics may be less likely on a super-Earth than on an Earth-mass planet. Also the interior structure (i.e. the core size) influences the likeliness of plate tectonics (as well as the duration of the active plate tectonics phase Noack et al., 2014).

The combined results of my above-mentioned studies from the past two years (especially Noack et al., 2014; Noack and Breuer, 2014, and unpublished material) suggest that the outer edge of the habitable zone of a star does not only depend on the distance from the star (which is the classical definition of e.g. Kasting et al., 1993), but is also limited by the possible volcanic outgassing that depends on the interior. These possible geophysical limitations on the habitable zone should be taken into consideration in the search for habitable terrestrial planets. Insufficient outgassing of CO_2 and thus a reduced habitable zone may be expected for planets:

1. without plate tectonics,
2. with a large planet mass, and/or
3. with a high iron content.

Contents

The main content of Sections 2, 3, 4 and 6 has been published in (Noack et al., 2014; Noack and Breuer, 2014). Section 5 and part of Section 3 is still unpublished material. Section 1 is based on an earlier publication (Noack and Breuer, 2013) but is added here as introduction to the topic.

1 Habitability in the solar system

Is there life outside of Earth? Has there been life on Mars? Is the ocean of Jupiter's moon Europa inhabited? Several scientists try to answer these questions, and most current or planned space missions try to find indicators of past or present life outside of Earth.

In the 19th and 20th century, scientists believed that life exists on different planets of the solar system (see review in Noack and Breuer, 2013). Venus is the planet in our Solar System, which is most similar to Earth and is often called Earth's sister planet. A thick opaque cloud layer, however, does not allow the direct observation of its surface, and speculations existed at the beginning of the last century about possible intelligent life on Venus (e.g. Mumford, 1909). Based on telescope observations of Mars, Giovanni Schiaparelli published a map of the Martian surface in 1877 (republished in Schiaparelli, 1893) showing not only river-like structures, but also a dichotomy of the northern and the southern hemisphere. The smooth and shallow surface in the North was interpreted as a water ocean (named *Mare Australe*) and the visible *canali* (chanels) gave way to wild speculations about intelligent life on Mars (e.g. Mumford, 1909), since they looked like artificial constructed channels. The canali have alternatively been interpreted to be either rivers connecting the poles with each other or "lines of vegetation" (Pickering, 1926). In 1647 Johannes Hevelius mapped the visible near-side of the Moon in detail including all larger craters as well as several black spots – the Mare (Hevelius, 1647). These regions have been interpreted as oceans, and life on the moon was thought to be a possibility.

The age of space missions put an end to these speculations. Space missions such as Venera 4 and Marina 5 (e.g. Wood et al., 1968) revealed that for Venus the dense atmosphere, with a surface pressure almost hundred times the pressure on Earth's surface, leads to very high surface temperatures of around 730K (Taylor and Grinspoon, 2009), and the existence of life at Venus' surface can be ruled out. Our second neighbour planet, Mars, contains a red (oxidized) surface without any evidence for present-day life – and no large canals could be observed. Most likely the canali were optical illusions. The idea of surface oceans on the Moon was confounded when more information became available, showing that surface life cannot survive on the Moon due to the missing atmosphere and the lack of water, as well as the low surface temperatures at the night side. The dark Mare can be explained instead by a basaltic composition of the surface material and correspond to the low terrains on the near side of the moon.

It has been suggested that there are habitable niches on present-day Mars at the equator (Cockell et al., 2016), and that life could be able to survive in Venus' atmosphere (Schulze-Makuch et al., 2004), but most speculation on possible habitable bodies has moved to the outer solar system (subsurface habitability of icy moons like Europa or Enceladus) or planets outside of the solar system, the exoplanets.

For Earth, it is speculated that plate tectonics plays an important role for its long-term habitability at the surface. This convection mechanism transports efficiently surface material by subduction into the planetary interior and allows life to grow and survive due to recycling of nutrients, the stabilization of the climate and the cooling of the deep interior. The latter further helps to maintain the magnetic field that protects the atmosphere from erosion and life from harmful radiation. On icy moons in contrast, the habitable environment would be restricted to a possible subsurface ocean; a stable atmosphere is not required. To sustain the subsurface ocean and to gain energy for possible life, volcanic activity in the underlying silicate mantle but also tidal heating play an important role. The volcanic activity, however, may be also related to plate tectonics in the silicate mantle but its existence is only speculative. In fact, plate tectonics on terrestrial bodies (i.e. a planet or moon with an iron core, a silicate mantle and a crust on top) is uncommon, and the Earth is the only planet that is known to operate in this convective regime. Other terrestrial bodies (e.g. Mars and Venus) operate today in the so-called stagnant lid regime where convection takes place underneath an upper stagnant layer – in their early evolution, however, plate tectonics may have been active. Alternatively, Venus may have experienced a convective resurfacing mechanism – as it has been proposed for the moon Enceladus (see also Noack et al., 2012) – or a strong magmatic resurfacing – which would be comparable to the resurfacing of the moon Io. Even though planets and moons differ in many aspects, they show a lot of similarities. Understanding the diversity and the common features of terrestrial bodies (i.e. planets and moons) in the Solar System is a main challenge in geodynamics and astrophysics. One important question is to understand how plate tectonics and other resurfacing mechanisms work and why no (present-day) plate tectonics exists on any other terrestrial body in our Solar System but on Earth.

It has often been argued that plate tectonics may be strongly linked to the habitability of Earth. In particular, the *Gaia hypothesis* proposes that life and the planet itself are closely connected to form a self-regulating complex system, maintaining the conditions for life on the planet (Lovelock and Margulis, 1974). This sensitive and complex

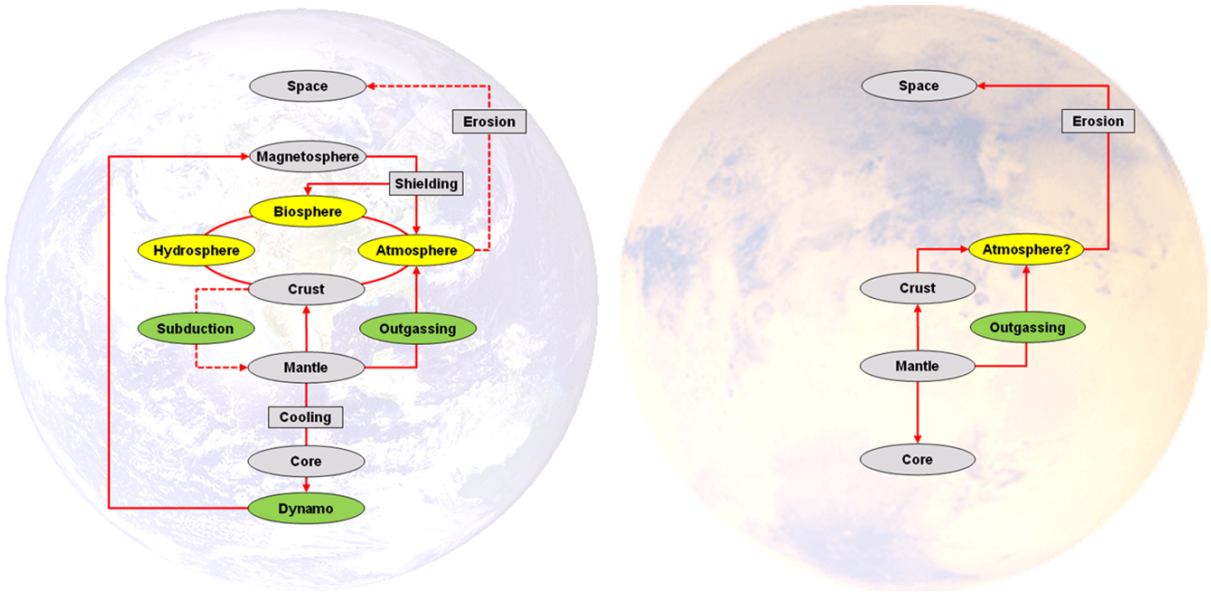

Figure 1: Visualization of the feedback cycles between interior and atmosphere for Earth and – in contrast – the limited coupling for a one-plate planet like Mars. Plate tectonics seems to be important for life due to regassing of volatiles, replenishing of nutrients, and stabilization of the atmosphere due to the long-term carbon cycle. Furthermore, surface recycling cools the mantle efficiently, which leads to a high heat flux at the core-mantle boundary and can be helpful in maintaining a magnetic field. From Noack and Breuer (2013) after van Thienen et al. (2007).

system, however, depends on several feedback mechanisms coupling the atmosphere with the surface (oceans and continental surface) and the interior.

Figure 1 (from Noack and Breuer, 2013) visualizes the potential role of plate tectonics for the origin and evolution of life (see e.g. Parnell, 2004; Ward and Brownlee, 2000). The left panel shows a simplified sketch that includes main processes on Earth, which are described in detail below. The sketch on right panel represents the processes on Mars on which plate tectonics is not active. The lack of plate tectonics may reduce the ability of a planet to become or remain habitable. Starting from the inside out, subduction of the cold surface layer leads to a strong cooling of the interior and hence to a larger heat flux at the core mantle boundary compared to a one-plate planet as Mars (Breuer and Spohn, 2003). This way, a magnetic dynamo generated in the fluid outer core of Earth may be maintained on long time scales (Stevenson, 2003). A magnetic field (i.e. the magnetosphere) protects the atmosphere against erosion from the solar wind (Dehant et al., 2007) and life from radiation. In case of the Earth, the magnetic field together with a strong gravitation protects the atmosphere from being strongly eroded – on Mars the weaker gravity and the missing magnetosphere at least since the last 4Ga may have resulted in the thin present-day atmosphere of only 6-10 mbar (compared to 1 bar on Earth), see for example Haberle et al. (2001).

The Earth's atmosphere contains greenhouse gases like carbon-dioxide, water, or methane, which are fed into the atmosphere by outgassing during volcanic activity. On Venus, these greenhouse gases lead to high surface temperatures of about 460°C (Taylor and Grinspoon, 2009), which makes life as we know it impossible at the surface of our sister planet. On Earth with its plate tectonics, the partial pressure of carbon dioxide in the atmosphere is buffered over geological time scales by a negative feedback mechanism in which the rate of weathering of silicate minerals (followed by deposition of carbonate minerals) depends on the surface temperature. The occurrence of the so-called global carbon-cycle as a consequence of plate tectonics saved the Earth from sharing the same fate as Venus with its dense atmosphere and high surface temperatures. Almost the total amount of carbon, which is present in the atmosphere of Venus, exists on Earth as well – but is deposited in chalk stones. Carbon is extracted from the atmosphere and incorporated into sediments via the silicate-carbon-cycle. The extraction rate depends on the strength of rainfall and the area of land masses. If the atmospheric temperature increases for instance due to an increase in volcanic activity, enhanced rainfall washes the carbon out of the atmosphere resulting in a decrease of the surface temperature – decreasing surface temperatures on the other hand lead to a reduction of rainfall and weathering and hence more CO_2 remain in the atmosphere resulting in a temperature

increase (Kasting et al., 1993). This negative feedback mechanism of the silicate-carbon-cycle keeps the surface temperature constant over a long time period. The biosphere is expected to play a substantial part in the short-term carbon-cycle due to both storage of carbon in shells and skeletons and by enhancement of the carbon-silicate cycle (Sundquist, 1993). Weathering leads to solution of carbon into water (carbonic acid) and possibly to an enrichment of the carbon concentration in the oceans. Dissolved carbon in the surface layer of the oceans can be exchanged with the atmosphere, such that the ocean can be seen as short-term regulating system of the carbon concentration in the atmosphere. However, the buffering mechanism of the oceans has its limitations. Since life is a main factor of the buffering mechanism of the oceans (i.e. organic carbon, carbon-silicate cycle and photosynthesis), an increased oceanic acidity due to an increasing carbon concentration may slow down the precipitation of calcium carbonates and thus decrease the amount of carbon that the oceans can absorb. Here, plate tectonics sets in. On long, geological time-scales, the oceanic crust including its carbon-rich upper layer (e.g. limestone built from organic carbon reservoirs) is subducted into the mantle. At the same time, new oceanic and continental crust (including replenished nutrients) is formed. It is questionable, if an enhanced Earth-like CO_2-cycle can exist without the interaction of life.

The subduction of oceanic crust further transports water into the mantle, which is stored as hydrated minerals in the subducted material, leading amongst others to a reduced melting point of the silicate. At shallow depths, subducted basaltic crust is therefore re-melted and forms the continental crust consisting of light granitic material. Parnell (2004) argued that this process was necessary for life to evolve in the way it was the case on Earth by influencing surface mineralogy. Furthermore, the existence of (proto-)continents may have been essential for the evolving complexity of life (Ward and Brownlee, 2000). An interesting connection between the origin of life and the rise of continents has been suggested by Rosing et al. (2006) in arguing that the energy needed for the formation of light granite has been provided by photochemical active microbes. Life may further contribute to the amount of water subducted into the mantle by enhancing erosion and sediment formation (Höning et al., 2014). Therefore plate tectonics would be important for the development of life, which then would help to form the continents, that are needed for more complex species to develop. Another process indicating the importance of plate tectonics for the origin of life may be found at the hydrothermal vents, where it has been suggested that life may have originated (Martin and Russell, 2003). These hydrothermal vents – so-called black and white smokers - are regions of volcanic activity in the oceans, mostly located directly at the plate boundaries, for example at the mid-ocean ridges. Even though the temperature of the water streaming out of the vents is much larger than in the surrounding oceans (up to about 400°C, (Martin and Russell, 2003)), several early-life forms can be detected around the smokers, and chemical reactions lead to a sufficient energy source (to be used instead of photosynthesis). This environment reflects the conditions expected for early Earth and led to the idea that life may have originated in hydrothermal vents. Without plate tectonics, these smokers that origin at the plate boundaries would most likely not exist. The only volcanic activity to be expected would be hotspots, which are magmatic plumes in the mantle, from which melt may be erupted to form island chains like for example the Hawaiian islands (due to the movement of the oceanic plate over the hotspot several islands evolve with time).

The arguments listed above suggest that plate tectonics might be important for the habitability of the Earth and the evolution of Earth-like life. In the Solar System plate tectonics is a rare phenomenon; the Earth is the only planet showing evidence of long-term plate tectonics. Thus, special conditions seem to exist on Earth and it can be shown that this surface recycling depends on a series of factors, e.g. planetary mass, age of the planet (i.e. mantle temperature), water content in the interior, surface temperature (compare e.g. Earth and Venus), mantle rheology (reference viscosity and phase transitions), partial melt (crust development, density variations in the mantle and dehydration), and the possible influence of life on the mechanism of plate tectonics and continent formation.

2 Extra-solar planets and habitable zone

Since the first detections in the early 1990s (Wolszczan and Frail, 1992; Mayor and Queloz, 1995), more than thousand extrasolar planets have been detected, and many additional candidates have been announced by the Kepler mission. The increasing instrumental sensitivity allows for the detection of small, potentially rocky planets (see Fig. 2a). For some of these planets – for example, CoRoT-7b (Léger and 160 co-authors, 2009; Hatzes et al., 2011), Kepler-10b (Batalha and 51 co-authors, 2011), 55Cnc e (Fischer et al., 2008; Winn et al., 2011; Demory et al., 2011) and GJ 1214b (Charbonneau et al., 2009) – radius and mass measurements have been carried out, providing a mean density. Only for these planets can it be inferred whether they are mainly rocky or hold a substantial amount of atmosphere. Furthermore, if the mean density is known to be high enough, accuracy constraints on the internal structure of the planets can be derived (e.g. Valencia et al., 2006; Wagner et al., 2012). CoRoT-7b and Kepler-10b, for example, both have a high average density that suggests an iron core with the size of approximately 70 % of the planet's size (Wagner et al., 2012). Note, however, that accurate measurements of radius and mass are necessary to assess possible interior structures of a detected exoplanet. Fig. 2b shows the possible range in the interior structure for an Earth-sized planet with one Earth mass but an inaccuracy of measurement of either 10 % (dark shadowed regions) or 20 % (light shadowed region) considering Earth-like mantle and core compositions.

For rocky planets (usually assumed to have masses less than 10 M_{Earth}), one of the main scientific objectives is whether they are habitable, that is, hold an environment that can sustain life (Steele et al., 2006). The most important prerequisite for life is liquid water because all life on Earth needs liquid water at least for a part of its lifetime. This constraint has led to the typical definition of habitability on extrasolar planets requiring liquid water on the planetary surface, because it is difficult to observe subsurface conditions of these distant worlds and life on gas planets seems unlikely. From this, the so-called habitable zone (HZ) for rocky planets is defined – that is, the range of orbital distances over which liquid water may be possible on the surface (e.g. Hart, 1979; Kasting et al., 1993; Kopparapu et al., 2013). Several low mass planets (super-Earths to mini-Neptunes) and planetary candidates close to or within the HZ have already been detected: e.g. Gliese 581 c,d (Mayor et al., 2009; Udry et al., 2007), HD 85512 b (Pepe et al., 2011), GJ 667C c (Anglada-Escudé et al., 2012; Delfosse et al., 2013; Bonfils et al., 2013), HD 40307 g (Tuomi et al., 2013), and Kepler 22b (Borucki and 83 co-authors, 2012). However, for none of these planets could mass or radius be determined accurately enough to judge their bulk composition.

The possible existence of liquid water on a planetary surface depends on the surface temperature and the water reservoir in the planet. This water reservoir derives from planetary formation and the subsequent delivery of water by impacts. Because both processes are difficult to assess even for the planets in the Solar System, the habitability of extrasolar planets is usually determined by atmosphere models that evaluate surface temperatures assuming a water reservoir of one Earth ocean (e.g. Kasting et al., 1993). This, for example, has been done for the

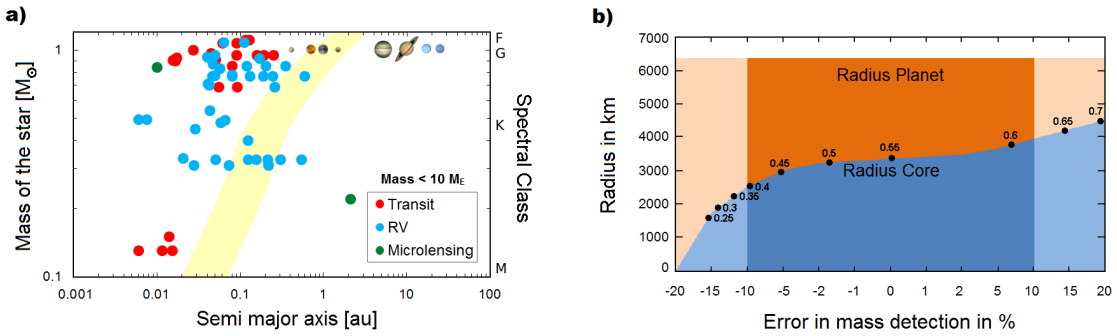

Figure 2: Left: Detected potentially rocky exoplanets with less than 10 M_{Earth} in comparison with the Solar System. The planets are depicted over their semi-major axis and mass of their central star. The colour coding indicates the detection methods: cyan depicts planets found by radial velocity measurements (RV), red depicts planets detected with the transit method, and green depicts planets found by microlensing. Note that planetary masses from RV measurements are lower mass limits. The yellow area indicates the HZ in line with Selsis et al. (2007) and based on Kasting et al. (1993). Right: Possible interior structures and resulting radius ratios (black dots) for an Earth-sized planet with one Earth mass plus/minus 10 % or 20 % inaccuracies of measurement assuming Earth-like mantle and core compositions, after Rauer and 154 co-authors (2014).

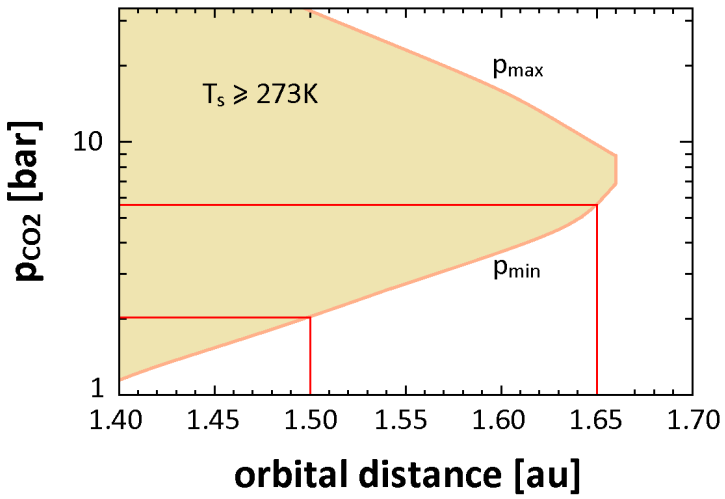

Figure 3: Range of CO_2 surface pressures compatible with habitable surface conditions (coloured area), with $T_{surf} \geq 273$ K (the solid line indicates the outer edge of the habitable zone with $T_{surf} = 273$ K) as a function of orbital distance for an Earth-like planet around the Sun. Upper limit of CO_2 pressure is fixed at 34 bar, which is the vapour pressure at 273 K. At an orbital distance of 1.5 astronomical units (au) a surface CO_2 pressure of 2 bar is needed for surface temperatures above 273 K; at 1.65 au, more than 5 bar are needed. The smaller the maximal possible surface pressure, the more the outer boundary of the HZ is shifted inwards toward the inner boundary (adapted from Kasting et al. (1993)).

extrasolar planet candidate Gl 581d by several groups (Wordsworth et al., 2010, 2011; Kaltenegger et al., 2011; von Paris et al., 2010; Hu and Ding, 2011; Selsis et al., 2007), leading to constraints for atmospheric composition and mass for habitable surface conditions. This planet may be habitable for carbon dioxide (CO_2) partial pressures of the order of one to several bars, assuming it is a rocky planet and holds a sufficiently large water reservoir. Thus, atmosphere modelling can help estimate if and for which atmospheric composition and mass an extrasolar planet could be habitable. However, whether these atmospheres are possible in terms of formation and evolution of planets has usually not been considered.

In addition to a primary atmosphere and the delivery of volatiles by impacts, the outgassing from the interior plays a major role in the buildup of an atmosphere. The outgassing of volatiles depends on the interior structure, composition and dynamics. On Earth, CO_2 is subject to the carbonate-silicate cycle, a negative feedback cycle that stabilizes the climate and the CO_2 content (e.g. Walker et al., 1981; Kasting et al., 1993). For Earth-like planetary atmospheres, CO_2 partial pressures have been estimated on the basis of a parameterization of this cycle (e.g. Edson et al., 2012; Abbot et al., 2012). Kite et al. (2009) apply a parameterized model calibrated to Earth to investigate mantle melting by varying both planetary masses and sizes. Modelling studies of rocky extrasolar planets have also estimated the primordial atmosphere on the basis of interior structure models (e.g. Elkins-Tanton and Seager, 2008b).

2.1 Geophysical influence on the habitable zone

The well-known circumstellar habitable zone (HZ) gives the distance to a star where surface liquid water may exist for a terrestrial planet. It assumes a fixed Earth-like CO_2-cycle including the life-enhanced carbon-silicate cycle and active volcanism which regulates the atmosphere via the amount of outgassed greenhouse gases or bound carbonates.

The concept of the HZ neglects the possible planetary diversity that we can already see in the Solar System. Here we investigate an update of the HZ by studying the effects of geophysical constraints on the outgassing efficiency and hence the atmospheric surface pressure. An inefficient outgassing at the outer boundary of the classical habitable zone does not allow for liquid water at the surface, thus reducing the width of the HZ.

The Earth is only one out of three planets in the HZ – with Mars and Venus at the boundaries. Both those classical solar planets lack active plate tectonics, a global magnetic field and (at least in the case of Mars) active volcanism. Planets like Mars without plate tectonics (apart from possible early plate tectonics, Sautter et al., 2015)

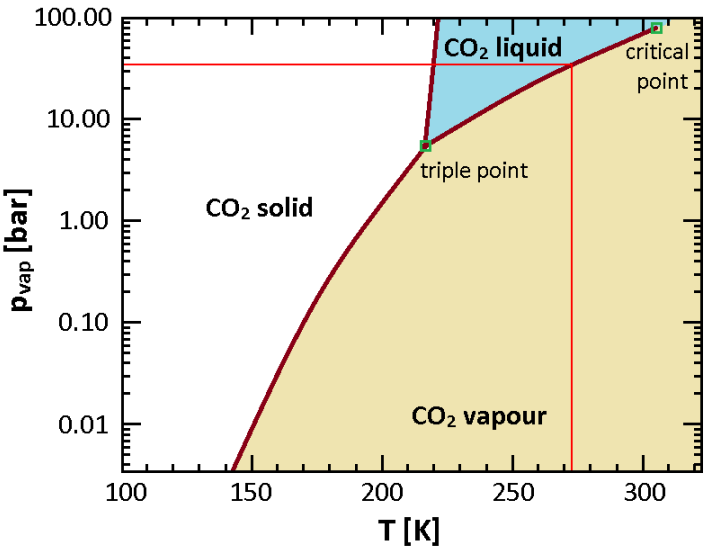

Figure 4: CO_2 phase diagram. Yellow region designates vapour phase; for these pressures, CO_2 could reside in the atmosphere. Larger atmospheric pressures would either lead to condensation of CO_2 (blue region) or seperation by freezing (white region). At 273 K, the pressure where CO_2 condensates lies at 34 bar.

and no or only limited volcanic events may not be considered as habitable at the outer boundary of the HZ, since the CO_2 greenhouse effect needed to ensure liquid surface water is strongly reduced.

Venus, on the other hand, built-up a dense CO_2 atmosphere. If the planet would be at the outer boundary of the habitable zone or if some of the CO_2 from the atmosphere would have been extracted by weathering and carbonate formation, Venus could be a habitable planet. At its orbit and with the current solar flux, a runaway greenhouse effect happens and Venus cannot have any liquid water at the surface. The early evolution of the planet, on the other hand, is still debated and varies between a runaway-greenhouse state similar to present day and an Earth-like planet with surface water and possibly even plate tectonics.

Kopparapu et al. (2014) investigated the possible influence of planet mass on the inner boundary of the HZ, showing that an increasing mass moves the inner boundary closer to the star, therefore widening the HZ. Kasting et al. (1993) and similar studies on the outer boundary of the HZ take the influence of the planet mass on the atmospheric surface pressure into account, but all these studies assume that the HZ is only constrained by atmospheric processes and that Earth-like amounts of CO_2 or larger could be outgassed if needed. However, the reservoir of atmospheric CO_2 may be limited by the interior.

2.2 Atmospheric constraints on habitability

To estimate the impact of interior structure and dynamics on the potential outgassing of an atmosphere, we apply a 2D interior convection model to calculate the production rate of partial melt for Earth-sized planets with different iron core sizes. From this, we estimate outgassing rates of CO_2 and compare them with the atmospheric modelling results of Kasting et al. (1993) to judge whether the outgassing from the interior may allow for a sufficiently large greenhouse effect at the outer edge of the HZ.

Previous research has assumed that the CO_2 reservoir for the atmosphere is not limited. Kasting et al. (1993) assumes that for the outer boundary of the HZ (see Fig. 3), as much CO_2 as needed will be brought into the atmosphere by the carbonate-silicate cycle, and as such, habitability is only constrained by atmospheric processes, such as the greenhouse effect or Rayleigh scattering.

However, the atmospheric CO_2 reservoir may also be limited by the interior, assuming that only a limited amount of carbon-dioxide is outgassed. The outer edge of the habitable zone is constrained by the ability to obtain surface temperatures of at least 273 K. At this temperature, the condensation pressure of carbon-dioxide is 34 bar, see Fig. 4. If the atmospheric pressure exceeds this value, either CO_2 will condense or surface temperatures will increase above 273 K. The minimal CO_2 pressure p_{min} needed for liquid water at the surface depends on the orbital distance, see Fig. 3 and section 4.4.2.

One of the questions we address in this work is whether (and under which constraints) the required p_{min} may not be obtained from outgassing of the planetary interior. This study is also inspired by detections of Earth-sized planetary candidates (e.g. Borucki and 69 co-authors, 2011), for which the mass of the planets is not measurable at all or not to the desired accuracy because of reasons such as the present-day detection limit, the low brightness of the observed objects or the uncertainties in host star parameters (e.g. stellar mass). Therefore, we examine whether the differences in planetary interior structure (and mass) that are possible for a rocky extrasolar planet with one Earth radius may influence the outgassing and, thus, planetary habitability.

3 Modelling the interior of terrestrial planets

Interior models are often used to investigate how the interior dynamics can influence the surface of a planet, focussing, for example, on plate tectonics (Tackley, 1998; Trompert and Hansen, 1998), on the formation of the crust (e.g. Morschhauser et al., 2011) or on the crustal dichotomy of a planet (Keller and Tackley, 2009; O'Neill and Nimmo, 2010). However, atmospheric influences, such as the greenhouse effect, and resulting variations in surface temperature are often neglected. Some studies have concentrated on the buildup of the atmosphere (e.g. Grott et al., 2011b; Leblanc et al., 2012) and possible feedbacks on mantle dynamics using simple gray 1D atmosphere models (e.g. Phillips et al., 2001; Noack et al., 2012; Gillmann and Tackley, 2014). The possible habitability of an Earth-like planet depends on the feedback between atmospheric processes and interior dynamics. In particular, plate tectonics, which depends on surface temperatures (e.g. Lenardic et al., 2008; Noack and Breuer, 2013), may have a strong influence on the evolution of the atmosphere.

Thus far, most of the numerical models treating interior dynamics (either 1D parameterized models or fully dynamical 2D and 3D models, which treat partial melting and volcanic outgassing self-consistently) have focused on the Solar System bodies, such as Mercury (e.g. Grott et al., 2011a), Venus (e.g. Armann and Tackley, 2012; Noack et al., 2012), the Earth (e.g. de Smet, 1999) and Mars (e.g. Morschhauser et al., 2011; Keller and Tackley, 2009; Sramek and Zhong, 2012). Numerical models for super-Earth planets have also been applied to investigate the effects of depth-dependent thermodynamic properties (Stamenkovic et al., 2012; Wagner et al., 2012), the propensity of plate tectonics (O'Neill and Lenardic, 2007; Valencia et al., 2007; Stein et al., 2011; van Heck and Tackley, 2011; Noack and Breuer, 2014) and the effects of variable surface temperature on the interior dynamics and its implications for the planet's volcanism (Gelman et al., 2011; van Summeren et al., 2011).

In this section, we employ a 2D interior dynamics model (Hüttig and Stemmer, 2008; Noack et al., 2015) to investigate whether the CO_2 outgassing rate of terrestrial planets depends on their interior structure, assuming that the planets comprise of iron and silicates. We also investigate the likelihood of plate tectonics and compare the outgassing potential between a plate-tectonics planet and a stagnant-lid planet. We use the resulting CO_2 pressures to discuss possible constraints on the outer boundary of the HZ depending on the interior structure of the planet and the surface regime (i.e. plate tectonics or stagnant-lid regime).

3.1 Extended Boussinesq

For the treatment of convection, we solve the following partial differential equation system for an extended-Boussinesq fluid (e.g. King et al., 2010) in a 2D spherical geometry using the finite-volume codes GAIA and CHIC (Hüttig and Stemmer, 2008; Noack et al., 2015). The mantle is heated by radioactive decay and by cooling of the iron core. We use free-slip boundary conditions and assume that the CMB temperature decreases over time due to core cooling. The equation system is non-dimensionalized as is typically done for convection simulations (Christensen, 1984; Noack et al., 2012). The conservation equations of mass, momentum and energy are as follows:

$$\nabla \cdot v = 0 \tag{1}$$

$$-\nabla P + \nabla \left[\eta \left(\nabla v + (\nabla v)^{\mathrm{T}}\right)\right] + RaT e_r = 0 \tag{2}$$

$$\begin{aligned} &\frac{\partial T}{\partial t} + v \cdot \nabla T + (T + T_0)\left(Div_r + \frac{\Delta S}{c_p}\left[\frac{\partial F}{\partial t} + v \cdot \nabla F\right]\right) \\ &\quad = \nabla^2 T + \frac{Di}{2Ra}\eta \left(\nabla v + (\nabla v)^{\mathrm{T}}\right)^2 + H. \end{aligned} \tag{3}$$

Here, P denotes the dynamic pressure induced by convection. T marks a transposed tensor, T denotes the temperature and T_0 denotes the non-dimensional surface temperature, which we obtain by dividing the actual surface temperature by the temperature contrast (ΔT) across the mantle. t is the time, v is the velocity vector, v_r is the radial velocity as e_r is the radial unit vector. Ra is the Rayleigh number, η is the viscosity and H is the radioactive heat source density, which decays over time (see section 4.2). ΔS is the entropy change on melting, c_p is the mantle heat capacity and F is the melt fraction. In our model, we assume that newly formed melt leaves the system instantaneously upon formation. The latent heat is added in Eq. (3) in form of a sink term that accounts for temporal changes of the melt fraction. To avoid the uncertainties caused by more complex melting and freezing processes in the lower mantle, the partial melt is only accounted for in the upper part of the mantle (above 12 GPa). Di is the dissipation number and depends on the thermal expansivity α, the gravitational surface acceleration g,

the mantle thickness D and the heat capacity of the mantle:

$$Di = \frac{\alpha g D}{c_p}. \tag{4}$$

3.2 Compressible mantle flow

In Section 5 we investigate the effect of compressible mantle flow (e.g. Schubert et al., 2001; King et al., 2010) on outgassing using the truncated anelastic liquid approximation (TALA). Reference profiles are employed for the pressure, density and temperature ($\bar{p}, \bar{\rho}, \bar{T}$), as well as lateral variation fields due to convection (p', ρ', T'):

$$\begin{aligned} T &= \bar{T} + T' \\ p &= \bar{p} + p' \\ \rho &= \bar{\rho} + \rho' \end{aligned}$$

The surface pressure is 1 bar. We furthermore use reference profiles for the gravitational acceleration, thermal expansion coefficient, heat capacity at constant pressure, bulk modulus and Gruneisen parameter ($\bar{g}$,$\bar{\alpha}$,$\bar{c_p}$,$\bar{K_T}$,$\bar{\gamma}$) as provided by the interior structure model for an initial reference temperature profile. This initial profile assumes a thermal boundary (including a possible lithosphere) at the top of the silicate mantle of 100 km thickness, an upper mantle temperature (starting at the bottom of the upper thermal boundary layer) and a surface temperature of 290 K. The temperature increases adiabatically throughout the silicate mantle, the temperature at the core-mantle boundary (T_c) is set as the resulting adiabatic temperature at the bottom of the mantle and increases further along the core adiabate towards the center of the planet. The same temperature profile is used as initial temperature profile for the simulations. Note that the temperature scale ΔT needed for non-dimensionalization and for the definition of the Rayleigh number below is therefore only a reference value and not the actual temperature drop across the mantle. The thermal conductivity ($\bar{k}$) is calculated following the scaling law derived in Tosi et al. (2013).

The conservation equations of mass and momentum for the TALA formulation are solved together in a coupled system and read in non-dimensional quantities

$$\nabla \cdot \left(\bar{\rho}\vec{v}\right) = 0 \tag{5}$$

$$-\nabla p' + \nabla \cdot \sigma = Ra\bar{\rho}\bar{g}\left(\bar{\alpha}(T - \bar{T}) - B\,(1 - d)\right)\vec{e}_r \tag{6}$$

$$\sigma = \eta\left(\nabla\vec{v} + \nabla\vec{v}^{\mathrm{T}} - \frac{2}{3}\nabla \cdot \vec{v}\right) \tag{7}$$

Here $\vec{v}$ is the convection velocity, p' denotes the pressure variations due to convection, and σ the convective stress tensor. η is the viscosity, T indicates a transposed matrix, and I is the identity tensor. The bulk modulus K_T is here non-dimensionalized like the convective pressure, that means it is multiplied with $D^2/(\eta_{ref}\kappa_0)$, and the formulation is derived from Schubert et al. (2001), whereas all other non-dimensionalization factors are as usual (see for example Christensen, 1984; Noack et al., 2012). Ra is the reference Rayleigh number ($Ra = \rho_0\alpha_0\Delta T g_0 D^3/(\kappa_0\eta_0)$ for reference temperature scale ΔT and reference thermal diffusivity $\kappa_0 = k_0/(C_{p,0}\rho_0)$). Buoyancy follows both from thermal and compositional variations, where B is the buoyancy number defined here as $1/(C_{p,0}\alpha_0)$ and d is the melt depletion (a value of 0 denotes primordial mantle material and 0.3 the maximal allowed depletion).

The conservation equation of energy solves the composite temperature field ($T = \bar{T} + T'$) and reads:

$$\begin{aligned} \bar{\rho}\bar{C}_p\left(\frac{\partial T}{\partial t} + \vec{v} \cdot \nabla T\right) &= \nabla \cdot \left(\bar{k}\nabla T\right) + Di\bar{\alpha}\bar{\rho}\bar{g}v_r(T + T_0) \\ &+ \frac{Di}{Ra}\Phi + \bar{\rho}H + \bar{\rho}\bar{C}_p(T + T_0)L\left(\frac{\partial F}{\partial t} + \vec{v} \cdot \nabla F\right). \end{aligned} \tag{8}$$

Here v_r denotes the radial velocity, T_0 the surface temperature divided by temperature scale ΔT, Φ the viscous dissipation (see van Heck and Tackley, 2008, for definition) and H are the radioactive heat sources. We assume Earth-like values following McDonough and Sun (1995) with present-day values of C_U=21 ppm, C_{Th}=85 ppm, C_K=280 ppm, that are recalculated to initial heat source amounts 4.5 billion years ago and then decrease with time. L is the latent heat and F the melt fraction.

3.3 Rayleigh number and viscosity

The Rayleigh number Ra is a measure of the vigour of convection and is given by

$$Ra = \frac{\alpha g \rho D^3 \Delta T}{\kappa \eta_{\text{ref}}}, \tag{9}$$

where ρ is the density of the mantle material, κ is the thermal diffusivity and $\eta_{\text{ref}} = \eta(T_{\text{ref}}, p_{\text{ref}})$ is a reference viscosity at a reference temperature and pressure. The viscosity η for diffusion creep is given in Pas and stands for the resistance of a material to motion; it follows an Arrhenius law (Karato and Wu, 1993):

$$\eta(T, p) = A \exp\left(\frac{E + pV}{RT}\right). \tag{10}$$

The viscosity depends on a material constant A (Karato and Wu, 1993), the activation energy E and activation volume V (which are both material dependent), the universal gas constant R, temperature T and hydrostatic pressure p; the influence of the dynamic pressure P is disregarded in Eq. (10).

3.4 Rheology of super-Earths

Due to lack of high-pressure data, we assume in our study that diffusion creep dominates both in the upper mantle (olivine minerals) and in the lower mantle (which consists in our models of perovskite or post-perovskite mixed with magnesiowustite). Tackley et al. (2013) derived a law for the activation volume perovskite for diffusion creep depending on pressure, based on the data of Ammann et al. (2010) (note that this is the upper bound of the activation volume in Tackley et al. (2013), the lower value only holds for dislocation creep, for which the other rheological parameters are yet unknown):

$$V_{pv}(p) = 3.65 \frac{\text{cm}^3}{\text{mol}} \exp\left(-\frac{p[\text{GPa}]}{200}\right) \tag{11}$$

and for post-perovskite

$$V_{ppv}(p) = 1.7 \frac{\text{cm}^3}{\text{mol}} \exp\left(-\frac{p[\text{GPa}]}{1100}\right) \tag{12}$$

Stamenkovic et al. (2011) derive a similar formula for perovskite material

$$V_{pv}(p) = 1.38 \frac{\text{cm}^3}{\text{mol}} + 2.15 \frac{\text{cm}^3}{\text{mol}} \exp\left(-0.065 \cdot (p[\text{GPa}] + 10)^{0.485}\right) \tag{13}$$

We use both formulations of Tackley et al. (2013) in Section 5 and Stamenkovic et al. (2011) in Section 6, where the results for the two formulations are comparable. The activation volume and thus lower mantle rheology plays an important role for mantle convection in super-Earths (Stamenkovic et al., 2012; Noack and Breuer, 2014; Tackley et al., 2013). All rheological parameters are listed in Table 1.

Parameter [unit]	ol	pv	ppv
$A\ [m^p/(Pa^n s^1)]$	$1.9{\cdot}10^{-11}$	$2.0{\cdot}10^{-12}$	$1.4{\cdot}10^{-9}$
E [kJ/mol]	300	370	780
$V\ [cm^3/mol]$	6	$V_{pv}(p)$	$V_{ppv}(p)$

Table 1: Rheological parameters for dry diffusion creep in the olivine (ol) mantle following Karato and Wu (1993) applying a fixed shear modulus of 80 GPa, a Burgers vector of 0.5 nm and a grain size of 1 mm, as well as for the perovskite (pv) and post-perovskite (ppv) mantle following Tackley et al. (2013).

3.5 Partial melting and outgassing

We calculate the amount of partial melt produced during the thermal evolution of Earth-sized planets with different interior structures, from which we estimate the amount of CO_2 outgassed from the interior. We simulate mantle

convection in a terrestrial planet using a 2D finite volume code for fluid dynamics. When convection in a silicate mantle transports hot material from CMB to the upper part of the mantle via upwellings, partial pressure-release melting can occur. Partial melting occurs when mantle rock begins to melt. Because mantle material comprises an assemblage of minerals with different melting temperatures, partial melting describes the coexistence of liquid and crystals when the temperature lies between the solidus (lowest melting point component in the mineral assemblage) and the liquidus (highest melting point component in the mineral assemblage). Partial melt (which is less dense than the surrounding rock for small pressures) rises to the lithosphere, leading to either volcanism at the surface (extrusive volcanism) or melt accumulations in the lithosphere or crust (intrusive volcanism). We consider outgassing of volatiles only for extrusive melt. Upwellings, as well as downwellings, that form beneath the cold lithosphere in the upper mantle also trigger large convective stresses that are applied to the lithosphere and may eventually lead to plastic deformation and plate tectonics, which also can have a large influence on the melt production.

We calculate melt volumes, following (Plesa and Breuer, 2014; Plesa and Spohn, 2012; Noack et al., 2012), assuming that either χ_{ex} =10 % or χ_{ex} =25 % of the melt is extrusive, whereas 90 % or 75 % of the melt including volatiles remain trapped in the lithosphere. These extrusive melt factors circumscribe the observed range of intercontinental extrusive melt ratios on Earth (e.g. Crisp, 1984).

We assume that the silicate mantle initially contains χ_{CO_2} =1 wt% CO_2 and is depleted in volatiles over time from partial melting. We assume that outgassing of CO_2 depends linearly on the degree of melting, which is a simplified approach. The enrichment of incompatible elements, including volatiles in the melt, is controlled by either their solubility or their partitioning during fractionated differentiation – the acting mechanism is the one providing the lowest concentrations in the melt. In case of CO_2, the abundance depends on its solubility, which depends more on oxygen fugacity or the redox state of the mantle material and less on temperature and pressure (Hirschmann and Withers, 2008). As a consequence, the degree of melting, as well as the amount of carbon in the mantle, plays a minor role in the degassing process, in contrast to degassing of H_2O (Grott et al., 2011b). Note that fractional differentiation controls the process when the concentration of carbon in the solid material sinks below a critical value. However, at least for the amount of carbon commonly assumed in terrestrial mantles, we are above this threshold (Hirschmann and Withers, 2008). By applying our approach with the degassed CO_2 being proportional to the melt volume, we thus assume a constant oxygen fugacity even when varying the mantle thickness.

We admit that the uncertainties in the outgassing rate are substantial, especially considering the limited knowledge about the interior of Earth with respect to volatile reservoirs and melt production on early Earth and thus the mantle volatile history. Knowledge about extrasolar planets is even sparser. However, in this study we are interested in how the interior structure may influence the outgassing rate. Thus, quantitatively the results obtained depend on model assumptions, but we can qualitatively constrain the influence of the interior structure and dynamics on the planetary atmosphere and, thus, habitability.

The melt fraction $F(t_n)$ depends on the temperature T_n and the melting temperatures of the silicates,

$$F(t_n) = \frac{T_n - T_{n,\text{solidus}}}{T_{\text{liquidus}} - T_{n,\text{solidus}}}, \tag{14}$$

where the solidus curve $T_{n,\text{solidus}}$ denotes the temperature at which the first minerals of the mantle material mixture melt at timestep n (i.e. partial melt) and rise to the surface. If the temperature reaches the liquidus curve T_{liquidus}, all components of the mantle material melt in the corresponding region. Note that the solidus temperature depends on the depletion of the material and is adapted if partial melt is extracted. In our model, $f\left(F(t_n)\right)$ is a linear function of the melt fraction that describes local changes of the mantle composition,

$$f\left(F(t_n)\right) = -\frac{F(t_n)}{\Delta t_n}. \tag{15}$$

The initial value of the compositional field C is set to 0.3 in line with Keller and Tackley (2009), and therefore the maximal possible depletion is restricted to 30 %.
We use the (initial) solidus and liquidus curve of peridotite (taken from de Smet, 1999) for pressures below 15 GPa:

$$T_{\text{solidus}} = 1409.15\,\text{K} + 134.2\,\frac{\text{K}}{\text{GPa}} \cdot p - 6.581\,\frac{\text{K}}{\text{GPa}^2} \cdot p^2 + 0.1054\,\frac{\text{K}}{\text{GPa}^3} \cdot p^3 \tag{16}$$

$$T_{\text{liquidus}} = 2035.15\,\text{K} + 57.46\,\frac{\text{K}}{\text{GPa}} \cdot p - 3.487\,\frac{\text{K}}{\text{GPa}^2} \cdot p^2 + 0.0769\,\frac{\text{K}}{\text{GPa}^3} \cdot p^3. \tag{17}$$

For these pressures, the latent heat consumption is included in the energy equation–see Eq. (3)–and the amount of both surface melt volume and outgassed volatiles is traced. For pressures above 15 GPa, the melting curves change (Zerr et al., 1998), and a different parameterization must be used for the melt curves. We make use of the extrapolated solidus function of Stamenkovic et al. (2011) for pressures up to 1.1 TPa (based on laboratory data up to almost 200 GPa) fitted to yield the same melting temperatures at 15 GPa. We assume that the temperature difference between solidus (T_{sol}) and liquidus temperature (T_{liq}) is constant for pressures above 15 GPa with 75 K (de Smet, 1999).

$$\begin{aligned} T_{sol} &= 1761\,\mathrm{K} + 36.918\,\frac{\mathrm{K}}{\mathrm{GPa}}\bar{p} \\ &\quad -0.065444\,\frac{\mathrm{K}}{\mathrm{GPa}^2}\bar{p}^2 + 7.6686\cdot 10^{-5}\,\frac{\mathrm{K}}{\mathrm{GPa}^3}\bar{p}^3 \\ &\quad -3.09272\cdot 10^{-8}\,\frac{\mathrm{K}}{\mathrm{GPa}^4}\bar{p}^4, \end{aligned} \tag{18}$$

$$T_{liq} = T_{sol} + 75\,\mathrm{K}. \tag{19}$$

However, at pressures above 12 GPa for a mantle with a composition similar to Earth's composition (Ohtani et al., 1995), melt is assumed to be denser than the surrounding material (disregarding the influence of phase transitions, see section 4.4.1). Therefore, to determine the melt volume that reaches the surface, assuming an Earth mantle composition, our model considers only melt production (with corresponding depletion) in the uppermost mantle with pressures below 12 GPa. However, depleted material can be advected into the deep mantle. As stated above, we assume that partial melt instantaneously leaves the system as soon as it is formed (Keller and Tackley, 2009; Spohn et al., 2001). The solidus increases to account for the change in mineral composition of the residual material. The increase of the solidus with depletion is assumed to be linear, where 100 % depletion would lead to a solidus temperature equal to the liquidus temperature. In our model, however, the depletion and, thus, the increase of the solidus temperature are limited to 30 %.

We determine the mass of outgassed CO_2 (M_{CO_2}) from the extrusive melt volumes at the surface:

$$M_{CO_2} = \chi_{ex}\chi_{CO_2}\sum_i F_i(t_n)V_i \tag{20}$$

where i is an index used for all cells in which partial melt occurred at time t_n (and the degree of melt $F_i(t_n)$ is greater than zero); V_i denotes the volume of cell i. We then derive the possible surface pressure p_{CO_2}, which is related to the outgassed volatile mass M_{CO_2}, the planetary gravity g and surface area A by

$$p_{CO_2} = \frac{M_{CO_2}\,g}{A}. \tag{21}$$

In all investigated models, the planetary surface A does not change. However, mass and gravity of our model planets vary (see tables 3 and 4), and equal melt volume does not lead to equal atmospheric pressure. Note that p_{CO_2} will not necessarily equal the atmospheric pressure because other processes, such as condensation or weathering, also influence the amount of CO_2 in the atmosphere.

3.6 Thermochemical convection

To track compositional changes in the mantle, an additional partial differential equation is solved:

$$\frac{\partial C}{\partial t} + v\cdot\nabla C - f(F) = 0, \tag{22}$$

where C represents the mantle composition that changes with the melt fraction F due to mantle depletion in crustal components during the melting process. The depletion value indicates the amount of processed mantle material (i.e. per cent of extracted melt) during the melting process, which is directly linked to the volatile distribution in the mantle. Eq. (22) is solved using a particle-in-cell method (Plesa et al., 2013). Massless particles are used to trace the amount of depleted material (C) and, thus, the amount of volatiles in the mantle, which decrease linearly with the degree of depletion. The advective part in Eq. (22) is treated by the particles flow, and at time t_n the equation reduces to

$$\frac{C_{n+1} - C_n}{\Delta t_n} = f\left(F(t_n)\right). \tag{23}$$

3.7 Plate tectonics simulation

The mantle material behaves like a viscous fluid in the convecting part of the mantle. However, in the lithosphere the deformation of the material is rather elasto-plastic. In convection simulations, typically only the plasticity is included, for example, via a pseudo-plastic approach (Tackley, 1998; Trompert and Hansen, 1998), which we also use in the present study.

In this approach, we do not allow the convective stress $\tau = 2\eta\dot{\varepsilon}_{\mathrm{II}}$ (where $\dot{\varepsilon}_{\mathrm{II}}$ is the second invariant of the strain rate and depends on the velocity gradient) to exceed a pre-defined depth-dependent yield stress σ_{YS}. The yield stress up to a lithostatic pressure of 200 MPa increases with hydrostatic pressure, depending on a friction coefficient μ (Byerlee, 1978), as

$$\sigma_{\mathrm{YS}} = \mu p. \tag{24}$$

For larger pressures, the yield stresses are slightly below those obtained with Eq. (24) and can be approximated by either using an exponent smaller than one for the pressure (Murray, 1965) or by applying a second yield stress formulation for these higher pressures, where a non-zero surface yield stress and a decreased friction coefficient (e.g. Byerlee, 1978) are employed. However, including pore pressures leads to a formulation similar to Eq. (24) with a reduced friction coefficient for shallow depths (Kohlstedt et al., 1995), see also Section 6.1.

If the convective stress exceeds the yield stress anywhere in the mantle or lithosphere, the viscosity is reduced to an effective viscosity to limit the convective stress to the yield stress:

$$\eta_{\mathrm{eff}} = \begin{cases} \eta & \text{, if } \tau < \sigma_{\mathrm{YS}} \\ 0.5\sigma_{\mathrm{YS}}/\dot{\varepsilon}_{\mathrm{II}} & \text{, otherwise} \end{cases} . \tag{25}$$

For the investigated stagnant-lid cases, a large enough friction coefficient is chosen such that no surface mobilization occurs. The friction coefficient strongly depends on the material properties. We test several different friction coefficients in section 6 and their influence on the occurrence of plate tectonics.

We investigate only the initiation time of plate tectonics, because surface mobilization leads to an increased transport of mantle material towards the surface and, thus, possibly enhanced pressure-release melting. For the outgassing rates of CO_2 due to plate tectonics, we are only interested in the beginning of the plate-tectonics phase and stop our simulations if a large amount of CO_2 (i.e. tens of bars of CO_2) has been outgassed. After that, formation of carbonates and regassing of carbon by subduction of oceanic plates may change the atmospheric mass of CO_2. In addition, we do not consider the influence of subduction of the basaltic crust, which affects both mantle convection and possible formation of continents. For our stagnant-lid cases, we do not expect any considerable sink of CO_2 and therefore can compare CO_2 pressures after 4.5 Gyr.

4 Earth-size planets: influence of composition

4.1 Interior structure assumptions

In this section, we investigate only rocky planets consisting of a silicate mantle and an iron-rich core and restrict our models to Earth-sized planets. We vary the interior structure (i.e. the size of the iron core), which then changes the mass of the planet. It should be noted though that the measurement of a planetary radius alone does not reveal whether the planet is rocky, holds a thick atmosphere or a thick surface water-ice layer. Even when mass and, thus, mean density are known, it still cannot be inferred unambiguously whether the planet comprises an iron core and a surrounding silicate mantle and their relative proportions (Elkins-Tanton and Seager, 2008a).

In the present study, we vary the ratio of core radius to planetary radius (*radius ratio* RR) from a Moon-like ratio of approximately 0.25 (Weber et al., 2011) to a Mercury-like ratio of 0.85 (Smith et al., 2012) and beyond to a maximum radius ratio of 0.9. The Earth has a radius ratio of 0.55. We fix the densities in the silicate mantle and the iron core for all models and use average values obtained from the Earth (for a compressible formulation with depth-dependent density see Section 5): the Earth's mantle density varies from 3380 kg/m^3 in the lithosphere to about 5570 kg/m^3 at the core-mantle boundary (CMB), leading to an average mantle density of 4700 kg/m^3 (Turcotte and Schubert, 2002; Stamenkovic et al., 2012). In the core, the density increases from almost 10,000 kg/m^3 to 13,000 kg/m^3 at the core center following the standard PREM model (Dziewonski and Anderson, 1981), here an average density of 11,000 kg/m^3 is employed for our model.

With fixing the average densities, we neglect the compressibility of the material, which for example would lead for a core larger than the Earth's core to a higher average core density and a lower average mantle density in comparison to the Earth case. We will later discuss that this simplification can be justified as our findings would be even strengthened when considering compressibility, which can also be observed in our compressible study in Section 5. Furthermore, the pressure in the mantle to calculate both the melting temperature and the viscosity is obtained by the product of gravity, density and depth and increases linearly with depth. This simplified approach does not consider the sphericity of the planet but as melting is only considered to the cross-over pressure of 12 GPa for melt to be buoyant (see below), the difference in pressure and thus in the melting curve is less than a few percent. The deviation in pressure between the 'flat' and the 'spherical' approach increases with depth and is in the range of a few tens percent at the core-mantle boundary. This has a direct influence on the calculated viscosity of the mantle. However, as we only consider Earth-sized planets in this section, the difference in viscosity is negligible for the mantle dynamics.

4.2 Model parameters and scenarios

As a reference case, we simulate an Earth-sized planet with an Earth-like core-to-planet radius ratio of 0.55. For all simulations, we use a 2D cylindrical shell. We use a larger reference viscosity (of 10^{22} Pas) than is typically assumed for Earth, which yields upper mantle viscosities of around $10^{20} - 10^{21}$ Pas to avoid numerical errors.

The temperature of the CMB is initially set to 3900 K and can change over time as a result of mantle cooling and heat flux at the CMB. Above the core, we set an initial thermal boundary with an initial thickness of 287 km (10 % of the reference mantle thickness), in which the temperature decreases using a sine curve (Buske, 2006) towards the initial temperature in the lower mantle of 2800 K (the temperature rises above the CMB and thus resembles the observed temperature difference in present-day Earth). Towards the upper part of the mantle, the temperature decreases linearly until the initial upper-mantle value of 2000 K (or 2400 K in the second scenario) is reached. A thermal boundary layer of 287 km thickness then connects the upper-mantle temperature with the surface temperature, which is fixed at 280 K. We disturb the initial temperature field by applying a weak spherical harmonics temperature variation to trigger initially four upwellings and four downwellings in the mantle.

We set the initial amount of internal heat sources to $H_0 = 2 \cdot 10^{-11}$ W/kg (Breuer, 2009) and the averaged decay constant to 0.3391 Gyr^{-1}. After 4.5 Gyr, the assumed present-day amount of radioactive heat sources of $4.35 \cdot 10^{-12}$ W/kg (e.g. McDonough and Sun, 1995) is obtained.

All parameters used for the reference calculation (i.e. for RR=0.55) are summarized in Table 2.

We then vary the radius ratio from 0.25 (i.e. the radius of the iron core is one-fourth of the planet radius) to 0.9. This way, our parameter space covers all radius ratios observed for terrestrial bodies in the inner Solar System, from a Moon-like interior structure with a small iron core (Weber et al., 2011) to a maximum radius ratio of 0.9, similar to the suggested Mercury-like interior structure with a radius ratio of up to 0.85 (Smith et al., 2012).

Parameter	Symbol	Value
Planet radius (km)	r_{planet}	6378
Core radius (km)	r_{core}	3508
Mantle thickness (km)	D	2870
Surface temperature (K)	T_{s}	280
Initial upper mantle temperature (K)	$T_{\text{um,ini}}$	2000
Initial lower mantle temperature (K)	$T_{\text{lm,ini}}$	2800
Initial CMB temperature (K)	T_{CMB}	3900
Mantle density (kg/m^3)	ρ_{m}	4500
Core density (kg/m^3)	ρ_{c}	11000
Surface gravity acceleration (m/s)	g	9.81
Specific mantle heat capacity ($\frac{\text{J}}{\text{kgK}}$)	c_{p}	1000
Specific core heat capacity ($\frac{\text{J}}{\text{kgK}}$)	$c_{\text{p,c}}$	700
Thermal expansion coefficient (1/K)	α_{m}	$2 \cdot 10^{-5}$
Thermal diffusivity (m^2/s)	κ_{m}	10^{-6}
Dissipation number	Di	0.48
Reference viscosity (Pas)	η_{ref}	10^{22}
Activation energy (kJ/mol)	E	240
Activation volume (cm^3/mol)	V	2.5
Rayleigh number	Ra	$7.56 \cdot 10^6$
Initial amount of heat sources (W/kg)	H_0	$2 \cdot 10^{-11}$
Decay rate of heat sources (Gyr^{-1})	λ	0.3391
Melting depth corresponding to 12 GPa (km)	z_{melt}	272
Friction coefficient	μ	0.06

Table 2: Parameter set for the reference simulation.

To test the robustness of our results, we use two initial mantle temperatures (scenarios 1 and 2 in Table 3), which lead to different melting rates in the mantle. The occurrence and initiation time of plate tectonics also depend on the relative core radius, as we show in the third scenario, in which we use different friction coefficients and determine whether (and when) plate tectonics occurs depending on the interior structure. Furthermore, we investigate how the occurrence of plate tectonics changes the outgassing rate for radius ratios of 0.55, 0.7 and 0.9.

The variation of the mass not only results in a different internal structure (i.e. different ratios of core to planetary radius) but also influences the convective parameters. First, the mass variation influences the surface gravity (see Table 4) and, thus, the hydrostatic pressure and the Rayleigh number. (Note that instead of employing a depth-dependent gravity acceleration, we assume a constant gravity acceleration across the mantle, which depends in our model only on the total planet's mass.) Second, the variation in interior structure leads to a variation in mantle thickness, which again influences the Rayleigh number and several non-dimensionalizations (see Christensen, 1984; Noack et al., 2012, for details on the non-dimensionalization factors). We take this into account in our model using consistent parameter sets, as summarized in Table 4.

To calculate partial melt and, thus, outgassing rates, we use the same grid resolution for all simulations to allow for comparison of the results. We chose a spatial resolution of ∼20 km between two neighboured grid points. Because the planetary radius is always set to Earth's radius of 6378 km, the number of grid points in radial direction varies between 32 (RR=0.9) and 220 (RR=0.25), see Table 4.

Scenario	RR	Initial temp. $T_{\text{um,ini}}$ (K)	Friction coeff. μ
SL – standard case	0.25-0.9	2000	0.06
SL – warm case	0.25-0.9	2400	0.06
PT – standard case	0.25-0.9	2000	0.0006-0.06

Table 3: Scenarios investigated in the study. SL denotes stagnant-lid cases and PT denotes plate-tectonics cases. We keep the surface radius fixed at a value of 6378 km and vary the ratio of core radius to planet radius (RR), the initial upper mantle temperature $T_{\text{um,ini}}$, and the friction coefficient.

RR	r_{core} (km)	D (km)	M (M_{Earth})	g (m^2/s)	z_{melt} (km)	P_{CMB} (GPa)	Di	sh	D^2/κ (Gyr)
0.25	1595	4783	0.824	8.09	330	174.1	0.66	220	721.6
0.30	1914	4464	0.838	8.22	325	165.1	0.63	200	628.6
0.35	2232	4146	0.856	8.40	317	156.7	0.60	186	542.0
0.40	2551	3827	0.881	8.64	309	148.8	0.57	172	461.8
0.45	2870	3508	0.912	8.95	298	141.3	0.54	156	388.0
0.50	3189	3189	0.952	9.34	286	134.0	0.51	142	320.7
0.55	3508	2870	1.000	9.81	272	126.7	0.48	128	259.8
0.60	3827	2551	1.058	10.38	257	119.1	0.45	114	205.2
0.65	4146	2232	1.126	11.05	241	111.0	0.42	100	157.1
0.70	4464	1914	1.206	11.83	225	101.8	0.39	84	115.4
0.75	4783	1595	1.298	12.73	209	91.3	0.35	72	80.2
0.80	5102	1276	1.403	13.76	194	79.0	0.30	56	51.3
0.85	5421	957	1.521	14.92	179	64.3	0.24	48	28.9
0.90	5740	638	1.655	16.24	164	46.6	0.18	32	12.8

Table 4: Parameter sets for the simulations with different radius ratios (RR). Listed are the radii of planet and core (r_{planet}/r_{core}), the mantle thickness D, the mass of the planet M, the gravity acceleration g, the melting depth z_{melt} (i.e. for which a pressure of 12 GPa is reached), the pressure at the CMB P_{CMB}, the number of shells sh and the diffusion time through the mantle, defined as D^2/κ, which is used for the non-dimensionalization of time.

4.3 Results

We first present the results obtained for the thermal evolution of the reference case. In the subsequent section, we compare the melting rate and the outgassing rate for stagnant-lid planets with one Earth radius but different core-mantle radius ratios. In addition, we show the influence of varying initial upper mantle temperatures on the outgassing rates, followed by an investigation of the likelihood of plate tectonics depending on the interior structure of a planet. Last, we show how the evolution of surface melt changes when the surface is mobilized via Earth-like plate tectonics.

4.3.1 Reference case

In the reference case, we employed an Earth-like interior structure and assumed a reference viscosity of 10^{22} Pas at a temperature of 1600 K, which leads to upper mantle viscosities in the range of suggested values for both Mercury and Venus (e.g. Grott et al., 2011a; Nimmo and McKenzie, 1998). This viscosity is stiffer than an Earth-like reference viscosity but still leads to average convective velocities in the mantle of approximately 21-42 mm/yr (Peclet numbers of 2000–4000), which is similar to the velocity of Earth's tectonic plates. The maximal convective velocities for our simulations are up to 10 cm/yr in the mantle.

Fig. 5 displays the temperature and mantle depletion for different time steps of the simulation: at the beginning of the simulation, when the first partial melt occurs (750 Myr); at 2.2 Gyr, when convection is strongest; and at the end of the thermal evolution (4.5 Gyr). The melting region is limited to the uppermost part of the mantle (where pressures are smaller than 12 GPa). Therefore, we only consider the process of depletion for pressures below 12 GPa but this depleted material can be convected into the lower mantle. We initially set the depletion of mantle material to 0 % everywhere in the mantle and assume that the maximum amount of possible depletion is 30 % (Keller and Tackley, 2009). As a result of convection in the mantle, depleted material and fresh material can mix. New and volatile-rich material is transported into the upper mantle, where pressure-release melting can occur. After 2.2 Gyr the mantle material is still inhomogeneous, and regions with strongly depleted material (yellow) appear next to weakly depleted regions (dark orange). However, after 4.5 Gyr, the mantle material (beneath the lithosphere) is well mixed, and the remaining volatiles in the mantle are equally distributed. In the lithosphere, no melt occurs because the temperatures in the lithosphere are lower than the solidus temperature. This region is stagnant, and thus no depleted material mixes with the lithosphere material, which acts as a chemical reservoir.

We determine the amount of CO_2 outgassed during the thermal evolution by assuming a constant amount of volatiles per melt volume. We consider only melt that reaches the surface and apply either 10 % or 25 % extrusive volcanism.

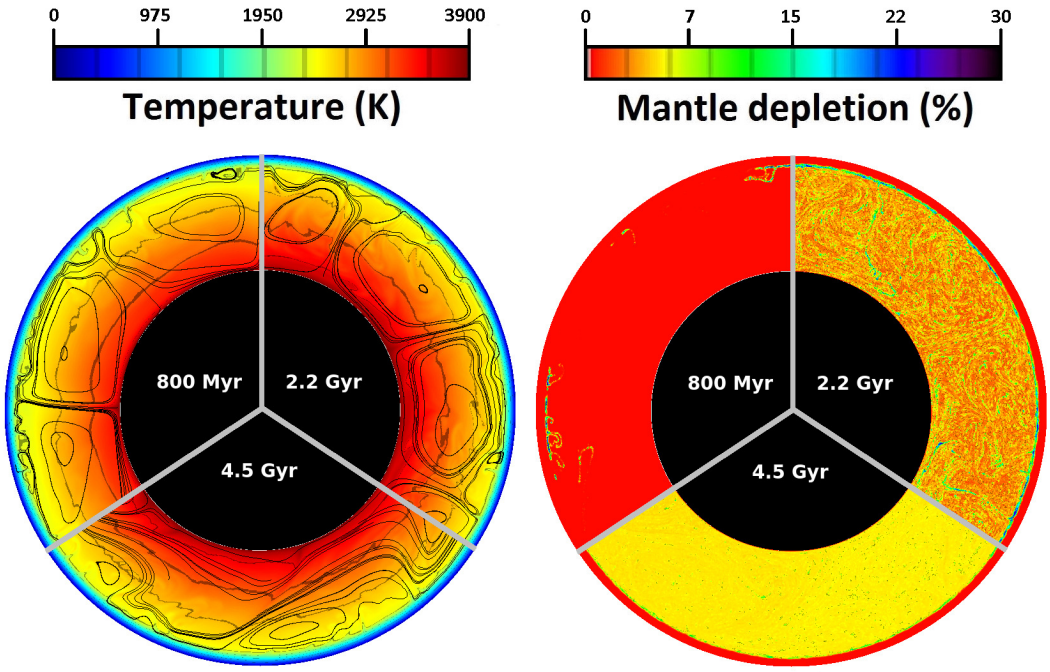

Figure 5: Temperature field and mantle depletion at different times for the reference case, with an initial mantle temperature of 2000 K and an Earth-like interior structure for a stagnant-lid Earth-sized planet.

Assuming 10 % of extrusive volcanism, the melt rate reaches 3.5 km^3/yr at 1.5 Gyr and decreases almost linearly over time until it drops below 1 km^3/yr, around 2.5 Gyr. The melting rate at the end of the thermal evolution is around 0.02 km^3/yr. The total melt volume extracted towards the surface during 4.5 Gyr is $4.305 \cdot 10^9$ km^3, when assuming 10 % extrusive volcanism, and $10.76 \cdot 10^9$ km^3, when assuming 25 % extrusive volcanism. This gives an outgassed amount of CO_2 with a partial pressure of 37.2 bar or 29.9 bar for the reference case with a radius ratio of 0.55, respectively, if no sinks (condensation, freezing or chemical cycles) of CO_2 are considered.

In addition to our standard case (see Table 3), in which we assume an initial upper mantle temperature of $T_{um,ini} = 2000$ K, we tested the robustness of our results by applying an additional value for the initial upper mantle temperature (second scenario) with $T_{um,ini} = 2400$ K. For these simulations, more melt is produced during the thermal evolution. The total volume of surface melt after 4.5 Gyr sums to $11.21 \cdot 10^9$ km^3 (10 % extrusive volcanism) or $28.04 \cdot 10^9$ km^3 (25 %) and results in an outgassed amount of CO_2 of 96.8 bar or 242 bar, respectively. The melting rate after 4.5 Gyr is ~ 0.0016 km^3/yr (for χ_{CO_2} =10 %), which is smaller than that for the standard case, because more melt has been produced during the early evolutionary stages of the planet. With the enhanced depletion of the mantle and the associated increase of the solidus temperature, less melt production is possible at 4.5 Gyr.

4.3.2 Variation of core size

In this section, we investigate how the melting rate (and, thus, the outgassing rate) changes when varying the iron core size between 25 % and 90 % of the planet's size. Although the total volume of silicates differs due to the varying mantle volume, the average depletion of volatiles per unit volume is expected to be similar to the reference case in case the production of partial melt is insensitive to the interior structure. This is, however, not the case, as shown in Fig. 6. The figure displays the temperature and mantle depletion fields of the 2D simulations after 4.5 Gyr for three cases: a Moon-like interior structure with a radius ratio of 0.25, the Earth-like case (RR=0.55) and a more Mercury-like interior structure (RR=0.9).

For all three cases, the mantle material is well mixed apart from the stagnant lithosphere, however, the average depletion strongly differs. For the largest radius ratio of RR=0.9, no melt has been produced in the mangtle during the entire evolution – thus, the depletion is zero. For the Earth-like interior structure (RR=0.55), the average

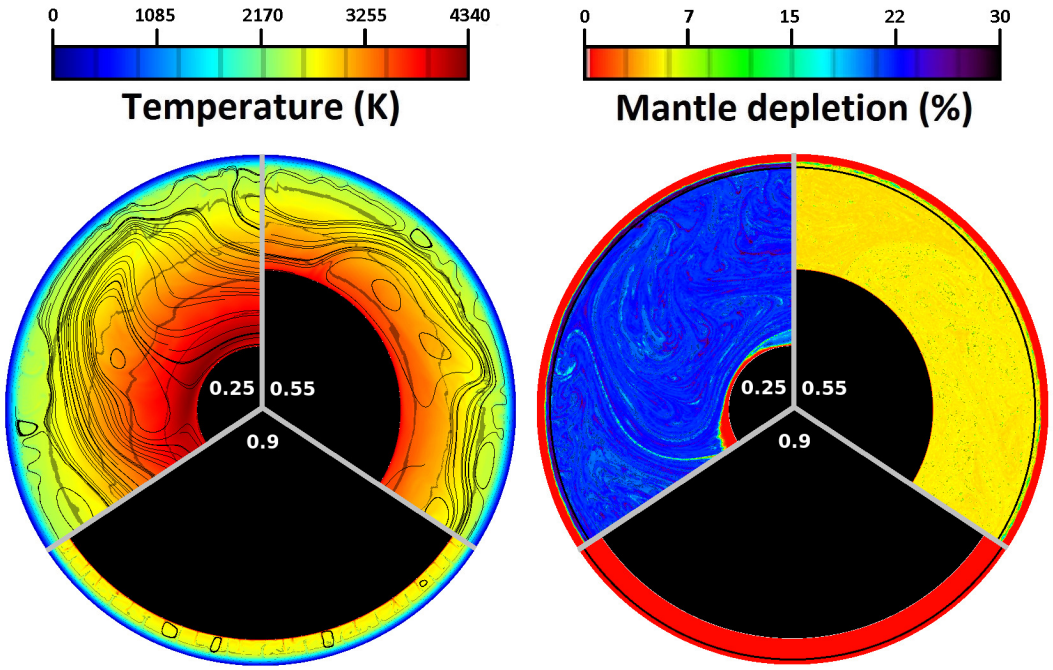

Figure 6: Temperature field and mantle depletion after 4.5 Gyr for the reference case (RR=0.55) in comparison with a Moon-like interior structure with a radius ratio of 0.25 and a more Mercury-like interior structure with a radius ratio of 0.9. For all simulations, the same planet radius is used. The 12 GPa isocurve is also plotted in the right figure.

depletion value in the mantle is 4.8 %, and for the Moon-like interior structure (RR=0.25), the average mantle depletion is 20.1 %.

Not only does the total amount of melt decrease when the mantle thickness is reduced, but also the amount of melt per unit volume (or, analogously, per kg). This finding is caused by the different pressure gradient in the mantle and thus melting temperature with depth when varyingg the interior structures. In the discussion we will elaborate on this effect in more detail. The temperature fields in Fig. 6 also show that the mantle temperatures strongly differ after 4.5 Gyr. For the radius ratio of 0.9, the average temperature in the mantle is 2276 K compared with 2894 K for a radius ratio of 0.25. Although for a thick mantle the Rayleigh number is larger and thus the heat transport by convection is more efficient in comparison to a thin mantle, the thick mantle cools slower due to its larger amount of radioactive heat sources (see Table 4).

The described trend of decreasing outgassing and mantle temperature with decreasing mantle thickness holds in general, as we show in Fig. 7, which plots the outgassed CO_2 pressure, the average mantle temperature and the melting rate over time. Table 5 lists the estimated amount of outgassed CO_2 for all simulations with a stagnant lid for both initial mantle temperatures and relative contribution of extrusive melt. As discussed above, the amount of atmospheric CO_2 may be reduced to much lower pressures as a result of thermodynamic limits (see von Paris et al., 2013) and other processes (e.g. weathering). Thus, even if an amount of several hundreds of bars is outgassed from the interior, the actual atmospheric pressure may be much lower.

For the low initial mantle temperature of 2000 K and a radius ratio above 0.75, no melting occurs in the mantle at all. For a radius ratio of 0.75, the melting lasts for only ~1.2 Gyr. Whereas for all smaller radius ratios, partial melt lasts until the end of the simulation (4.5 Gyr) and the rate of partial melting increases with increasing mantle thickness.

In Fig. 8, we compare the melting efficiency after 4.5 Gyr for all investigated radius ratios. We achieve the following results: first, the depletion of the mantle after 4.5 Gyr decreases with increasing radius ratio for initial mantle temperatures of both 2000 K (blue circles) and 2400 K (red boxes). Second, more melt occurs for both higher initial mantle temperatures and higher amounts of extrusive melt. Third, for a radius ratio higher than 0.75, the amount of partial melt is strongly reduced for both initial temperatures, leading to an atmospheric pressure of outgassed CO_2 of less than 1 bar.

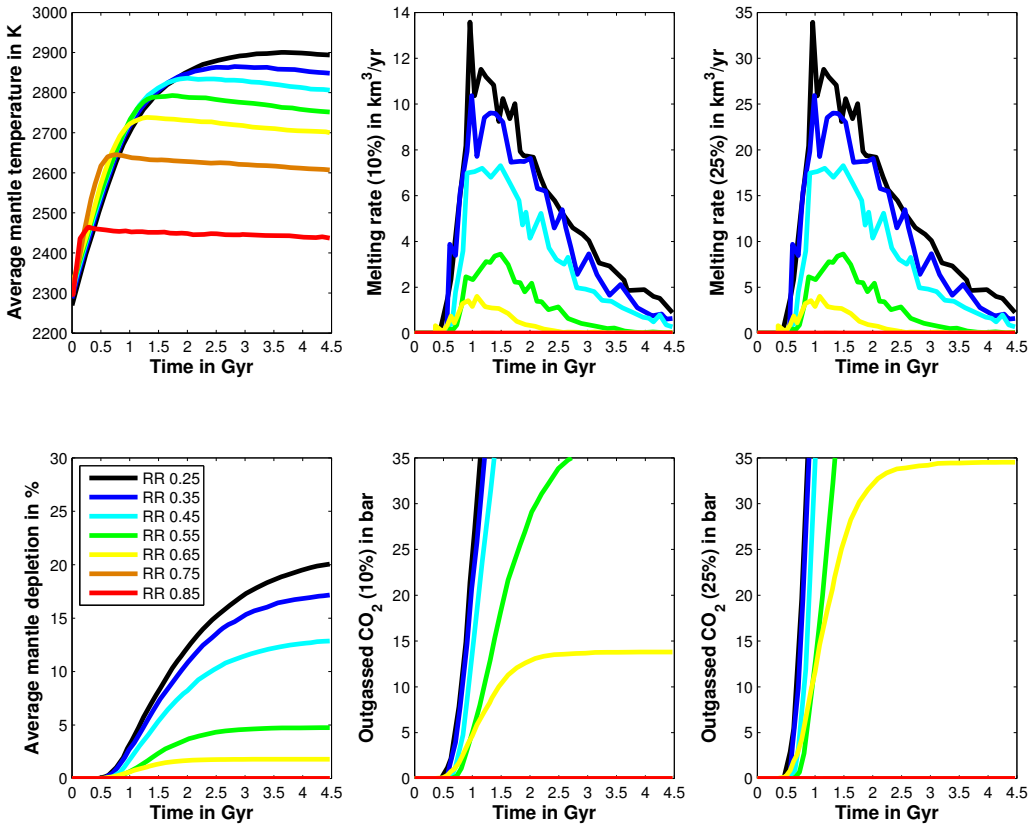

Figure 7: Thermal evolution of an Earth-sized planet with different radius ratios (RR) varying from 0.25 (small iron core and large silicate mantle) to 0.85 (large iron core) in steps of 0.1. Top row: volume-averaged mantle temperature (left) and melting rate at the surface for either 10 % (centre) or 25 % (right) extrusive melt. Bottom row: average mantle depletion (left) and outgassed amount of CO_2 for the two extrusive melt amounts (centre: 10 %; right: 25 %).

Note that the calculated values of the atmospheric pressures represent only general trends as they depend on assumed initial values, rheological parameters and CO_2 content in the melt. Furthermore, from a numerical point of view, different solutions can be obtained, depending on resolution and initial perturbations of the temperature field, leading to slightly different pathways during the evolution and, thus, in outgassing efficiency. However, independent of the applied parameter sets, the tendencies summarized for varying mantle thickness should hold in general.

4.3.3 Plate tectonics

To evaluate the question of how likely plate tectonics is for Earth-sized planets with varying internal structures and how efficient the mantle outgassing may be, we performed a parameter study with the parameters as stated for scenario 3 in Table 3.

For all radius ratios, we determine the initiation time of plate tectonics depending on varying friction coefficients μ in Eq. (24). We set the initiation time to the time when the maximal surface velocity exceeds a specific threshold value, which is set to a value of 100 for the non-dimensional velocity (corresponding to ~1 mm/yr). We use different friction coefficients between 0.0006 and 0.02; note that the friction coefficient for Earth, as measured in laboratory experiments, is larger (e.g. Byerlee, 1978). Water can reduce the yield stress in the lithosphere; the influence of the pore water pressure on the yield stress gradient can be formulated with a reduced friction

RR	SL standard			SL warm		
	V_{melt}^{in+ex} 10^9 km^3	$p'^{10\%}_{CO_2}$ bar	$p'^{25\%}_{CO_2}$ bar	V_{melt}^{in+ex} 10^9 km^3	$p'^{10\%}_{CO_2}$ bar	$p'^{25\%}_{CO_2}$ bar
0.25	214.6	153	382	246.1	175	438
0.3	181.8	132	329	227.0	164	411
0.35	178.5	132	330	226.1	167	418
0.4	187.6	143	357	230.6	175	439
0.45	127.1	100	250	171.0	134	335
0.5	106.1	87.3	218	162.9	134	335
0.55	43.05	37.2	92.9	112.1	96.8	242
0.6	4.08	3.73	9.31	73.4	67.1	168
0.65	14.19	13.8	34.5	79.0	76.8	192
0.7	2.10	2.18	5.46	33.0	34.4	86.0
0.75	<0.001	<0.1	<0.1	0.314	0.35	0.88
0.8	0	0	0	<0.001	<0.1	<0.1
0.85	0	0	0	<0.001	<0.1	<0.1
0.9	0	0	0	<0.001	<0.1	<0.1

Table 5: Resulting melt volume that rises towards the surface (intrusive and extrusive) and estimated amount of CO_2 outgassing after 4.5 Gyr for stagnant-lid (SL) cases with different amounts of extrusive volcanism and different initial mantle temperatures using either the standard (2000 K) or the warm scenario (2400 K) from Table 3. Note that the amount of outgassed CO_2 (denoted by p'_{CO_2}) does not necessarily equal the atmospheric partial pressure (p_{CO_2}).

coefficient (e.g. Kohlstedt et al., 1995).

Fig. 9 shows the variation of the initiation time for different friction coefficients and radius ratios assuming an initial mantle temperature of 2000 K. For small friction coefficients ($\mu \leq 0.0036$), plate tectonics is initiated for all radius ratios in the first 550 Myr but the initiation time is slightly reduced with increasing radius ratio (and, thus, decreasing mantle thickness). With increasing yield stresses (i.e. friction coefficients above 0.006), however, we find that only models with an intermediate radius ratio between 0.65 and 0.85 show plate tectonics. We discuss this result in more detail in section 4.4.3.

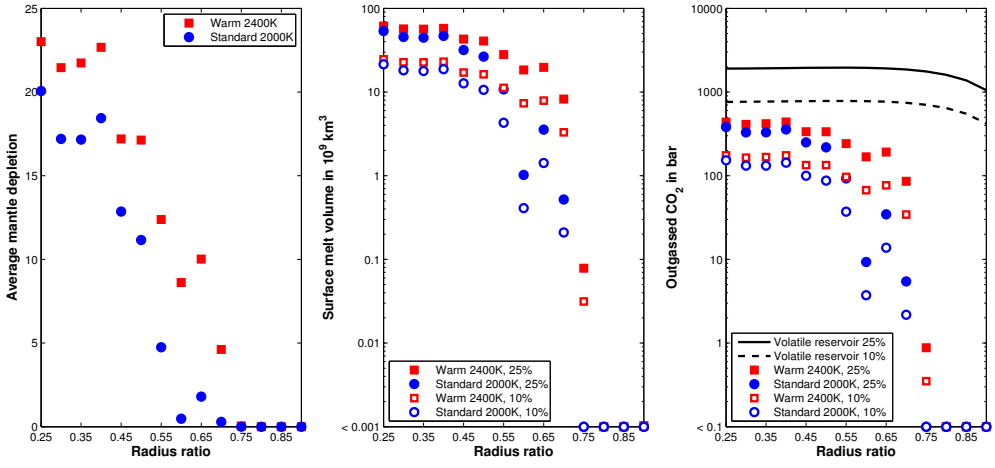

Figure 8: Average mantle depletion after 4.5 Gyr (left), total surface melt volume (centre) and estimated amount of outgassed CO_2 (right) for all radius ratios and for an initial mantle temperature of either 2000 K (blue circles) or 2400 K (red boxes). The surface melt volume is plotted for 10 % (open symbols) or 25 % (full symbols) of extrusive melt.

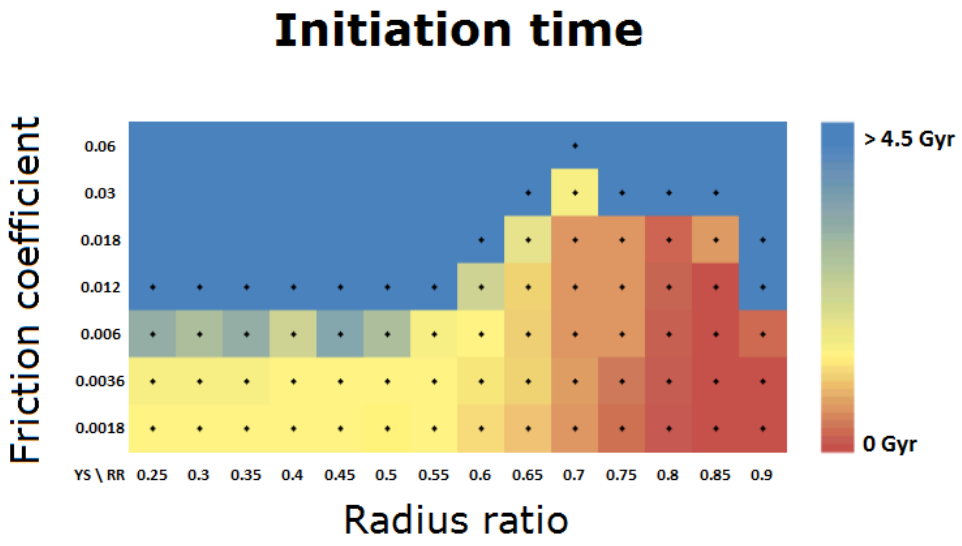

Figure 9: Initiation time of plate tectonics for different friction coefficients and radius ratios employing an initial mantle temperature of 2000 K and a reference viscosity of 10^{22} Pas. The black dots denote the cases that have been simulated.

To determine the influence of plate tectonics on the outgassing rate, we compare a stagnant-lid simulation (friction coefficient of 0.06) with a plate-tectonics simulation (friction coefficient of 0.006) with respect to mantle temperature and atmospheric evolution for different radius ratios of 0.55, 0.7 and 0.9 (Fig. 10). We further employ an initial upper mantle temperature of 2000 K and determine the amount of melt that rises to the surface as well as the outgassing of volatiles as described in section 3.

In all cases, after initiation of plate tectonics, the mantle temperature drops immediately. This enhanced cooling of the mantle may have an impact on the outgassing rates at later evolutionary stages of the mantle by less production of partial melt. Nevertheless, because of ridge formation and, thus, convective transport of hot material to the surface, the outgassing rate (determined by using the correlation factors listed in Table 5) is much larger for the plate-tectonic cases than for the stagnant-lid cases. The amount of outgassed CO_2 increases to several tens of bars shortly after the initiation time of plate tectonics. This finding is independent on the radius ratios. Although the efficient cooling of the mantle may reduce the outgassing rate with time, a dense atmosphere can be obtained for all radius ratios if one does not consider any sink of CO_2. For simplicity, we stopped the plate-tectonics simulations after at least 34 bar of CO_2 have been outgassed, which is the condensation pressure of carbon dioxide at a surface temperature of 273 K (see Fig. 4).

4.4 Discussion

This research is motivated by atmospheric modelling studies that investigate the habitability of extrasolar planets at the outer edge of the HZ, in which the amount of greenhouse gases, mainly CO_2, is usually treated as a free parameter. However, interior dynamics may strongly restrict the possible amount of CO_2 available at the surface. We estimate the CO_2 outgassing from the interior for Earth-sized planets with different interior structures, using different mixing ratios of silicate and iron and, therefore, different ratios of iron core to planet radius between 25 % and 90 %. Our main points addressed in the study are as follows: We want

1. to determine the melting rate (and, thus, the outgassing of volatiles) for a stagnant-lid planet,
2. to investigate whether possible constraints for the outer boundary of the HZ exist,
3. to investigate the influence of plate tectonics on outgassing (independent of regassing of CO_2), and
4. to examine whether the likelihood of plate tectonics depends on interior structure.

For our investigations, we use one set of planetary interior parameters (initial and rheological parameters) chosen to be Earth-like. We investigate how partial melt, outgassing and plate tectonics change with varying interior

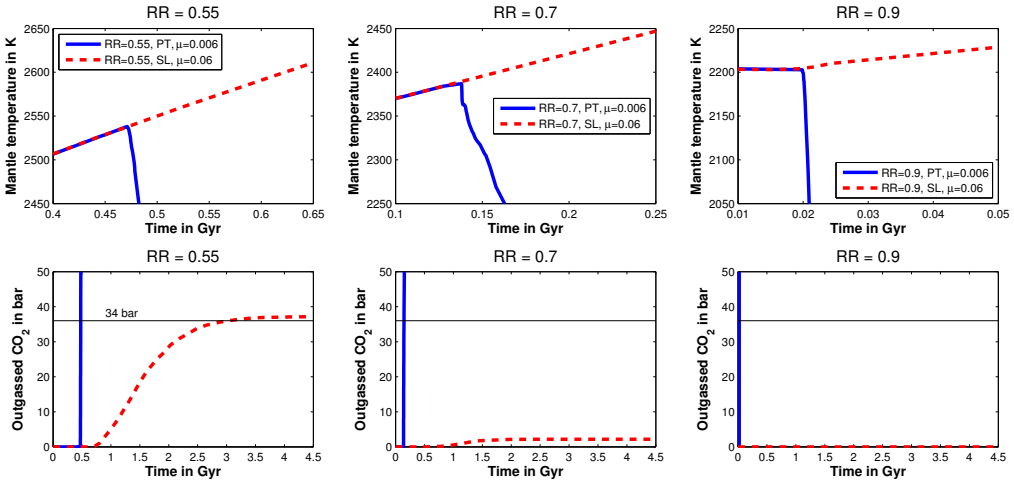

Figure 10: Evolution of mantle temperature and outgassed CO_2 after plate tectonics (PT – blue) initiated in comparison with a stagnant-lid case (SL – red) for a radius ratio of 0.55 (left), 0.7 (centre) and 0.9 (right).

structure while keeping the planet radius constant (i.e. Earth radius). To test the robustness of our results, we also use a second set of parameters employing a higher initial mantle temperature. Our results show that for stagnant-lid planets with a relatively thin mantle (in our study with RR≥0.75), the outgassing is strongly limited (for planets of one Earth radius, which likely also holds for larger planets). The outer boundary of the HZ may thus be restricted because of insufficient CO_2 outgassing. If plate tectonics sets in, however, sufficient outgassing can be obtained also for large core-mantle radius ratios, indicating that plate tectonics is indeed an important process for planetary habitability.

However, it should be noted that a planet around another star may have a different composition and thus also a different concentration of radioactive heat sources, melting temperature or amount of volatiles in the melt than assumed in our model. This might shift the critical RR at which the habitable zone is restricted by the interior structure for stagnant-lid planets. Investigation of planets that include a thick ice-ocean layer, would also be interesting. For those planets, however, the existence of a liquid subsurface layer above the silicate shell would be more important for potential habitability. This aspect is beyond the scope of our study, which focusses only on surface habitability.

4.4.1 Limitations for melting and outgassing

In our melting model, we assume according to the work of Ohtani et al. (1995), that melt below 12 GPa is denser than the silicate matrix and therefore does not contribute to mantle depletion and outgassing. However, more recent studies (e.g. Mosenfelder et al., 2009) suggest that though melt becomes denser than olivine, it is less dense than wadsleite and ringwoodite, up to a pressure of ∼25 GPa. Assuming a composition for the lower mantle of 20 % periclase and 80 % perovskite, Beuchert and Schmeling (2013) calculate that the melt becomes denser than lower mantle material at pressures higher than 100 GPa. Therefore, our models may severely underestimate the amount of melting and should be regarded as lower bounds.

The results imply that for stagnant-lid planets, the amount of partial melt and, thus, outgassing decreases with increasing radius ratio. For the smallest radius ratios (0.25–0.4), the outgassing rates are similar because, for these cases, the iron core is too small to affect the melting temperature and, thus, outgassing efficiency, in contrast to models with larger cores. The mass of a planet with a radius ratio of 0.9 is twice the mass of a planet with a radius ratio of 0.25, even though we ignored compressibility for the sake of simplicity. Conversely, the mass has a direct influence on the pressure gradient in the silicate mantle, which determines the melting temperature at a specific depth. Only when the mantle temperature is equal to or above the solidus temperature partial melting and, thus, outgassing can occur. Fig. 11 shows the melting temperatures for the different radius ratios as a function of depth.

The left panel of Fig. 11 shows the solidus temperatures for different scenarios for pressures below 12 GPa. At a depth of 100 km, the planet with a radius ratio of 0.25 has a peridotite melting (solidus) temperature of 1815 K; for

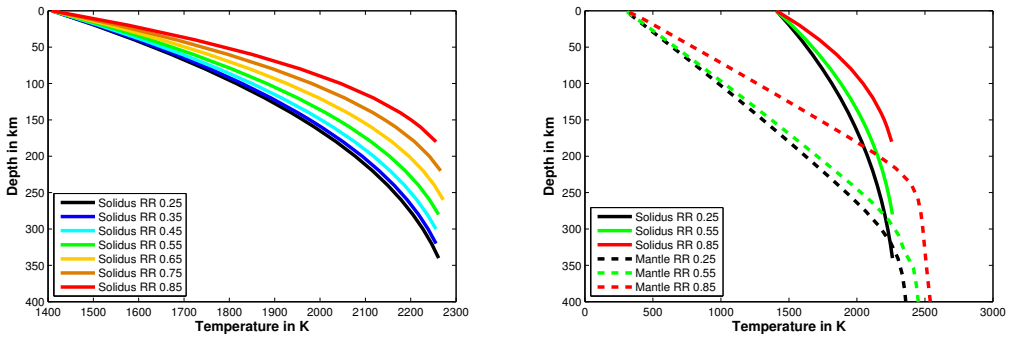

Figure 11: Left: Solidus temperatures for pressures below 12 GPa for an Earth-sized planet with different core sizes and, thus, different planetary masses. The radius ratios are varied in 0.1 steps for a better overview. With the change in gravity and, thus, pressure, the melting temperatures at a specific depth rises with increasing iron core size. Right: Solidus melting temperature (solid lines) versus average mantle temperature (dotted) for three different radius ratios after 4.5 Gyr.

a radius ratio of 0.85, the melting temperature is higher with 2045 K. For the largest radius ratio of 0.9 (not shown in Fig. 11), the solidus temperature is 2079 K, which is 264 K larger than for the Moon-like interior structure with a radius ratio of 0.25 at the same depth. In addition to the higher melting temperatures, the melting depth, at which melt is still less dense than the surrounding material and buoyancy leads to rising of the melt, strongly varies, as shown by the cutoff lines in the left panel of Fig. 11. For a radius ratio of 0.25, the melting depth is 330 km; for a radius ratio of 0.9, it is only half this depth, with 164 km. Finally, the Rayleigh number, which is a measure of the vigour of convection, decreases with decreasing mantle thickness, see Eq. (9).

The possible amount of melt that reaches the surface is therefore restricted by three factors for large core cases in comparision to small core cases: 1) the shallower melting region, 2) the higher solidus temperature at the same depth, which needs to be reached to obtain partial melt, and 3) the weaker convective vigour. The reason for the first two factors is the increased pressure gradient ($p = \rho g z$) for planets with a larger core. For the case with a radius ratio of 0.9 the pressure is twice the value of the case with 0.25 radius ratio at the same depth due to the variation in mass and, thus, gravity. Note that the neglection of sphericity in the calculation of the pressure gradient has a minor effect on the solidus temperature as only melt up to 12 GPa is considered. For the three cases plotted in the right panel in Fig. 11, only for the smallest radius ratio of 0.25 the average mantle temperature is still higher than the solidus temperature after 4.5 Gyr of thermal evolution. Local temperatures can however be higher than the average value, and therefore locally partial melting may occur for all cases.

To exclude that the observed decrease in outgassing with increasing core size is correlated only with the Rayleigh number, we conduct two additional runs for an Earth-like radius ratio of 0.55: the standard case (2000 K) with 10 % extrusive melt. Only the melting temperatures and melting depth differ from the reference case and are taken from a radius ratio of either 0.25 or 0.9. In particular, the Rayleigh number is not changed. For the melting curves of a radius ratio of 0.9, no melting in the uppermost part of the mantle and, thus, no outgassing occur during 4.5 Gyr. In contrast, for the melting curves calculated for a radius ratio of 0.25, an immense amount of outgassing occurs already in the beginning of the thermal evolution, similar to the standard case with a radius ratio of 0.25 (and adapted parameters). This shows that the pressure effects on the melting temperature and melting depth have the strongest influence on our outgassing results. Note that we only consider melting for a pressure range between 0 and 12 GPa for an Earth-sized planet. This allows us to calculate the pressure with the simplified approach of a 'flat' planet ($p = \rho g z$).

We further neglect the compressibility of the core and mantle material (which is treated in Section 5) with fixing the densities of mantle and core in our models. As a consequence, we underestimate the core density and overestimate the mantle density with increasing core size and vice versa. A lower mantle density may imply a lower pressure gradient than assumed in our models but a higher core density results in an increase of g and thus can compensate or even overcompensate the effect of the reduced mantle density when calculating the pressure up to 12 GPa. In fact, as iron has a larger compressibility than silicates, a larger core would result in a even higher pressure gradient in the mantle than assumed in our simplified appraoch – thus support our findings that with increasing core size the degassing of the mantle is strongly reduced.

In addition, we used several simplifications in our interior model, which we do not expect to change the observed trend of an decrease in outgassing efficiency for increasing core sizes. We assume that partial melt instantaneously leaves the system after melt formation, which may lead to a decrease in density for the residual material. In our model, we further consider only depletion effects and outgassing of CO_2 and ignore possible dehydration of mantle material. Both effects have been shown to reduce the outgassing of a stagant-lid planet Plesa and Breuer (2014). In fact, we assume that both compositional changes and dehydration have a weaker effect on melt production than the reference viscosity and initial mantle temperature. We use an increased reference viscosity of 10^{22} Pas for numerical reasons, which leads to less partial melt than might be expected for a mantle with a smaller reference viscosity. Conversely, our initial upper mantle temperatures have been either 2000 K or 2400 K. The different initial temperatures already lead to a large variation in outgassing efficiency. However, although more melt is produced for the warmer initial mantle temperature (analogous to a reduced reference viscosity), the observed main tendency of outgassing potential depending on the interior structure seems to be unaffected.

4.4.2 Constraints on habitability

Towards the outer edge of the HZ, habitability is constrained by the surface temperature T_{surf}, which needs to remain equal to or above 273 K, which is the triple point temperature of water. With increasing orbital distance, the stellar insolation decreases. At larger orbital distances (au), the atmosphere must therefore provide a stronger greenhouse effect to warm the surface. Building on the concept of the carbonate-silicate cycle on Earth, previous studies on the HZ (e.g. Kasting et al., 1993; Kopparapu et al., 2013) have assumed an increase in atmospheric CO_2 at the outer edge of the HZ. Such an increase results in a stronger greenhouse effect and, thus, increased surface warming. However, an increase in CO_2 also leads to enhanced backscattering of stellar radiation via Rayleigh scattering, which favours surface cooling. The interplay of cooling and the greenhouse effect produces a distinct maximum of surface temperatures (instead of a steady increase) when CO_2 increases, which is called the maximum greenhouse effect (e.g. Kasting et al., 1993). Fig. 3 illustrates this behaviour. At a given value of stellar insolation, usually two values of CO_2 pressure can be derived. The first is the minimum pressure, p_{min}, which is at least necessary to obtain 273 K surface temperature. The second is the maximum CO_2 pressure, p_{max}, above which Rayleigh scattering leads to temperatures below 273 K. In addition, from this interplay between cooling and warming, the amount of atmospheric CO_2 may be limited by the phase diagram (see Fig. 4). At a given surface temperature below the critical temperature (303 K), the vapour pressure curve limits the amount of gaseous CO_2 in the atmosphere. Adding more CO_2 then just causes condensation or freezing at the surface (von Paris et al., 2013). For example, at 273 K, a maximum of 34 bar of CO_2 in the gaseous phase is possible in equilibrium with the surface. At 288 K, 55 bar of atmospheric CO_2 would be permitted. The upper limit of permitted atmospheric CO_2 depends on surface temperature and, thus, on orbital distance and characteristics such as central star type or planetary gravity. In most cases, the upper limit for gaseous atmospheric CO_2 is higher than p_{max}.

For Earth-sized planets with a stagnant-lid, the results imply that for large core-mantle radius ratios, the amount of outgassed CO_2 is small. Assuming that the major source of atmospheric CO_2 is outgassing from the interior (and thus ignoring a possible primordial atmosphere), this limits the habitability of such planets at the outer edge of the HZ. If less than ~1 bar of CO_2 is outgassed from the interior, as we found for radius ratios larger than 0.7, Earth-sized planets at the outer edge of the HZ with orbital distances larger than 1.4 au may not hold enough CO_2 to warm the surface through the greenhouse effect (see Fig. 3). For small core-to-planet radius ratios, the atmospheric amount of gaseous CO_2 provided by outgassing from the interior is much larger. The actual atmospheric partial pressure of CO_2 for these cases is then limited by other processes, such as condensation or freezing of CO_2 for surface temperatures below 303 K. The amount of CO_2 in the atmospheres of planets also depends on weathering at the surface, which is also part of the carbonate-silicate cycle. Thus, the actual amount of atmospheric CO_2 may depend on many factors, including continental coverage, surface temperature, water reservoir or chemical reactions.

Fig. 12 illustrates the influence of the interior structure on the size of the HZ. For this figure, we only considered secondary atmospheres and, thus, the possible limitations of the interior structure on the outgassing potential. Furthermore, we assumed that the outer boundary of the HZ is close to the inner boundary if only a negligible amount of CO_2 (and, thus, also other volatiles) has been outgassed. Our four different outgassing results (two initial mantle temperatures and two relative extrusive melt amounts) show the same trend of a strongly reduced HZ for large iron cores. This result therefore seems to be robust and mostly independent of the applied convection

parameters.

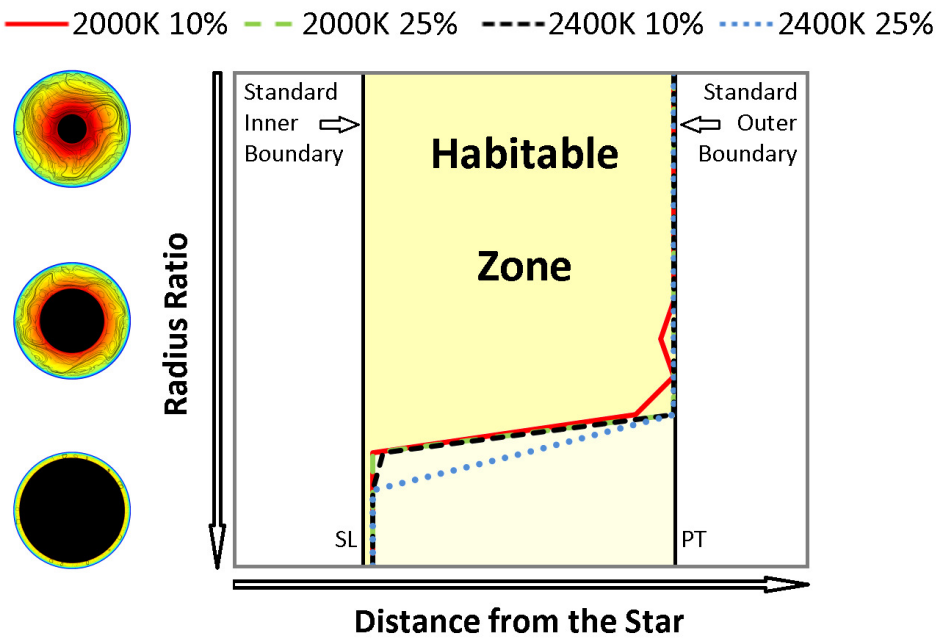

Figure 12: Sketch of the HZ for Earth-sized planets with different interior structures using the results presented in this study. For simplicity, we assume that the outer HZ is only restricted by the amount of CO_2 that can be outgassed from the interior. Note that different restrictions of the HZ may be obtained depending on the interior and atmospheric modelling details.

Stellar evolution, which leads to brightening of main-sequence stars over time, also influences habitability. It might be that at early evolutionary stages, the outgassed amount of CO_2 from the interior is not sufficient to heat the surface above the melting point of water. When the star brightens, however, depending on orbital distance, the outgassed amount of CO_2 may be sufficient to reach temperatures above 273 K. Note, however, that even if the amount of CO_2 outgassed from the interior is not enough to obtain temperatures above the freezing point of water, other greenhouse gases, such as methane or nitrous oxide, or atmospheric particles may lead to a sufficient warming of the surface (e.g. Selsis et al., 2007).

To understand the influence of the interior structure on habitability of a planet, it is also necessary to consider the possible changes in outgassing efficiency of plate-tectonics planets. The complex interaction among plate tectonics, the subduction of water and the CO_2 cycle is still not well understood, though first attempts to model this interaction have been developed (e.g. McGovern and Schubert, 1989; Parai and Mukhopadhyay, 2012; Wada et al., 2012). The occurrence of plate tectonics leads to a change in the outgassing process and rate as a result of three factors. First, efficient cooling of the mantle by subduction of the cold lithosphere can lead to a reduction in melt production and, thus, outgassing rate after a long time span, similar to the cooling effect of a suggested mobilized surface in the case of early Venus (Noack et al., 2012). Second, subduction of oceanic plates leads to a release of water in shallow regions of the upper mantle, which reduces the solidus temperature of the silicates above the subducted slabs and therefore leads more easily to partial melting (e.g. Katz et al., 2003). Third, with the mobile lithosphere, warm material can rise to the surface (which is not the case for stagnant-lid planets, on which an upwelling is stopped at the cold lithosphere), and pressure-release melting beneath a ridge is likely. These three effects counteract each other, but the third one is likely important at the time of plate-tectonics initiation, resulting in a strong increase of outgassing at that time.

Another inconclusive point is the influence of plate tectonics on the evolution of the secondary atmosphere. The long-term CO_2 cycle leads to subtraction of carbon from the atmosphere by formation of carbonates (via the carbonate-silicate cycle), which are then subducted with the oceanic plates into the silicate mantle. On Earth, it seems that the sinks of carbon (the long-term CO_2 cycle) with respect to the atmosphere and the source of carbon (via outgassing) have been in equilibrium since around 2.5 Gyr, when life started to enhance the formation of carbonates and most of the CO_2 had been subtracted from the atmosphere (Reddy and Evans, 2009).

The outgassing efficiency is indeed different for the plate-tectonics simulations than for stagnant-lid planets. When surface mobilization initiates, warm mantle material reaches the surface along the ridges (analogous to the mid-ocean ridges on Earth), and pressure-release melting leads to large outgassing rates. Even for the simulation with the largest radius ratio of 0.9, almost 100 bar of CO_2 are outgassed in the first 200 Myr. This is even larger than the maximal possible partial pressure of CO_2 at a surface temperature of 273 K (see Fig. 4) because, for pressures above 34 bar, CO_2 condenses. Therefore, the outer edge of the HZ is likely not limited by the outgassing from the interior if the planet is in the plate-tectonics mode, but rather by atmospheric processes, such as the maximum greenhouse effect (e.g. Kasting et al., 1993).

In case an Earth-sized planet is detected at the outer edge of the HZ with a high planetary mass indicating a Mercury-like rather than an Earth-like interior structure, we might expect that the planet did not build up a thick CO_2 atmosphere. (It should be noted though that a primordial atmosphere can change this assumption.) Thus, our model results could be tested by spectral characterization of such a hypothetical planet by future missions. For this type of investigation, however, highly accurate measurements of radius and mass are inevitable.

Fig. 2b plots the influence of error in mass detection on a possible interior structure (using an Earth-sized planet with one Earth mass as reference). Black dots indicate some possible initial structures depending on the accuracy of the detection method. For an inaccuracy of 20 % in mass, the iron core can have possible sizes ranging from 0 km to 4500 km (and even more if a surface ocean layer or a different core composition is considered). Only when the detection inaccuracy decreases below 10 % is it possible to infer whether our predicted atmosphere dependency on the interior structure (i.e. denser atmospheres for smaller masses for planets of one Earth radius) applies for exoplanets at the outer edge of the HZ.

4.4.3 Plate tectonics

For a large range of radius ratios (0.25 to 0.7), we obtain an increase of plate-tectonics likelihood with increasing radius ratio and, thus, with decreasing mantle thickness. However, further decreasing the mantle thickness (RR$\geq$0.75) shows that plate tectonics becomes less likely. The latter trend fits with the expected likelihood of plate tectonics depending on mantle thickness when applying standard scaling arguments for convective velocities and stresses. For the parameter sets used in our study, we can easily show that the convective stress divided by the yield stress in the lithosphere (and, therefore, also the likelihood of plate tectonics) decreases with decreasing mantle thickness.

In contrast, the observed trend for smaller radius ratios (i.e. below 0.7) may depend on the assumed initial conditions (we start from a non-convective initial stage). It may be also different when constant heat sources are used and the CMB temperature adapts to a quasi-steady-state temperature over time. However, the thermal evolution plays an important role, as well as initial values, such as, for example, the initial mantle and CMB temperature.

The cooling of a silicate mantle is more efficient for a thin mantle than for a thick mantle, which can keep its heat for a longer time. For each mantle thickness, rheology, set of initial parameters, and critical yield stress there is a specific time window in which plate tectonics can be initiated. After a short initialization phase for mantle convection, convective stresses may be large enough to initiate plastic yielding. However, with time when the mantle cools, the lithosphere thickens, and convective stresses finally fall below a critial value and plate tectonics may cease. The larger the yield stress, the larger the convective stresses must be, and thus the time window for possible plate-tectonics initiation is smaller. For a planet with a thin mantle, plate tectonics may start rapidly (because the first cooling phase is shorter than that on planets with a thick mantle) but may also end faster as convection becomes faster sluggish and not efficient enough for plate tectonics to maintain (see Table 4). Fig. 7 shows that the average temperature for stagnant-lid planets drops rapidly when plate tectonic starts, leading to decreasing temperatures after a short initial heating phase and indicating the cooling phase of the thermal evolution. The highest likelihood of plate tectonics for Earth-sized planets (i.e. the largest friction coefficients in which plate tectonics can be initiated) is obtained for a radius ratio of 0.7 for our chosen parameter set. Note that for a different rheology and different initial parameters, this peak may shift to other radius ratios.

Furthermore, we use a constant surface temperature of 280 K in all our model calculations presented herein. For higher surface temperatures, plate tectonics is less likely, because only for cold and stiff lithospheres pseudo-plastic yielding is efficient (Lenardic et al., 2008; Landuyt and Bercovici, 2009). Higher surface temperatures also lead to dry surfaces and may affect the water reservoir in the lithosphere; this would have severe consequences for the initiation of plate tectonics because the yield stress in a dry lithosphere is larger than that for hydrated silicates, even though larger stresses may then be obtained as suggested by Noack and Breuer (2014). The likelihood of plate tectonics therefore depends on past outgassing of volatiles from the mantle. The main interest of

our study, however, is whether CO_2 outgassing is influenced by the interior structure of the planet and therefore influences the outer edge of the HZ.

4.5 Summary

We show that for Earth-sized stagnant-lid planets, the outgassing of CO_2 depends on the interior structure. We find the weakest outgassing for Earth-sized planets with a Mercury-like interior structure (i.e. planets with a large core-to-planet radius ratio of roughly 0.85 up to 0.9). The outer boundary of the habitable zone (HZ) is mostly constrained by the amount of CO_2 in the atmosphere, which indicates that not all Earth-sized planets have the same outer boundary of the HZ as the Earth. Stagnant-lid planets with a thin mantle with radius ratios above 0.65 in our study seem to have a smaller HZ than planets with an Earth-like interior structure.

The efficiency of outgassing changes significantly if plate tectonics initiates on a planet. A substantial peak in the melt production and outgassing rates together with an efficient cooling of the mantle can be expected as soon as plate tectonic sets in. The maximum partial pressure of 34 bar (before condensation sets in at a surface temperature of 273 K) is easily outgassed, extending the outer boundary of the HZ to its maximum. The latter is then restricted by the maximum greenhouse effect.

We find that plate tectonics is easier to be initiated for an intermediate range of radius ratios than planets with relatively thin or thick mantles. The peak of plate-tectonics likelihood, however, depends on the employed mantle rheology and initial parameters.

In summary, planets of one Earth radius or even larger with a thin mantle (RR$\approx$0.9) and situated at the outer edge of the conventional HZ may not be habitable because their secondary atmospheres are too thin to reach habitable surface temperatures. Plate tectonics is unlikely on such planets, and only little partial melt can be expected, because the large iron core leads to a large pressure gradient in the silicate mantle and, thus, high melting temperatures at shallow depth. Furthermore, even if plate tectonics can be initiated on such planets, we do not expect it to continue for a long time, because the thin mantle cools rapidly and conduction will dominate the energy transport in the silicate mantle. Nevertheless, even a short time of active plate tectonics may be long enough to outgas an amount of volatiles sufficient for a habitable surface pressure, and without a sink (e.g. CO_2 cycle), liquid water may be stable over long time scales.

Our simulations show a wide range of possible outgassing scenarios and variations in plate-tectonics likelihood for a planet of one Earth size but different possible planet masses. This diversity (e.g. plate tectonics vs. stagnant-lid planet, broad vs. narrow HZ) shows that accurate detections of both mass and radius are required to be able to investigate the possible surface habitability of a rocky planet in more detail.

5 Super-Earth planets

5.1 Interior structure

In order to understand how the interior of a planet may influence its potential surface habitability, we investigate how the mass and interior structure of terrestrial planets may influence the outgassing efficiency as well as the likelihood to form long-term plate tectonics using the convection code CHIC (Noack et al., 2015).

We construct interior structure models to obtain profiles for the depth-dependent pressure, gravity acceleration, density, thermal expansion coefficient and heat capacity by integrating the equation of hydrostatic equilibrium and the Poisson equation and using equations of states of the relevant materials (Noack et al., 2015). We assume an initial temperature profile with a pre-defined thermal boundary layer (including a possible lithosphere) at the top of the silicate mantle of 100 km thickness, an upper mantle temperature of 2000 K (starting at the bottom

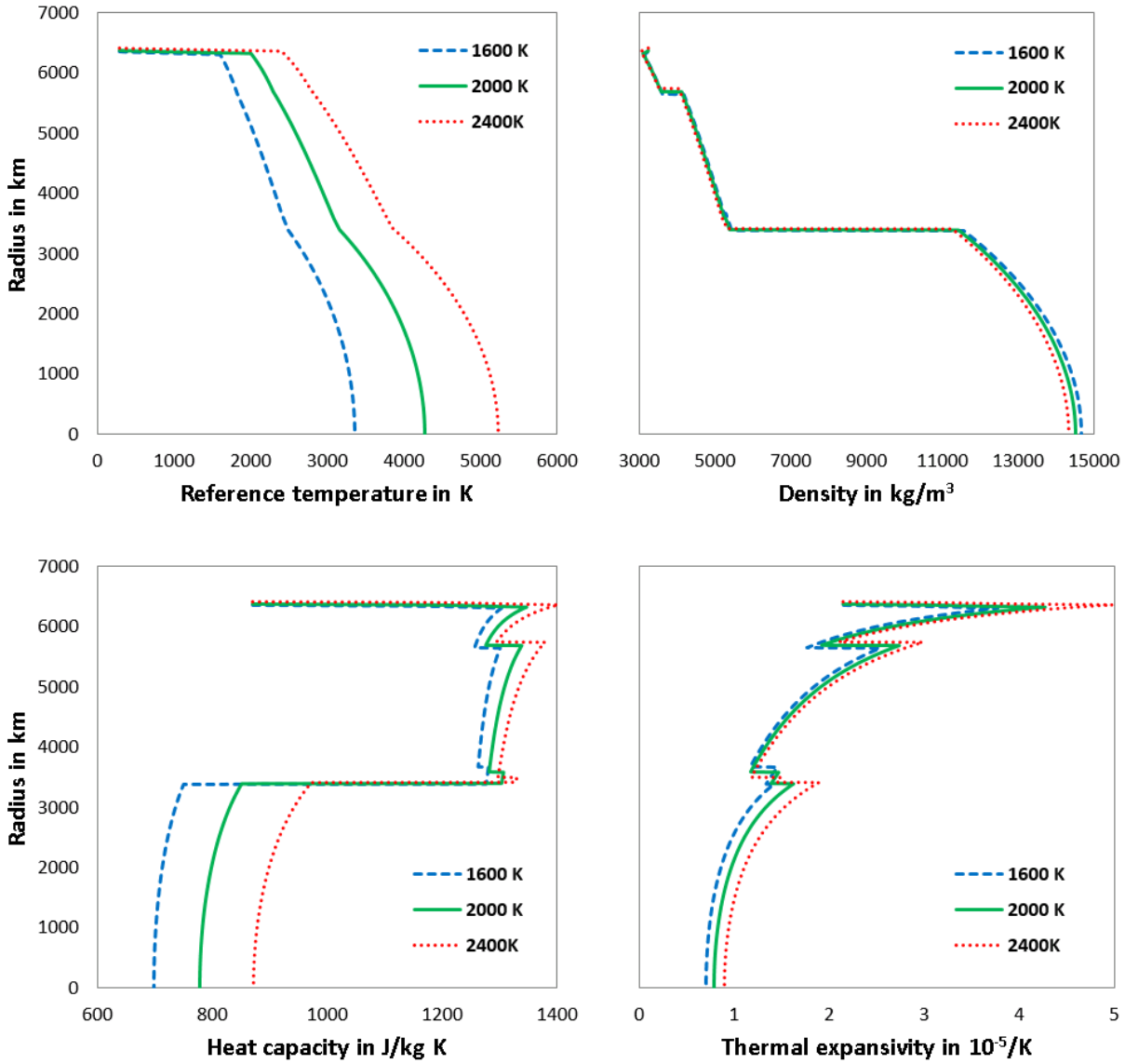

Figure 13: Profiles of reference temperature, density, heat capacity and thermal expansivity for a planet of 1 Earth mass applying an upper mantle temperature of either 1600[K] (blue, dashed), 2000[K] (green, solid) or 2400[K] (red, dotted). The temperature profile is then determined adiabatically as described in section 3.2. A core-mass fraction of 35% is applied.

of the upper thermal boundary layer) and a surface temperature of 290 K. The temperature increases adiabatically throughout the silicate mantle, the temperature at the core-mantle boundary (T_c) is set as the resulting adiabatic temperature at the bottom of the mantle and increases further along the core adiabate towards the center of the planet. We consider the planet mass and the amount of iron as input values, assuming a pure iron core and a magnesium-silicate mantle (for minerals olivine, Mg-perovskite, Mg-post-perovskite and magnesiowustite).

The temperature profile has only a very small effect on the resulting profiles of thermodynamic parameters, as is shown in Fig. 13 for a planet of one Earth mass with a core-mass-fraction of 35% for the example profiles of reference temperature, density, heat capacity and thermal expansivity for initial upper mantle temperatures of 1600 K, 2000 K and 2400 K. A fixed crustal density of 3200 kg/m^3 is applied over the uppermost 5 km. The resulting density profiles are mostly indistinguishable, but a difference can be seen in the planet radius. An increase of upper mantle temperature by 400 K leads to an increase of the planet radius by 25 km. We observe a larger influence of the reference temperature on the resulting heat capacity profile (mainly in the core) and on the thermal expansivity. We therefore apply different initial upper mantle temperatures in the results section to investigate the influence of different reference temperature profiles (and respective heat capacity/expansivity/density profiles) on the melting behaviour.

Model-dependent, global parameters (as well as mantle-averaged values) are listed in Table 6 and are obtained from the interior structure model for the initial reference temperature profile. The simulations use the depth-dependent profiles determined for a reference temperature profile with an upper mantle temperature between 1600 K and 2400 K.

5.2 Influence of mass and interior structure

Using the finite-volume code CHIC (Noack et al., 2015), we investigate the long-term evolution of rocky one-plate planets with varying mass and composition in a 2D spherical annulus under the TALA compressible approximation (see Section 3.2).

We employ depth-dependent profiles for all thermodynamics properties, which have been determined for the initial temperature profile (depending on the initial upper mantle temperature). The profiles self-consistently determine the mineral phases (olivine/perovskite/post-perovskite) and the density jump at the phase boundaries. Since we use reference profiles for the thermodynamic properties, the phase transitions are constant over time.

Table 6 lists all 70 runs for masses between 0.1 and 10 Earth masses and for iron contents χ_{Fe} between 5 and 95 wt-%. The table further lists the planet and core radius as obtained from the interior structure model and the resulting radius ratio, as well as mantle- or core-averaged values for all thermodynamic properties to show the influence of mass and composition on these values. Note, that for the simulations we do not use average values but the actual profiles. The last column lists the initial CMB-temperature $T_{c,ini}$, which is determined from the initial adiabatic profile (here 2000 K as example). No temperature jumps at the CMB are taken into account for the initial temperature profile, but can develop self-consistently with time (depending for example on the phase transitions in the mantle).

Figure 14 shows the evolution of the temperature and depletion field over time for a planet of one Earth mass with an iron content of 35 wt-% and an initial upper mantle temperature of 2000 K. The simulation starts with an adiabatic temperature profile; in later time steps the adiabatic profile develops self-consistently due to the compressible TALA formulation. Mantle depletion starts close to the lithosphere, where the pressure-dependent melting temperature is low enough for partial melting to occur. Due do efficient convection, depleted material is then transported into the mantle, and warm, non-depleted material is brought upwards, where it partially melts due to pressure-release melting. The lowermost part of the mantle does not contain any depleted material in the first half of the simulation. The reason for this is that the phase transition between perovskite and post-perovskite and the related density jump hinder efficient convection in this region. With time, for the same reason, the post-perovskite layer heats up and enhances the convective vigor, leading to homogeneous material mixing in the last part of the simulation.

The influence of the iron content and the planet mass on the mantle depletion is shown in Fig. 15. The top row shows four cases with different planet masses from Mars- to super-Earth mass employing a fixed iron content of 35 wt-% (Note that the ratio of core to surface radius is not constant, since the iron is more compressed for large-massive planets than for small-massive planets). For the smallest planet (0.1 Earth masses) the entire mantle beneath the lithosphere is homogeneously mixed and the maximal depletion value of 30% is reached

Run	M	χ_{Fe}	Rp	Rp	Rc	RR	g_s	ρ_m	Cp_m	α_m	k_m	γ_m	ρ_c	Cp_c	$T_{c,ini}$
	M_E	%	R_E	km	km		m/s^2	kg/m^3	J/kgK	$1/K$	W/mK		kg/m^3	J/kgK	K
1	0.1	5	0.548	3492	919	0.263	3.27	3240	1313	3.31	2.38	0.99	9178	939	2302
2	0.1	15	0.535	3411	1320	0.387	3.42	3242	1312	3.30	2.39	0.99	9302	932	2304
3	0.1	25	0.522	3326	1561	0.469	3.60	3241	1312	3.30	2.39	0.99	9375	928	2296
4	0.1	35	0.508	3238	1743	0.538	3.80	3236	1312	3.32	2.37	0.99	9419	925	2282
5	0.1	45	0.494	3145	1894	0.602	4.03	3227	1313	3.36	2.33	1.00	9445	924	2262
6	0.1	55	0.478	3046	2024	0.665	4.29	3214	1313	3.42	2.28	1.00	9454	923	2236
7	0.1	65	0.462	2941	2141	0.728	4.60	3196	1315	3.51	2.21	1.01	9447	922	2202
8	0.1	75	0.444	2827	2247	0.795	4.98	3172	1316	3.64	2.14	1.03	9427	921	2162
9	0.1	85	0.424	2702	2346	0.868	5.46	3141	1316	3.82	2.06	1.05	9391	918	2106
10	0.1	95	0.402	2561	2439	0.952	6.07	3119	1290	3.91	2.13	1.07	9334	914	2029
11	0.5	5	0.884	5632	1489	0.264	6.28	3863	1308	2.54	4.05	1.11	10797	874	2858
12	0.5	15	0.864	5503	2131	0.387	6.58	3862	1307	2.54	4.05	1.11	11054	865	2848
13	0.5	25	0.843	5370	2516	0.469	6.91	3849	1307	2.55	4.02	1.11	11190	860	2819
14	0.5	35	0.821	5233	2809	0.537	7.27	3825	1307	2.57	3.95	1.11	11264	858	2775
15	0.5	45	0.799	5090	3051	0.599	7.69	3790	1307	2.61	3.85	1.11	11295	857	2718
16	0.5	55	0.776	4941	3263	0.660	8.16	3737	1307	2.66	3.71	1.10	11287	856	2642
17	0.5	65	0.751	4784	3455	0.722	8.71	3655	1306	2.73	3.50	1.08	11242	856	2551
18	0.5	75	0.725	4616	3633	0.787	9.34	3534	1304	2.82	3.21	1.04	11154	858	2440
19	0.5	85	0.696	4436	3802	0.857	10.13	3312	1294	2.92	2.72	0.95	11024	858	2291
20	0.5	95	0.658	4192	3968	0.946	11.33	3180	1294	3.51	2.24	1.02	10846	860	2115
21	1	5	1.080	6881	1809	0.263	8.42	4236	1302	2.17	5.27	1.14	12036	838	3280
22	1	15	1.055	6720	2584	0.385	8.82	4235	1302	2.17	5.28	1.14	12400	828	3273
23	1	25	1.029	6555	3048	0.465	9.27	4221	1302	2.18	5.23	1.14	12593	822	3229
24	1	35	1.002	6385	3399	0.532	9.77	4193	1302	2.20	5.13	1.14	12705	819	3159
25	1	45	0.975	6209	3692	0.595	10.33	4149	1301	2.22	4.98	1.13	12751	815	3062
26	1	55	0.946	6024	3949	0.656	10.98	4087	1302	2.28	4.77	1.13	12739	816	2965
27	1	65	0.915	5828	4182	0.718	11.72	3999	1303	2.37	4.48	1.13	12671	818	2844
28	1	75	0.882	5620	4401	0.783	12.62	3866	1303	2.50	4.09	1.12	12544	821	2688
29	1	85	0.846	5393	4614	0.855	13.69	3648	1300	2.69	3.52	1.07	12344	823	2476
30	1	95	0.804	5122	4826	0.942	15.19	3255	1287	3.11	2.51	0.98	12050	828	2191
31	2.5	5	1.394	8883	2302	0.259	12.63	4918	1295	1.70	8.29	1.17	14613	786	4209
32	2.5	15	1.360	8667	3278	0.378	13.26	4920	1294	1.69	8.33	1.17	15180	776	4201
33	2.5	25	1.326	8448	3861	0.457	13.95	4902	1294	1.70	8.24	1.17	15480	770	4138
34	2.5	35	1.290	8221	4303	0.523	14.74	4869	1294	1.72	8.08	1.17	15667	766	4027
35	2.5	45	1.254	7989	4672	0.585	15.60	4807	1294	1.75	7.77	1.17	15735	764	3894
36	2.5	55	1.216	7745	4996	0.645	16.61	4720	1295	1.80	7.33	1.17	15721	763	3724
37	2.5	65	1.175	7489	5295	0.707	17.77	4595	1295	1.87	6.76	1.16	15613	764	3507
38	2.5	75	1.132	7214	5578	0.773	19.14	4416	1295	1.98	6.00	1.15	15406	764	3227
39	2.5	85	1.085	6911	5858	0.848	20.84	4147	1295	2.18	5.03	1.14	15073	766	2866
40	2.5	95	1.030	6562	6152	0.938	23.11	3592	1288	2.65	3.47	1.05	14544	775	2375
41	5	5	1.674	10664	2722	0.255	17.53	5681	1285	1.33	13.31	1.14	17674	735	5203
42	5	15	1.632	10395	3868	0.372	18.45	5690	1285	1.33	13.44	1.14	18480	724	5197
43	5	25	1.589	10123	4550	0.449	19.44	5670	1285	1.34	13.30	1.14	18922	719	5121
44	5	35	1.545	9845	5068	0.515	20.54	5625	1284	1.35	12.98	1.14	19174	715	4966
45	5	45	1.500	9559	5500	0.575	21.80	5546	1285	1.38	12.35	1.15	19281	714	4795
46	5	55	1.454	9263	5884	0.635	23.22	5429	1285	1.42	11.48	1.15	19255	715	4574
47	5	65	1.405	8951	6238	0.697	24.87	5261	1287	1.49	10.34	1.16	19090	717	4288
48	5	75	1.352	8616	6579	0.764	26.82	5022	1288	1.60	8.91	1.17	18783	720	3922
49	5	85	1.294	8246	6920	0.839	29.31	4662	1290	1.79	7.14	1.17	18294	722	3387
50	5	95	1.226	7812	7289	0.933	32.66	3985	1287	2.29	4.60	1.12	17491	730	2622
51	7.5	5	1.852	11802	2984	0.253	21.46	6283	1278	1.13	18.95	1.11	20132	701	5917
52	7.5	15	1.805	11498	4234	0.368	22.61	6295	1278	1.13	19.20	1.11	21130	690	5909
53	7.5	25	1.757	11192	4978	0.445	23.85	6274	1278	1.13	18.99	1.11	21677	686	5821
54	7.5	35	1.708	10880	5542	0.509	25.25	6220	1278	1.15	18.37	1.12	21995	683	5680
55	7.5	45	1.658	10560	6015	0.570	26.79	6128	1279	1.17	17.36	1.12	22121	683	5483
56	7.5	55	1.606	10232	6436	0.629	28.52	5981	1279	1.21	15.91	1.13	22065	684	5220
57	7.5	65	1.551	9880	6823	0.691	30.60	5788	1280	1.26	14.25	1.14	21890	685	4852
58	7.5	75	1.492	9507	7199	0.757	33.07	5498	1282	1.37	11.97	1.15	21503	689	4422
59	7.5	85	1.428	9096	7581	0.833	36.10	5061	1285	1.56	9.19	1.17	20868	696	3824
60	7.5	95	1.351	8607	8001	0.930	40.31	4260	1284	2.02	5.56	1.13	19841	702	2843
61	10	5	1.986	12651	3175	0.251	24.90	6799	1274	1.00	25.13	1.09	22274	678	6554
62	10	15	1.933	12318	4502	0.365	26.26	6818	1273	0.99	25.69	1.09	23443	666	6481
63	10	25	1.881	11985	5289	0.441	27.74	6797	1273	1.00	25.41	1.09	24094	661	6389
64	10	35	1.828	11647	5887	0.505	29.37	6737	1273	1.01	24.51	1.09	24458	659	6233
65	10	45	1.774	11302	6388	0.565	31.20	6630	1273	1.03	23.06	1.10	24615	659	6008
66	10	55	1.718	10945	6835	0.624	33.25	6471	1274	1.06	21.02	1.10	24568	660	5727
67	10	65	1.659	10571	7250	0.686	35.61	6239	1275	1.12	18.40	1.11	24323	664	5360
68	10	75	1.596	10169	7653	0.753	38.50	5907	1277	1.21	15.17	1.13	23866	669	4881
69	10	85	1.527	9726	8063	0.829	42.14	5406	1280	1.39	11.40	1.16	23124	674	4160
70	10	95	1.443	9196	8522	0.927	47.06	4493	1281	1.85	6.54	1.15	21887	682	3040

Table 6: Average thermodynamic parameters for all runs.

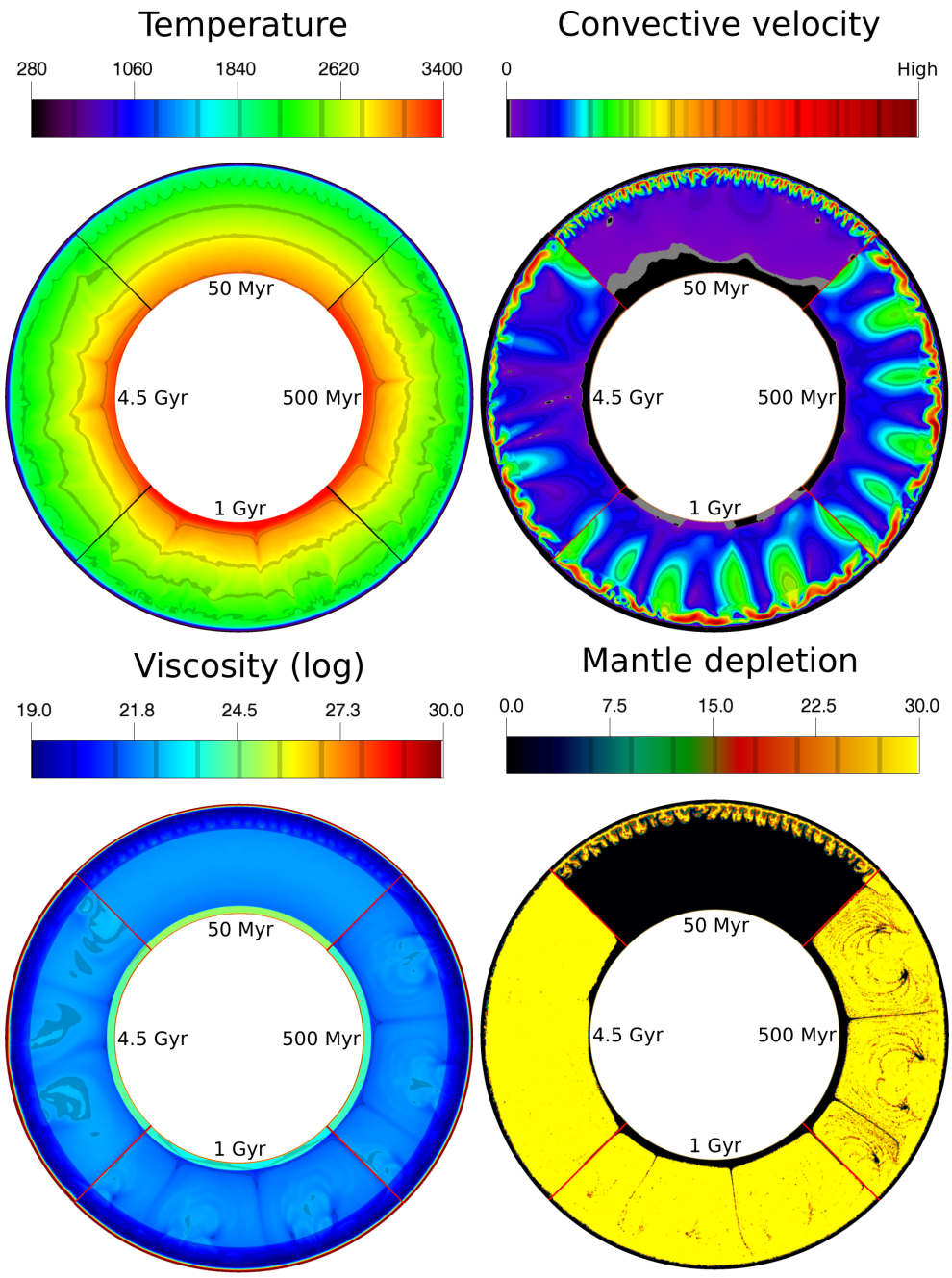

Figure 14: Thermal evolution of a planet of one Earth mass and an iron content of 35 wt-%.

almost everywhere in the mantle. For the Earth-mass planet, the phase transition between perovskite and post-perovskite leads to an in-homogeneously depleted layer at the bottom of the mantle, but otherwise the mantle is well depleted.

For larger masses, the larger surface gravitational acceleration (which approximately scales with the mass to power 0.4) leads to a steep pressure gradient. For the 2.5 Earth masses simulation, the temperature of hot, uprising plumes exceeds the melting temperature only in a very thin region, where the melt would still be buoyant. In less shallow depths (as well as in the case of more-massive planets) partial melting might occur, but due to the higher compressibility of molten material in comparison to solids, the melt would sink instead of rise towards the surface (Ohtani et al., 1995). To measure the amount of outgassable CO_2, we neglect possible negatively buoyant melt as well as melting possibly produced in the lower mantle, which in that depth might be buoyant Beuchert

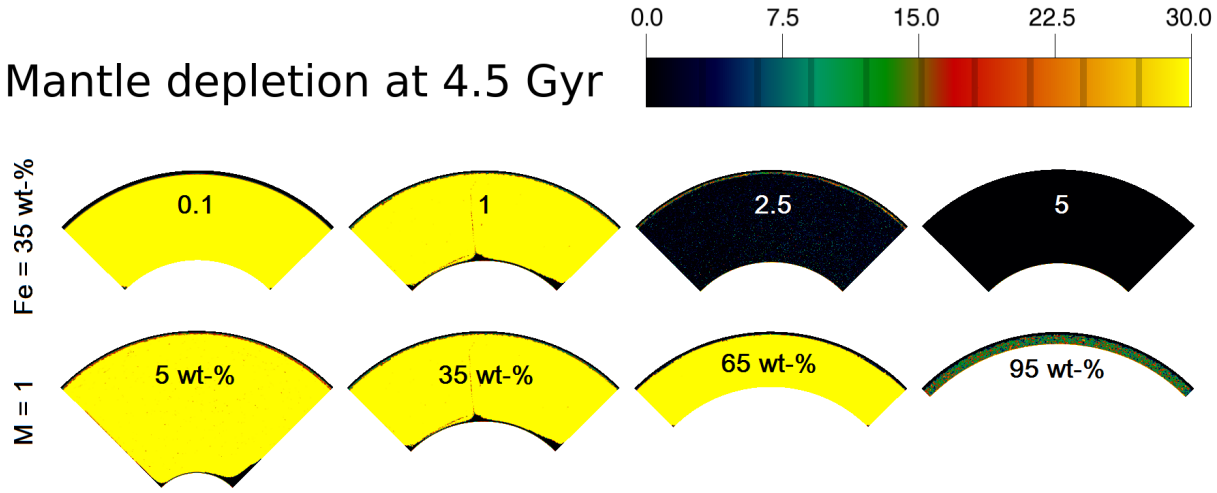

Figure 15: Mantle depletion after 4.5 Gyr for planets with an iron content of 35 wt-% and variable mass in Earth masses (top row) or for a one-Earth-mass planet with variable iron content (bottom row).

and Schmeling (2013).

The bottom row in Figure 15 visualizes four different iron contents for a planet of one Earth mass. For the smallest iron content, in the beginning of the simulation only the olivine and perovskite layers mix efficiently. The post-perovskite layer heats up (as has been observed in Fig. 14), and mixing with the perovskite layer happens later during the simulation (from approximately 2 Gyr on). After 4.5 Gyr, the layers are mix homogeneously apart from the region directly above the CMB, where the geometry effect described in the previous section hinders efficient convection.

For the planet with an iron content of 65 wt-% no post-perovskite layer (as in two left cases) appears, and the geometry further allows for efficient mantle mixing. For the largest iron content of 95 wt-%, on the other hand, different factors combined suppress efficient mantle depletion:
1) The high iron content leads to a small planet radius, which leads to a high surface gravitational acceleration of 15.24 m/s^2 (confer Table 6) and therefore a steeper pressure gradient compared to the other three cases. The pressure underneath the lid influences both the melting temperature and the depths of possible buoyant melt.
2) The shallow mantle cools efficiently, and mantle temperatures are below the melting temperature after a short

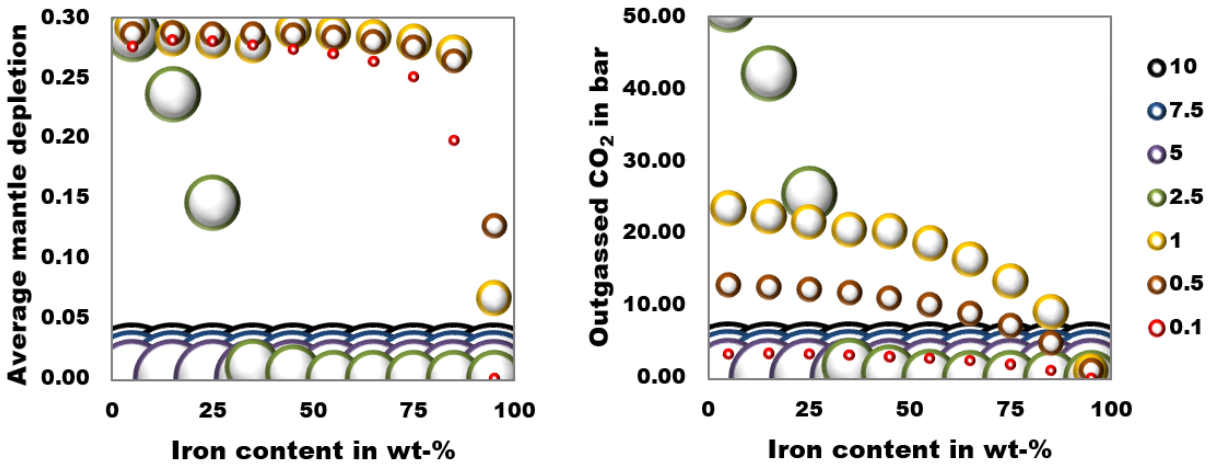

Figure 16: Average mantle depletion values (left) and total outgassed amount of CO_2 in bar (right) for different iron contents and planet mass (symbolized by circles of increasing sizeforincreasing mass) for an initial upper mantle temperatureof 2000 K.

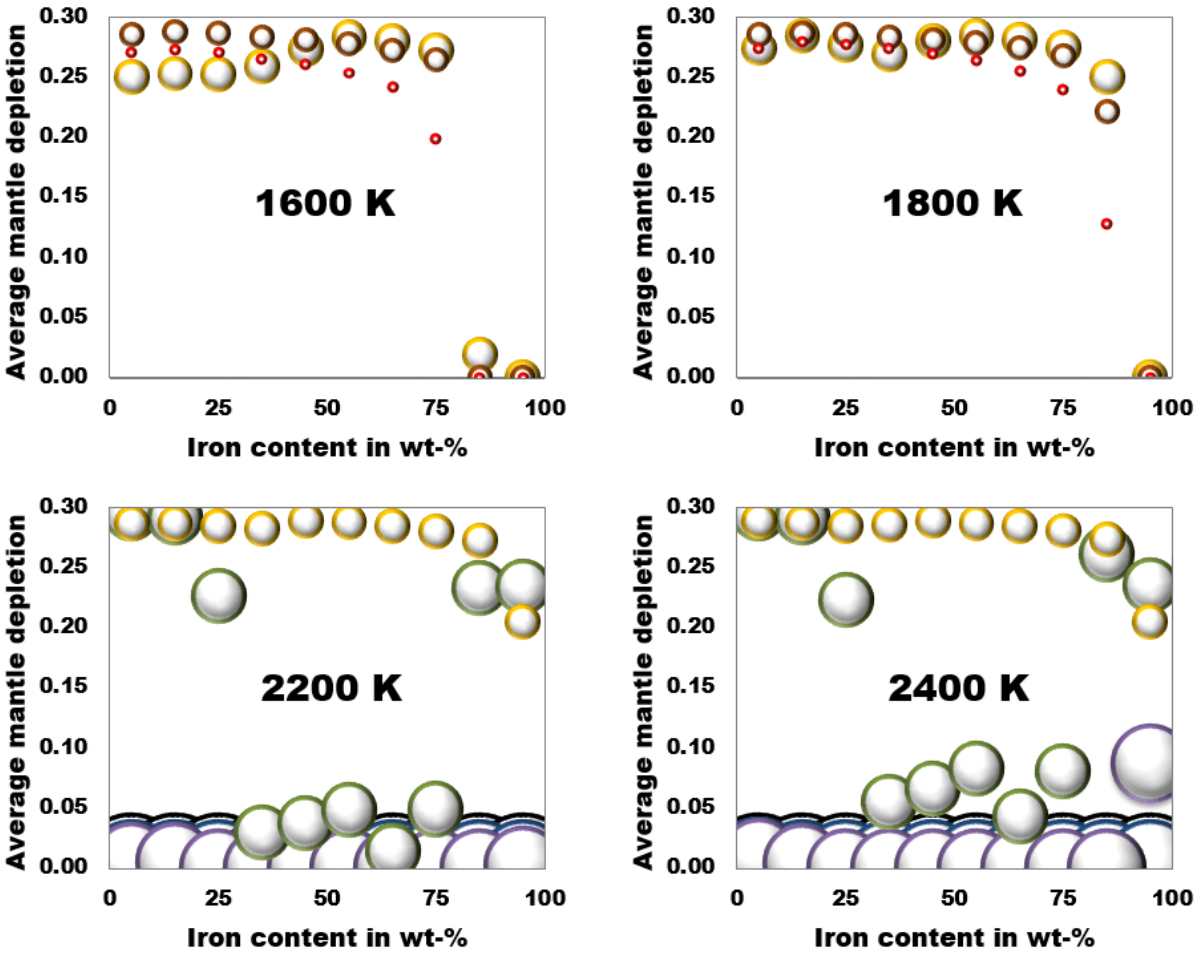

Figure 17: Average mantle depletion after 4.5 Gyr for different initial upper mantle temperatures, planet masses and iron content. The same legend as in Fig. 16 applies.

time.
3) The shallow mantle leads to a small Rayleigh number, which leads to less efficient mantle mixing and time-independent convection cells with non-depleted material in their center (as seen also in Case 1).

Figure 16 combines both investigations from Figure 15 by varying both the iron content and the planet mass simultaneously. We observe that even for small iron contents, planets from 5 Earth masses on will not be depleted efficiently, leading to average mantle depletion values (and outgassed bar of CO_2) of either zero or close to zero after 4.5 Gyr. Small-mass planets (0.1 to 1 Earth mass) show depletion of more than 15% for an iron content of up to 85 wt-%, and the amount of outgassed CO_2 is mainly limited by the mass of the planet, and not by the interior structure (with maximal 3.35 bar CO_2 for the 0.1 Earth mass planet compared to maximal 23.5 bar CO_2 for the 1 Earth mass planet (considering 10% extrusive volcanism and an initial CO_2 mantle content of 1000 ppm).

A planet with a larger mass leads to a larger amount of outgassed CO_2 atmosphere than a smaller planet with the same mantle depletion value. This can be observed when comparing the cases with 1 and 2.5 Earth masses. The planet of 2.5 Earth masses experiences in general less efficient mantle depletion than the 1 Earth mass planet (or any less-massive planet), but the highest amount of CO_2 is reached for the 2.5 Earth mass planet for iron contents of 25 wt-% or less.

Finally we investigate the influence of the initial upper mantle temperature on the average mantle depletion for all planet masses of our study. We vary the initial upper mantle temperature between 1600 K and 2400 K. For small-mass planets (0.1 - 0.5 Earth mass), initial mantle temperatures above 2000 K are unreasonable, whereas

values below 2000 K are unlikely as initial mantle temperatures for super-Earths (above one Earth mass). These cases are therefore excluded, see Figure 17. The upper and lower temperature bounds of 1600 K and 2400 K can be seen as extreme cases to cover a temperature range as large as possible.

Figure 17 plots the average mantle depletion at the end of the simulation over iron content for different initial upper mantle temperatures and planet masses (as has been done in Fig. 16 for an upper mantle temperature of 2000 K). The average depletion value is almost independent of the initial upper mantle temperatures, only for a planet of 2.5 Earth masses a clear increase of depletion with mantle temperature (also for high iron contents) can be observed. For the planets of 5, 7.5 and 10 Earth masses the average depletion value is less than 0.01 or zero for all temperatures and iron contents (apart from the 5 Earth mass planet and 2400 K). For larger cores, for the 2.5 and 5 Earth mass planet an increase in depletion can be observed for 2200-2400 K and 2400 K, respectively. In these cases, the initially high temperature leads to a thinning of the lithosphere and shallow melting, before the mantle cools down and moderate temperatures exclude the possibility of further melting. The high depletion value is therefore coupled to the improbably high initial mantle temperature that was applied here.

5.3 Influence of mantle composition

Theoretical considerations and observations predict that bulk compositions of planets are comparable to the stellar composition (see Dorn et al., 2015, and references therein). Relative abundances of Fe, Mg and Si in the solar system are similar among the Sun, the terrestrial planets and meteorites. For several stars that are known to host exoplanets, iron-silicate and magnesium-silicate ratios have been measured. We assume that for these systems, bulk planet compositions are also correlated to stellar ratios, and investigate how variable iron and magnesium contents (from 50% to 150% Sun-like values) influence the interior structure of exoplanets and their volcanic activity.

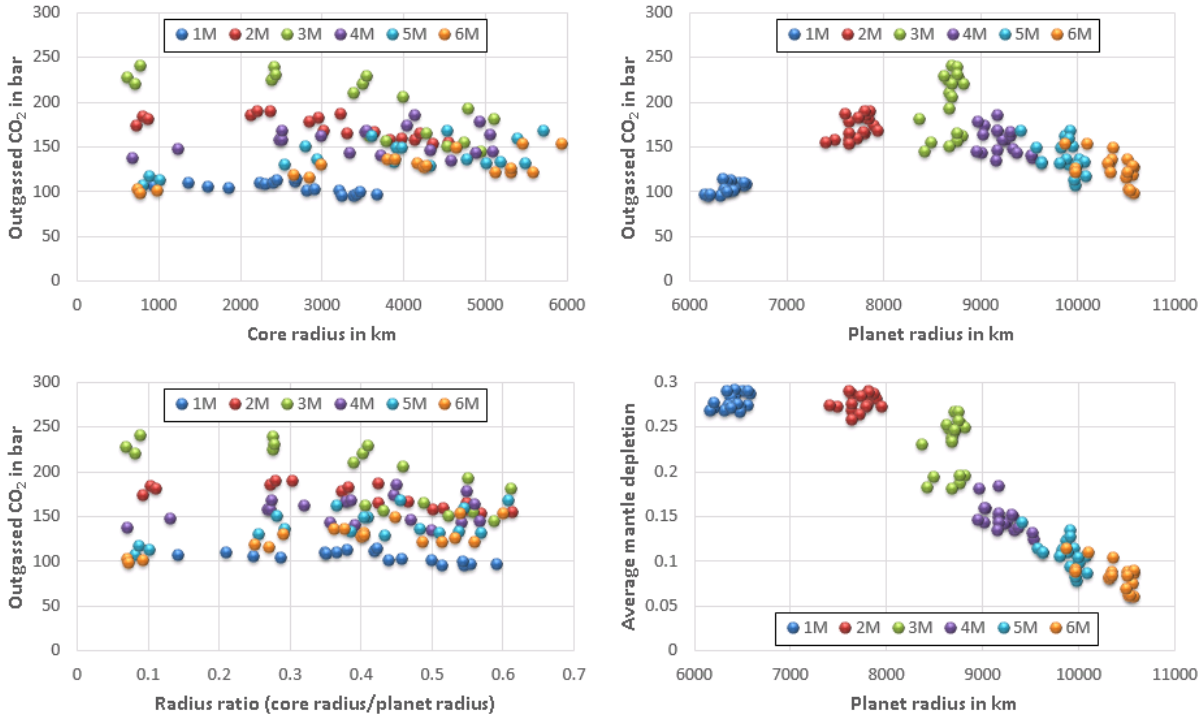

Figure 18: Outgassed CO_2 in bar and average mantle depletion plotted over core radius, planet radius or radius ratio. The coloured dots refer to different planet masses in Earth masses M.

Figure 18 shows the outgassed amounts of CO_2 and the average mantle depletion after 4.5 Gyr of thermal evolution for different one-plate exoplanets of variable composition (iron-silica and magnesium-silica ratios are either 0.5, 1 or 1.5 times the Sun value and either all iron in the core or an iron-enriched silicate mantle).

Low-mass planets (below ~3 Earth masses) are able to efficiently deplete the mantle and show a large amount

of volcanic outgassing even for the cases with large iron cores (radius ratio up to 0.6). The largest influence on the amount of volcanic outgassing comes from the core radius, as larger cores lead to thinner mantles and thus smaller amounts of carbon in the mantle – assuming 200 ppm Co_2 in the mantle (Elkins-Tanton et al., 2007).

For more-massive planets (from ~3 Earth masses on), the average mantle depletion decreases independently of the interior composition, leading to decreasing amounts of outgassed CO_2 with increasing planet mass. The results are therefore comparable to the results above for Earth-like mantle compositions.

5.4 Summary

We showed that for stagnant lid planets, outgassing is strongly limited if the pressure in the upper-most part of the mantle is large enough such that the melting temperatures are above the adiabatic mantle temperature and/or the melt is negatively buoyant and does not lead to volcanism and outgassing at the surface.

These large pressures can occur for either large iron cores (since iron is denser than silicates, influencing the surface gravity and thus pressure, Noack et al., 2014), or for high planet masses. Both effects are visualized in Figure 15.

The following results have been found in this study:

- Phase transitions (as the perovskite to post-perovskite phase transitions) can influence the efficiency of mixing of depleted and non-depleted material and can lead to inhomogeneous mantles.
- Large iron contents can inhibit efficient outgassing (depending on the planet mass).
- Large-massive planets (here from ~5-6 Earth masses on) may not outgas a dense CO_2 atmosphere, if they do not form plate tectonics nor start with very high initial upper mantle temperatures.

Here we investigated only stagnant lid planets. However, if plate tectonics occurs, hot mantle material can reach the surface, leading to immediate pressure-release melting, as shown in Noack et al. (2014) for Earth-size planets. A similar result is expected for planets with both smaller and larger masses than Earth.

The depletion of the mantle depends on the mantle temperature (but not very strong), and similar effects are expected for different amounts of radioactive heat sources, tidal heat sources as well as a possible heat source enrichment in the (possibly primordial) crust. These effects have been neglected in this study.

The existence of a dense-enough CO_2 atmosphere is important for the model of the habitable zone, where it is assumed that rocky planets can have an efficient, temperature-dependent carbon-silicate cycle and release of carbon at the outer boundary of the habitable zone is possible without limitations.

6 Plate tectonics on super-Earths

Several numerical studies have been published in the past years speculating about the existence of plate tectonics on large exoplanets. They focus on aspects like the mass of a planet, the interior heating rate and the occurrence of water in the mantle. Different trends in the propensity for plate tectonics have been observed in particular when varying the planetary mass: with increasing mass the surface mobilization is found to be either more, equally or less likely than on Earth. These studies and their implications are, however, difficult to compare as they assume different initial conditions and parameter sets, and either neglect the pressure effect on the viscosity or assume a rather small influence of the pressure on the rheology. Furthermore, the thermal evolution of the planets (i.e. cooling of core and decrease in radioactive heat sources with time) is typically neglected.

In the study published in Noack and Breuer (2014) and re-published below, we use a 2D finite volume code and apply a pseudo-plastic rheology. We investigate how a strong pressure-dependence of the viscosity influences not only the convective regime in the lower mantle, but also in the upper mantle and hence the likelihood to obtain plate tectonics. We investigate how our results change when either assuming a wet or a dry rheology or when employing different initial conditions, foccussing on the initial temperature in the lower mantle and at the core-mantle boundary.

6.1 Plate tectonics

To understand the factors that influence the global habitability of a planet, geodynamic models treating the convection in the mantle are common. One main focus of the geodynamic studies in the past years deals with the likelihood of plate tectonics on Earth-like planets with a mass larger than Earth's. First, interior structure models have been developed to obtain scaling laws for the interior structure of an Earth-like planet depending on mass and composition of a planet (Valencia et al., 2006; Wagner et al., 2011). Convection models in two or three dimensions or parameterized models applying these scaling laws (e.g. Valencia et al., 2007; O'Neill and Lenardic, 2007; van Heck and Tackley, 2011; Korenaga, 2010) have been applied to investigate the likelihood of plate tectonics on rocky exoplanets.

Different trends in plate tectonics likelihood with increasing mass have been found in these studies. O'Neill and Lenardic (2007) and Stein et al. (2013) showed that surface mobilization may drop for planets larger than Earth, while other studies argued for increasing plate tectonics likelihood with increasing mass (Valencia et al., 2007; van Heck and Tackley, 2011). Papuc and Davies (2008) find an increasing plate velocity for plate tectonics planets with increasing mass. Foley et al. (2012) infer that plate tectonics is most likely on large planets with a cool surface (in line with the studies by Lenardic et al., 2008; Landuyt and Bercovici, 2009; Noack, 2012) or a cool interior. The latter conclusion is also consistent with the results of various parameters studies, showing that a hot mantle (in terms of a large internal heating rate) may favour the formation of a stagnant lid (O'Neill et al., 2007; O'Neill and Lenardic, 2007; Stein et al., 2011, 2013), while large Rayleigh numbers (in terms of reduced reference viscosity) favour the plate tectonics regime (Stein and Hansen, 2008; Stein et al., 2013; Valencia et al., 2007). Finally, Korenaga (2010) concludes from revised scaling laws that plate tectonics does not depend on the size of a planet, but rather on the presence of surface water.

The pioneering works described above are typically based on various simplifications to model the mantle dynamics in exoplanets: the effect of pressure on the viscosity is often neglected (van Heck and Tackley, 2011; Valencia et al., 2007; Korenaga, 2010), time-independent parameters are employed (i.e. constant radioactive heating rate and either a mantle isolated from the core by employing zero heat flux at the core-mantle boundary (CMB) or a constant core temperature, (O'Neill and Lenardic, 2007; van Heck and Tackley, 2011; Stein et al., 2011). Furthermore, larger reference viscosities are used that make the material more sluggish and the computations faster (e.g. Stamenkovic et al., 2012; van Heck and Tackley, 2008) – or analogously higher reference surface temperatures leading to the same effect (e.g. van Heck and Tackley, 2011). The physics in the mantle is in addition often simplified by neglecting phase transitions. Especially the effect of pressure on the viscosity can have a strong effect on the resulting convection pattern in the mantle and hence also on the surface regime. The increase of the viscosity with pressure depends strongly on the activation volume of the mantle material. The activation volume of olivine has been determined by experiments for low pressure (e.g. Karato and Wu, 1993), and it has been suggested that the activation volume slightly decreases with increasing pressure (Karato, 2008). However, the actual decrease of the activation volume with depth and the resulting viscosity profile are not uniquely determined and also depends on the phase changes (Wagner et al., 2011; Stamenkovic et al., 2011). Also, it has recently been argued that at very high pressures, deformation by interstitial diffusion may become more effective than by vacancy diffusion,

possibly leading to a reduced viscosity with pressure along an adiabat (Karato, 2011).

Most studies use the viscosity of olivine or perovskite mineral phase and extrapolate it to higher pressure. However, the lower mantle of a large super-Earth is likely better represented by a post-perovskite mineral phase, which may lead to a different viscosity profile. Ab initio calculations and few experiments suggest that post-perovskite is weaker than perovskite (Dobson et al., 2012; Ammann et al., 2010) but also suggest a strong increase of the viscosity along the adiabat (Tackley et al., 2013). Considering the upper and lower bound of activation enthalpy derived by the study of Tackley et al. (2013), the derived viscosity increase is similar to the findings by Wagner et al. (2011) and Stamenkovic et al. (2011). In the present study we use the activation volume derived by Stamenkovic et al. (2011) for perovskite and neglect a possible change in diffusion mechanism Karato (2011).

The influence of pressure on the convective behaviour of a large exoplanet has already been investigated in Stamenkovic et al. (2012) with 1D and 2D models. In case of an activation volume of at the CMB of a 10 Earth mass planet (Stamenkovic et al., 2011), the lower mantle may be very viscous and can be stagnant – the formation of such a stagnant lower mantle (called CMB-lid) depends on the initial temperature structure, however (Stamenkovic et al., 2012). In the latter study, an adiabatic mantle temperature profile has been applied for 2D convection models, which was extrapolated from Earth's temperature profile to larger pressures. These temperatures are in line with mantle and CMB temperatures used in the literature for exoplanets (e.g. Valencia et al., 2006; Papuc and Davies, 2008). A more recent study by Wagner et al. (2011) suggests even higher mantle temperatures for super-Earths.

Next to neglecting the pressure-dependence of the viscosity, constant parameters are typically used for the convection models of exoplanets, as it has been mentioned above. This includes a fixed temperature at the CMB (if the mantle is not isolated from the core) as well as a constant amount of radioactive heat sources (e.g. van Heck and Tackley, 2011; Stein et al., 2011; O'Neill and Lenardic, 2007) – we call these runs "quasi-steady-state" (QSS) simulations here. The approach of using constant parameters has one main advantage: influences of parameter variations (like the mass of a planet) can easily be determined and compared, since the time factor plays no role, even though recent studies show that different steady-state solutions may be obtained depending on the initial parameters (Lenardic and Crowley, 2012; Weller and Lenardic, 2012). However, quasi-steady-state simulations lack the information about the time evolution. Model runs, which show a plate tectonic regime in steady state calculations, might never shift into that regime if planetary cooling is considered due to a change in the convective behaviour and the associated stress regime. For the terrestrial planets it has been argued that quasi-steady-state calculations give a good approximation to the dynamics of cooling-planet calculations as the adjustment time is rapid. This time, however, may be significantly larger for more-massive planets and the so-called thermostat effect regulating the interior temperature is inefficient (Stamenkovic et al., 2012): For instance, the existence and thickness of a possible CMB-lid in super-Earths strongly depends on the initial mantle temperature profile. In general, a heated system tries to remove efficiently its heat, which is by convection if possible. Thus, when using QSS models, the CMB-lid heats up until convective heat transport – although sluggish – sets in and a CMB-lid can hardly be obtained. The time scale to obtain this quasi-steady-state can easily take up several tens of billion years (Stamenkovic et al., 2012).

We therefore use and compare both approaches (quasi-steady-state and thermal evolution models) in the present study to investigate the likelihood of plate tectonics on exoplanets between 0.1 and 10 Earth masses for both wet and dry rheology. We further vary the initial CMB temperature for the largest investigated planet with 10 Earth masses.

We first compare an Earth-size planet with a 10 Earth mass planet for reference viscosities between 10^{22} – $10^{24} Pas$ and for an activation energy of either 240 kJ/mol with the corresponding wet yield stress formulation,

$$\sigma_{YS,wet} = 50MPa + \mu(\rho - \rho_w)gz, \tag{26}$$

or 300 kJ/mol while applying the dry yield stress formulation

$$\sigma_{YS,dry} = 50MPa + \mu\rho gz, \tag{27}$$

for a thermal evolution model (see Karato and Wu, 1993).

Laboratory experiments show that most surface materials on Earth have a friction coefficient around μ =0.6. However, these experiments have been done for low pressures up to 1.7 GPa. For higher pressures, the friction coefficient might be smaller than this value. We therefore introduce a scaling factor f_{frict}, which is multiplied to the depth-dependent part of the yield stress in Eq. (27), i.e. $f_{frict}\mu\rho gz$, and analogous for the wet yield stress formulation in Eq. (26). This factor has been varied between 0 and 0.02 (which yields an increase of the yield stress

with depth of 0.88 MPa/km, analogous to the value used by Rolf and Tackley (2011) of 0.83 MPa/km) to determine the critical scaling factor (and hence yield stress) for which surface mobilization can take place depending on the rheology, internal heating rate and planetary mass.

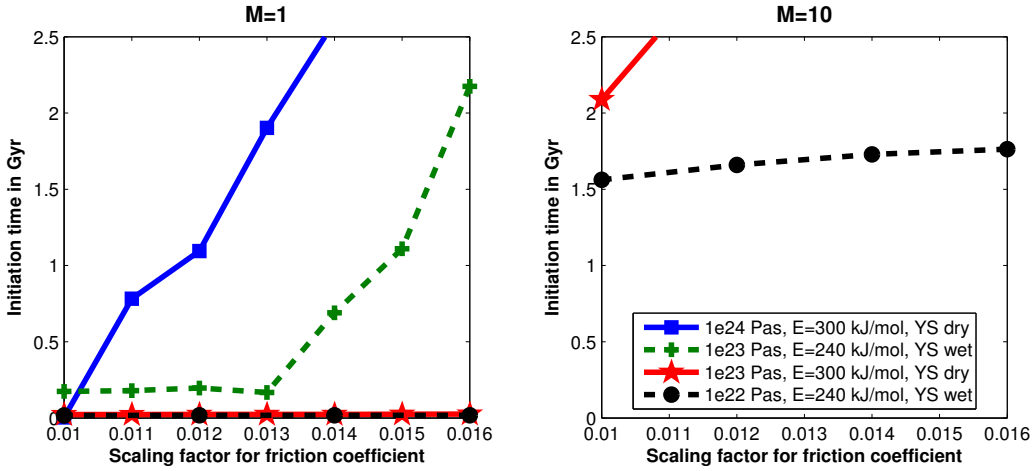

Figure 19: Initiation time of plate tectonics for different scaling factors limited to the first 2.5 Gyr of the thermal evolution. We plot the times for an Earth-like planet of either one (left) or ten Earth masses (right). Four different parameter sets have been investigated with reference viscosities between 10^{22} and 10^{24} Pas and employing either a wet activation energy of E=240 kJ/mol (applying also the wet yield stress formulation) or E=300 kJ/mol (with the dry yield stress formulation).

Fig. 19 shows the initiation time of plate tectonics for the different cases. For the planet of 10 Earth masses, plate tectonics only occurs for the smallest investigated scaling factors f_{frict} or using a small reference viscosity. Using a reference viscosity of $10^{24} Pas$ and E=300 kJ/mol or a reference viscosity of $10^{23} Pas$ and E=240 kJ/mol does not lead to plate tectonics in 2.5 Gyr for any of the used scaling factors and the corresponding lines are therefore not visible in the right panel in Fig. 19. Using a reference viscosity of $10^{23} Pas$ a scaling factor of 0.01 or less leads to plate tectonics for the larger activation energy – in contrast to the case with E=240 kJ/mol with the same reference viscosity (but adapted yield stress formulation). For E=240 kJ/mol and the smallest applied reference viscosity plate tectonics initiates for all yield stress factors in the shown parameter range.

For the case with one Earth mass, plate tectonics is in general initiated faster compared to the 10-Earth-mass planet and hence also for larger scaling factors (left panel in Fig. 19). For a reference viscosity of $10^{23} Pas$, the larger activation energy leads to a faster initiation time (and hence also larger scaling factors leading to plate tectonics) than the smaller activation energy, similar to what has been found for the 10 mass planet.

The use of the smaller activation energy is motivated by a wet rheology in the mantle. However, three different aspects have to be investigated when trying to understand the influence of a wet rheology on the occurrence of plate tectonics.

- The yield stress gradient is smaller for wet rheology compared to dry rheology, since the pressure with which the yield stress increases with depth is reduced by pore water pressure (Korenaga, 2007).
- The activation energy in the upper mantle (e.g. olivine mantle) depends on water and is smaller for wet rheology than for dry rheology (Karato and Wu, 1993).
- The reference viscosity for a wet mantle is reduced compared to a dry mantle by a factor of about 100 (Karato and Wu, 1993; Hirth and Kohlstedt, 2003).

The first effect (having a smaller yield stress gradient) is in general assumed to lead more easily to plate tectonics as long as the convective stress is large enough such that plate tectonics (and not some kind of sluggish surface mobilization) can take place. In Fig. 19 we find that the two first effects of a wet rheology (smaller yield stress gradient and reduced activation energy) combined with each other rather shift a planet into the stagnant lid regime compared to a mantle with the same reference viscosity but a larger activation energy and yield stress $\sigma_{YS,dry}$. The reduction of the depth-dependent yield stress does not compensate for the reduced convective stresses due to smaller activation energy.

The last effect, the decrease of the reference viscosity due to the presence of water, could not be investigated in a realistic parameter range. Nevertheless, the results plotted in Fig. 19 (dry rheology with $10^{24} Pas$ vs. wet rheology with $10^{22} Pas$) would suggest that a decrease of the reference viscosity favours the initiation of plate tectonics. It is, however, debated whether with further decreasing reference viscosity (and thus larger Rayleigh number) vigorous convection in the mantle may lead at some critical value of the viscosity to some kind of decoupling of mantle and lithosphere.

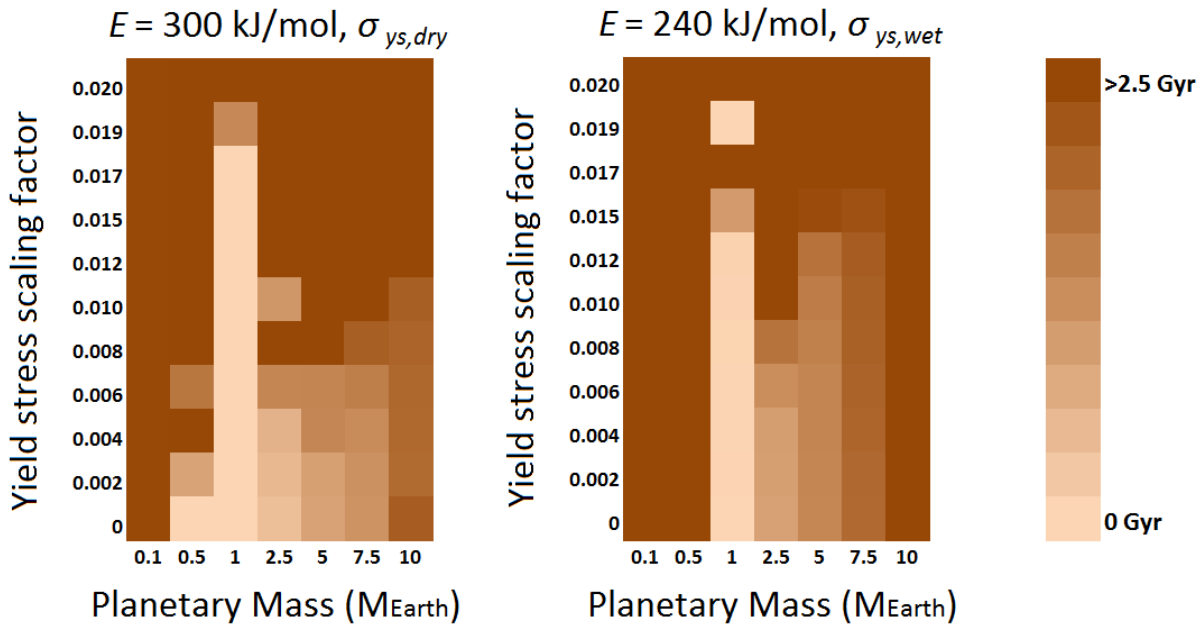

Figure 20: Initiation time of plate tectonics for different scaling factors for the two different activation energies investigated in the first 2.5 Gyr. The darkest brown colour stands for the cases where no plate tectonics initiated in that time, at all. A reference viscosity of 10^{23} Pas has been employed. The cases with 1 and 10 Earth masses correspond (for scaling factors between 0.01 and 0.016) to the black and blue lines in Fig. 19.

In Fig. 20 we compare planets with masses varying between 0.1 and 10 Earth masses with each other for both activation energies (and the corresponding yield stress formulations) and different yield stress scaling factors f_{fact}. For planets much smaller than Earth (e.g. of Mars size with 0.1 Earth masses), plate tectonics is less likely than for an Earth-size planet for both activation energies. In those cases, the mantle cools fast resulting in a thickening of the lithosphere, which makes plate tectonics unlikely. Only in the early evolution plate tectonics may be possible, but in our simulations the high forces induced by mantle plumes, that would be needed to initiate strong local deformation, could not be obtained. For one Earth mass, higher scaling factors (and thus yield stresses) lead to Earth-like plate tectonics in 2.5 Gyr. A further increase in mass, however, leads again to a decrease in plate tectonics likelihood.

The initial CMB temperatures used for the simulations in Fig. 20 (confer 7) have been calculated along an adiabat according to Stamenkovic et al. (2011). For the 10-Earth-mass planet and an initial CMB temperature of 6100 K, the viscosity strongly increases with pressure, leading to a stagnant lower mantle (CMB-lid Stamenkovic et al., 2012). Since the viscosity depends not only on pressure but also on temperature, we also applied initial temperatures at the CMB of 7100 K and 8100 K for a 10-Earth-mass planet for an activation energy of E=300 kJ/mol and the dry yield stress formulation. After 500 Myr (without plate tectonics), the CMB temperatures slightly increase to 7103 K and 8108 K. The CMB temperature is therefore almost time-independent due to the isolating effect of the CMB-lid (or sluggish lower mantle in the case of 8100 K) as shown already in Stamenkovic et al. (2012).

Nevertheless, we find that an increase of the CMB temperature (and hence lower mantle temperature) by 1000 K or 2000 K has a strong effect on the mantle dynamics and surface regime, as can be observed in Fig. 21. In the left panel we plot the thickness of the CMB-lid for a 10-Earth-mass planet for all three initial CMB temperatures. When increasing the CMB temperature, the thickness of the CMB-lid decreases. The CMB-lid, however, influences the convection in the remaining mantle.

Mass	0.1	0.5	1	2.5	5	7.5	10
$T_{m,up}$ [K]	2000	2000	2000	2000	2000	2000	2000
$T_{m,low}$ [K]	2050	2400	2850	3450	4050	4500	5000-7000
T_{CMB} [K]	3000	3400	3900	4500	5100	5600	6100-8100
p_{CMB} [GPa]	17	66	127	297	566	828	1092
V_{CMB} $[cm^3/mol]$	2.5	2.3	2.1	1.9	1.8	1.75	1.7
Di	0.13	0.34	0.47	0.60	0.76	0.89	1.02
Ra	2.03e4	2.275e5	7.56e5	3.53e6	1.15e7	2.36e7	4.04e7
H_0'	15.76	35.19	45.50	66.86	87.83	100.85	108.42
r_P [km]	3448	5301	6378	8161	9848	10972	11863
D [km]	1462	2343	2780	3754	4599	5179	5635
g $[m/s^2]$	3.417	7.14	9.81	14.93	20.5	24.7	28.5
ρ $[kg/m^3]$	3500	3970	4500	5300	6000	6470	6800
shells/nodes	33/362	52/554	64/671	84/862	102/1031	115/1149	125/1241

Table 7: Parameters for all investigated models. The masses are given in Earth masses. The mantle temperatures increases from upper mantle ($T_{m,up}$) to lower mantle ($T_{m,low}$). CMB temperatures T_{CMB}, CMB pressures p_{CMB}, activation volumes at the CMB V_{CMB} and dissipation numbers Di follow Stamenkovic et al. (2011), planet radius r_P, mantle thickness D, gravity acceleration g and mantle density ρ are taken from (Valencia et al., 2007). The reference Rayleigh number Ra at a reference viscosity of $\eta_{ref} = 10^{23}$Pas and the non-dimensional internal heating rate $H_0' = \rho H_0 D^2 (\kappa \Delta T)^{-1}$ listed, as well.

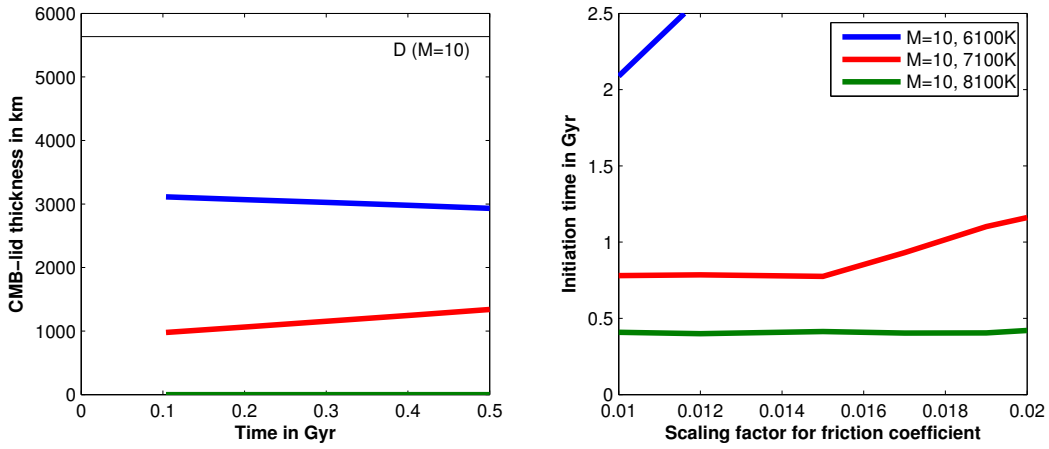

Figure 21: Left: CMB-lid thickness for a 10-Earth-mass planet in the first 500 Myr of the thermal evolution of stagnant-lid models depending on initial CMB temperature and hence initial lower mantle temperature. Note, that the lid thickness is plotted from 100 Myr on, since convection initiates after some tens of Myr, leading initially to lid thicknesses comprising the entire mantle. The black line is the mantle thickness of the 10-Earth-mass planet of 5635 km. Right: initiation time of plate tectonics for the corresponding thermal evolution models. For all simulations plotted here, an activation energy of E=300 kJ/mol, a reference viscosity of 10^{23} Pas and the dry yield stress formula (2.8) have been used.

For the case of the lowest CMB temperature (6100K), only yield stress factors smaller than 0.012 lead to a mobilization of the surface (right panel in Fig. 21). Increasing the CMB temperature to 7100K still leads to a CMB-lid of about one fifth of the mantle thickness, and plate tectonics occurs for all investigated yield stress factors. For a CMB temperature of 8100K no CMB-lid did form for the rheology parameters we used in our study, and plate tectonics initiated in the first 500Myr in the investigated range of yield stress scaling factors. We now compare our thermal evolution model with a quasi-steady-state model. In the latter case, the heat sources are constant over time and more heat can be produced in the mantle than in the case of a thermal evolution model. The direct consequence therefore is an increase in convective velocity and convective cell size, leading to an increased likelihood of plate tectonics. This can be observed in the left panel in Fig. 22, where we plot the initiation time

of a thermal evolution model versus a QSS model for a planet of either 1 or 10 Earth masses. Note that for QSS models the time does actually not play a role, since the simulations are run until a quasi-steady-state is achieved. However, we still plot how long these models need until plate tectonics occurs to show the influence of the internal heat sources on the plate tectonics likelihood. For the 10-Earth-mass planet the investigated range of yield stress scaling factors is larger than for the 1-Earth-mass planet, since plate tectonics occurs for larger scaling factors when using a QSS model (in contrast to the thermal evolution model). Here, the simulations run for 4.5 Gyr or until plate tectonics occurs. For the 1-Earth-mass planet, a difference between the thermal evolution model and the QSS model can only be observed for f_{frict} =0.02. However, for the 10-Earth-mass planet the usage of constant heat sources leads to the initiation of plate tectonics in the first 3 Gyr for all investigated yield stress scaling factors.

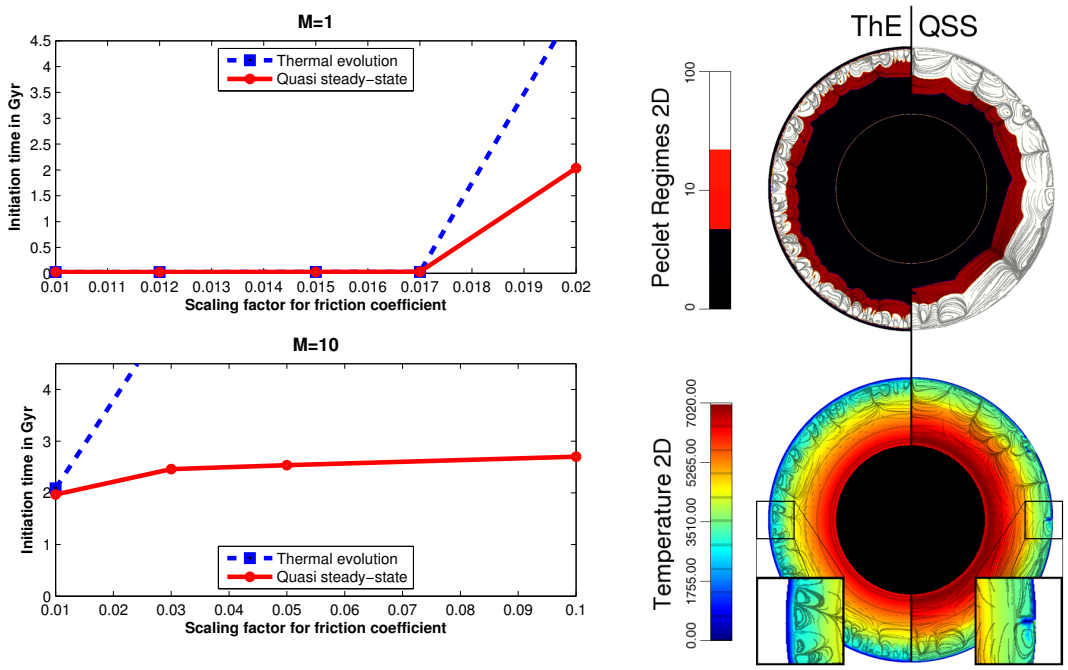

Figure 22: Left: Initiation time of plate tectonics for 1 (top) and 10 Earth masses (bottom) for either thermal evolution models or quasi-steady-state models. Right: Convective regimes (via the Peclet number) and temperature fields for a 10 Earth-mass planet for either a thermal evolution model (ThE, left) or a quasi-steady-state model (QSS, right). A yield stress factor of 0.05, an activation energy of 300 kJ/mol, a dry yield stress formulation and a reference viscosity of 10^{23}Pas have been used. The snapshots were taken at 2.9 Gyr.

In the right panel in Fig. 22 we plot snapshots of the convective (Peclet) regimes and temperature fields for a thermal evolution and a QSS model after 2.9 Gyr for a yield stress scaling factor of 0.05. Even though the quasi-steady-state for the second model has not yet been reached at that time, it can already be observed that the mantle temperatures strongly differ for both models solely due to using either constant or time-dependent heat sources. Furthermore, plate tectonics does only occur for the QSS model. The main difference between the two simulations is that in the QSS model constant heat sources lead to a strong decrease in CMB-lid thickness (black region in the Peclet regime field) and thus larger convective cells. After a longer simulation time, no CMB-lid will be observed at all, since more and more heat is stored in the lower mantle until weak convection starts (Stamenkovic et al., 2012; Tackley et al., 2013). This is not the case for thermal evolution models, where less energy is provided by the internal heat sources, which decay with time.

Applying constant heat sources leads to an increase in convective velocity in the lower mantle and a decrease in CMB-lid thickness compared to a thermal evolution model after the same simulation time. In the thermal evolution model, the amount of radioactive heat sources is with $H(2.9Gyr) = 7.6 \cdot 10^{-12} W/kg$ considerably smaller than $H_{QSS} = 2 \cdot 10^{-11} W/kg$ when using constant heat sources.

By either increasing the initial temperatures in mantle and core (Fig. 21) or by using time-independent parameters (QSS), plate tectonics initiates faster and for larger yield stresses than in the reference 10-Earth-mass case,

which is a thermal evolution model with a CMB temperature of 6100K.

6.2 Discussion and future outlook

For our plate tectonics simulations we find that the pressure effect on the viscosity and the associated formation of a CMB-lid has a large effect on the initiation of plate tectonics. For a thick CMB-lid the effective convective mantle is reduced in its thickness (i.e. the mantle thickness minus the CMB-lid). The effective Rayleigh number which describes the global convection efficiency is therefore reduced, as well. Following standard scaling arguments (e.g. Turcotte and Schubert, 2002), a CMB-lid, which takes up half of the silicate mantle, leads to a reduction in effective Rayleigh number to one-eighth of the global Rayleigh number of a planet without a CMB-lid and the convective velocity is therefore reduced to one fourth (following $v \sim Ra^{2/3}$) of the corresponding velocity. This strongly influences the likelihood of plate tectonics, since the reduced convective velocity in the upper mantle leads to smaller convective stresses and makes plate tectonics less likely.

We find that depending on initial mantle and core temperature (and thus CMB-lid thickness), the likelihood of plate tectonics on large exoplanets can either decrease or increase with mass. For CMB temperatures in the range of 8100 K (e.g. Wagner et al., 2011), a large super-Earth will more likely have plate tectonics than an Earth-size planet. For the lowermost investigated CMB temperature of 6100 K (Papuc and Davies, 2008; Sotin et al., 2007; Valencia et al., 2006) it is the other way around and a super-Earth will rather be in the stagnant-lid regime in comparison to a planet with a lower mass. Our results show that considering the thermal evolution of the mantle (e.g. in terms of decreasing internal heat sources with time) and varying the initial conditions have a strong influence on the resulting surface convective regime, a result similar to what has been found by recent studies using quasi-steady-state models (Lenardic and Crowley, 2012; Weller and Lenardic, 2012).

Note, that the absolute values given in the last section (i.e. initiation time of plate tectonics) depend on the chosen initial values and parameters sets. The initiation times in Fig. 19 to 21 may shift when using a different rheology, for example a different reference viscosity, non-Newtonian rheology, elasticity or change in diffusion creep (Karato, 2011; Stein et al., 2011). Applying a lower-mantle post-perovskite rheology may have a further influence on the possible emergence of a CMB-lid, since the phase transition from perovskite to post-perovskite may lead to a decreased viscosity above the CMB (Ammann et al., 2010), even though this is currently debated (Karato, 2011). On the other hand, the size of the CMB-lids observed in our study can be assumed to be larger when changing from 2D to 3D convection models (due to the reduced mantle temperature Noack and Tosi, 2013) or when using a depth-dependent activation volume instead of the CMB value, which presents the smallest activation volume in the mantle (Stamenkovic et al., 2011). However, the main tendencies observed in the present study (the existence of a possible peak in the plate tectonics likelihood depending on the CMB-lid thickness as well as the dependence of the CMB-lid thickness on the initial temperatures and heat sources) should be independent of the rheology.

Korenaga (2010) suggested that the strongest influence on the likelihood of plate tectonics is the occurrence of water in the lithosphere. Our results summarized in Fig. 19 may also suggest a strong increase in plate tectonics probability for a wet lithosphere and mantle (i.e. applying a reduced activation energy, reduced yield stress and smaller reference viscosity). However, all simulations have been done with increased reference viscosities (e.g. $\eta_{ref} = 10^{24}$Pas for the dry rheology vs. $\eta_{ref} = 10^{22}$Pas for the wet rheology) for numerical reasons. The reference viscosity of wet and dry olivine in Earth's upper mantle is actually smaller by three orders of magnitude (i.e. $\eta_{ref} = 10^{19}$Pas and $\eta_{ref} = 10^{21}$Pas, (Karato and Wu, 1993)). One may argue that a stronger convective vigour (due to smaller reference viscosity) should always lead to an increase in plate tectonics likelihood (which is also the trend that can be observed in Fig. 19).

To address this question, we perform a simple parameter study applying a small predefined viscosity contrast of 10^5 (employing the Frank-Kamenetskii approximation for the sake of simplicity) and investigate the effect of varying Rayleigh number (bottom-heated convection) or internal heat sources (mixed-heated convection). We use a 2D box model with a resolution of 80x80. In Fig. 23 we plot the root-mean-square (rms) mantle velocity against the rms surface velocity as well as the mobilization factor (black dashed line), which is defined as rms surface velocity divided by rms mantle velocity. This factor is a standard evaluation tool for plate tectonics simulations (e.g. Tackley, 2000; Stein et al., 2013) indicating if a surface is rather in the stagnant-lid regime (small mobilization factor) or in the plate tectonics regime. Note that all simulations have been run until a (time-averaged) steady-state has been reached. When varying the Rayleigh number, we assume that the reference viscosity defined at T'=1 in the parameter studies changes (e.g. dry vs. wet rheology). The non-dimensional yield stress depends on the reference viscosity, as well ($\sigma'_{YS} = \sigma_{YS} D^2/(\kappa\eta_{ref})$), and has to be adapted accordingly. We use a constant non-dimensional yield stress of 10^5 at a Rayleigh number of 10^6 and either vary the Rayleigh number (with H'=0)

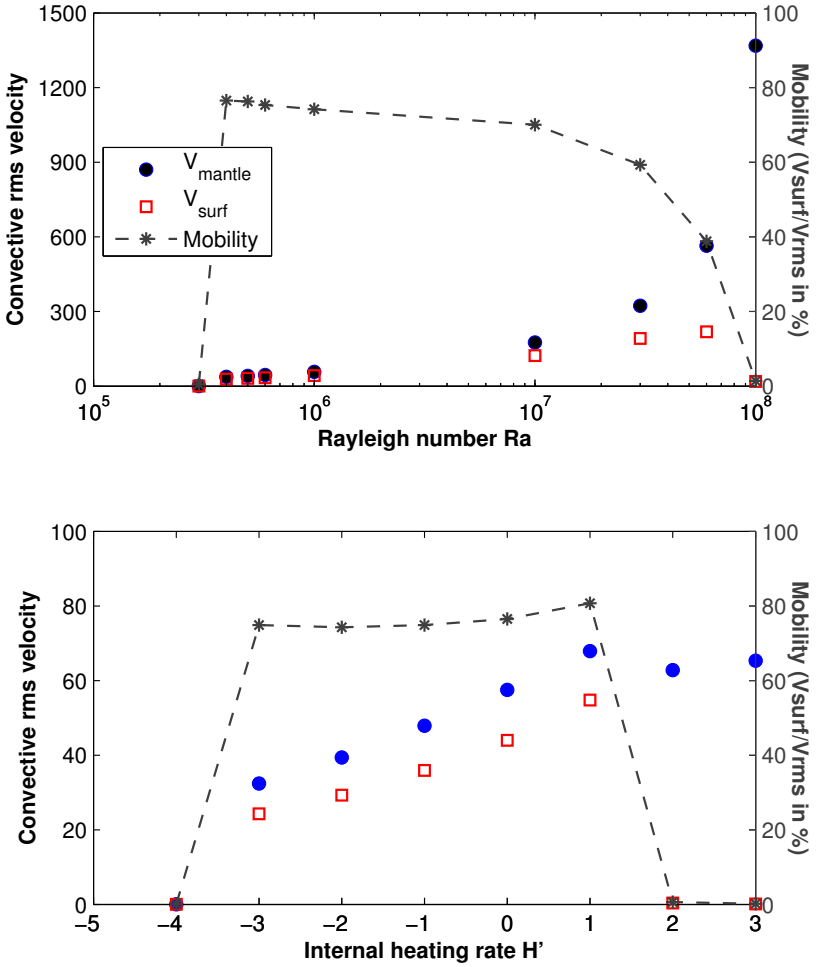

Figure 23: Average convective velocity in the mantle (root-mean square (rms) velocity V_{mantle}, dots) and at the surface (V_{surf}, squares) for varying Rayleigh numbers (top) or internal heat sources (bottom). The mobility of the surface (grey dashed line) is defined as the ratio of surface to rms mantle velocity (e.g. Tackley, 2000; Stein et al., 2013). Negative values for H' denote cooling. Since a 2D box has been used for this simple parameter study and since average mantle temperatures in a box are larger than in a sphere (Noack and Tosi, 2013; Stein et al., 2011), negative internal heating rates correspond to standard values when applying a 3D sphere geometry. The cases with Ra= $3 \cdot 10^5$(top) and $H' = -4$ (bottom) are in the conductive regime.

or the internal heating rate (for Ra=10^6). The upper panel in Fig. 23 shows that in the small-Rayleigh-number regime the surface velocity increases with increasing Rayleigh number. However, the surface velocity decreases at a critical Rayleigh number, the mobility factor drops to 1% and the stagnant lid regime is favoured for Rayleigh numbers above 10^8 (following the standard criterion that a stagnant lid is obtained when the surface velocity is equal or less than 1% of the rms mantle velocity, e.g. Hüttig and Breuer, 2011). A similar trend can be observed for variations in the amount of internal heat sources (lower panel in Fig. 23). For a high internal heat source density the surface mobility drops until the stagnant lid regime is obtained (analogous to O'Neill et al., 2007; O'Neill and Lenardic, 2007; Stein et al., 2011).

In general, large Rayleigh numbers in the mantle therefore seem to decouple the mantle from the lithosphere due to strong convection in the mantle in the sense that plate motion is inhibited and plate velocities do not scale with mantle velocities (Stein et al., 2013; Crowley and O'Connell, 2012). For large Rayleigh numbers small-scale

convection occurs and convection cells decrease in size. The force acting locally at the lithosphere is therefore smaller than for large-scale convection cells (i.e. so-called super-plumes) and mantle flow arranges itself self-consistently beneath the lithosphere. In terms of reference viscosity, a wet rheology (including a larger Rayleigh number compared to a dry rheology) might therefore rather lead to a stagnant-lid regime than when employing a dry rheology.

As a conclusion, we therefore speculate that a range of both optimal mantle heat (in terms of radioactive heat sources and thus age) and Rayleigh numbers (in terms of reference viscosities and rheology) may exist for any planet for the occurrence of plate tectonics and thus an enhanced habitability. However, it should be noted that we used a rather small viscosity contrast in our two parameters studies (as is typically also the case in the above-mentioned published parameter studies). For an Earth-like viscosity, the results may be different, and the range of reference Rayleigh numbers and internal heat sources that allow for plate tectonics to occur may be shifted. Due to limited computation resources, parameter studies with a realistic Earth-like rheology are not yet feasible and remain to be observed with mantle convection models. However, computational resources will strongly increase in the next decade and computational models are currently developed, that can solve mantle convection more efficiently (e.g. using adaptive grid refinement methods). Hence in the near future convection models using realistic Earth-like parameters (especially for the rheology) will answer the question, whether larger Rayleigh numbers (e.g. for a wet rheology) lead more easily to plate tectonics, or not. Also, changes in Rayleigh number due to variations in mantle thickness (and planetary mass) should be investigated, since the effect on the surface regime may be different compared to our parameter study where we have varied only the reference viscosity. However, our mass-dependent investigations plotted in Fig. 20 suggest that for different mantle sizes a change in the Rayleigh number alone may not reflect the mantle dynamics of larger planets, and influences of the pressure on the viscosity should not be neglected.

As the initial temperature distribution seems to be critical for the existence of plate tectonics in particular on planets more-massive than Earth, more advanced models to study the thermal state of a planet after accretion, differentiation and possible magma ocean solidification are needed. Depending on the initial thermal state, a 10 Earth mass planet may have a smaller, equal or larger likelihood to initiate plate tectonics than on Earth, depending on how much heat is available to (partly) compensate the strong pressure effect in large terrestrial exoplanets.

6.3 Summary

We find that the initial temperature conditions have a first-order influence on the likelihood of plate tectonics on large exoplanets. For standard literature values for initial temperatures of super-Earths, surface mobilization is less likely than on Earth, for warm initial temperature the result is vice versa. Simulations that neglect the time-dependence of internal heat sources on the other hand tend to lead to an increasing likelihood of plate tectonics with increasing mass. Finally, our investigations suggest that a wet rheology does not necessarily favour plate tectonics, but – depending on the reference viscosity – may rather lead to a stagnant-lid regime.

References

Abbot, D., Cowan, N., and Ciesla, F. (2012). Indication of insensitivity of planetary weathering behavior and habitable zone to surface land fraction. *The Astrophysical Journal*, 756:178.

Ammann, M. W., Brodholt, J. P., Wookey, J., and Dobson, D. P. (2010). First-principles constraints on diffusion in lower-mantle minerals and a weak d" layer. *Nature*, 465:462–465.

Anglada-Escudé, G., Arriagada, P., Vogt, S. S., Rivera, E. J., Butler, R. P., Crane, J. D., Shectman, S. A., Thompson, I. B., Minniti, D., Haghighipour, N., Carter, B. D., Tinney, C. G., Wittenmyer, R. A., Bailey, J. A., O'Toole, S. J., Jones, H. R. A., and Jenkins, J. S. (2012). A Planetary System around the nearby M Dwarf GJ 667C with At Least One Super-Earth in Its Habitable Zone. *The Astrophysical Journal Letters*, 751:L16.

Armann, M. and Tackley, P. (2012). Simulating the thermo-chemical magmatic and tectonic evolution of Venus' mantle and lithosphere 1. two-dimensional models. *J. Geophys. Res.*, 117(E12003):E12003.

Batalha, N. M. and 51 co-authors (2011). Kepler's First Rocky Planet: Kepler-10b. *The Astrophysical Journal*, 729:27.

Beuchert, J. B. and Schmeling, H. (2013). A melting model for the lowermost mantle using Clapeyron slopes derived from experimental data: Consequences for the thickness of ultralow velocity zones (ULVZs). *Geochem. Geophys. Geosyst.*, 14(1).

Bonfils, X., Delfosse, X., Udry, S., Forveille, T., Mayor, M., Perrier, C., Bouchy, F., Gillon, M., Lovis, C., Pepe, F., Queloz, D., Santos, N. C., Ségransan, D., and Bertaux, J.-L. (2013). The HARPS search for southern extra-solar planets XXXI. The M-dwarf sample. *A&A*, 549:A109.

Borucki, W. J. and 69 co-authors (2011). Characteristics of Planetary Candidates Observed by Kepler. II. Analysis of the First Four Months of Data. *The Astrophysical Journal*, 736:19.

Borucki, W. J. and 83 co-authors (2012). Kepler-22b: A 2.4 Earth-radius Planet in the Habitable Zone of a Sun-like Star. *The Astrophysical Journal*, 745:120.

Breuer, D. (2009). Dynamics and thermal evolution. In Trümper, J., editor, *Landolt-Börnstein, New Series VI/4, Astronomy and Astrophysics 4B - Astronomy, Astrophysics, and Cosmology - Solar System*, pages 254–280. Springer.

Breuer, D. and Spohn, T. (2003). Early plate tectonics versus single-plate tectonics on mars: Evidence from magnetic field history and crust evolution. *J. Geophys. Res.*, 108(E7):5072.

Buske, M. (2006). *Dreidimensionale thermische Evolutionsmodelle für das Innere von Mars und Merkur*. PhD thesis, Georg-August-Universität zu Göttingen.

Byerlee, J. (1978). Friction of rocks. *Pageoph*, 116:615–626.

Charbonneau, D., Berta, Z. K., Irwin, J., Burke, C. J., Nutzman, P., Buchhave, L. A., Lovis, C., Bonfils, X., Latham, D. W., Udry, S., Murray-Clay, R. A., Holman, M. J., Falco, E. E., Winn, J. N., Queloz, D., Pepe, F., Mayor, M., Delfosse, X., and Forveille, T. (2009). A super-Earth transiting a nearby low-mass star. *Nature*, 462:891–894.

Christensen, U. (1984). Convection with pressure- and temperature-dependent non-newtonian rheology. *Geophys. J. R. astr. Soc.*, 77:343–384.

Cockell, C., Bush, T., Bryce, C., Direito, S., Fox-Powell, M., Harrison, J., Lammer, H., Landenmark, H., Martin-Torres, J., Nicholson, N., Noack, L., O'Malley-James, J., Payler, S., Rushby, A., Samuels, T., Schwendner, P., Wadsworth, J., and Zorzano, M. (2016). Habitability: A review. *Astrobiology*, 16(1):89–117.

Crisp, J. (1984). Rates of magma emplacement and volcanic output. *Journal of Volcanology and Geothermal Research*, 20(177-211).

Crowley, J. and O'Connell, R. (2012). An analytic model of convection in a system with layered viscosity and plates. *Geophys. J. Int.*, 188(61).

de Smet, J. (1999). *Evolution of the continental upper mantle: numerical modelling of thermo-chemical convection including partial melting*. PhD thesis, Utrecht University.

Dehant, V., Lammer, H., Kulikov, Y., Grießmeier, J., Breuer, D., Verhoeven, O., Karatekin, O., Van Hoolst, T., Korablev, O., and Lognonne, P. (2007). Planetary magnetic dynamo effect on atmospheric protection of early earth and mars. *Geology and Habitability of Terrestrial Planets, Space Sciences Series of ISSI*, 24:279–300.

Delfosse, X., Bonfils, X., Forveille, T., Udry, S., Mayor, M., Bouchy, F., Gillon, M., Lovis, C., Neves, V., Pepe, F., Perrier, C., Queloz, D., Santos, N. C., and Ségransan, D. (2013). The HARPS search for southern extra-solar planets XXXV. Super-Earths around the M-dwarf neighbors Gl433 and Gl667C. *A&A*, 553:A8.

Demory, B.-O., Gillon, M., Deming, D., Valencia, D., Seager, S., Benneke, B., Lovis, C., Cubillos, P., Harrington, J., Stevenson, K. B., Mayor, M., Pepe, F., Queloz, D., Ségransan, D., and Udry, S. (2011). Detection of a transit of the super-Earth 55 Cancri e with warm Spitzer. *A&A*, 533:A114.

Dobson, D., McCormack, R., Hunt, S., Ammann, M., Weidner, D., Li, L., and Wang, L. (2012). The relative strength of perovskite and post-perovskite nacof3. *Mineralogical Magazine*, 76(4):925–932.

Dorn, C., Khan, A., Heng, K., Connolly, J., Alibert, Y., Benz, W., and Tackley, P. (2015). Can we constrain the interior structure of rocky exoplanets from mass and radius measurements? *A&A*, 577(A83):1–18.

Dziewonski, A. and Anderson, D. (1981). Preliminary reference Earth model. *Physics of the Earth and Planetary Interiors*, 25:297–356.

Edson, A., Kasting, J., Pollard, D., Lee, S., and Bannon, P. (2012). The Carbonate-Silicate Cycle and CO2/Climate Feedbacks on Tidally Locked Terrestrial Planets. *Astrobiology*, 12(6):562–571.

Elkins-Tanton, L. and Seager, S. (2008a). Coreless terrestrial exoplanets. *The Astrophysical Journal*, 688:628–635.

Elkins-Tanton, L. and Seager, S. (2008b). Ranges of atmospheric mass and composition of super-Earth exoplanets. *The Astrophysical Journal*, 685:1237–1246.

Elkins-Tanton, L., Smrekar, S., Hess, P., and Parmentier, E. (2007). Volcanism and volatile recycling on a one-plate planet: Applications to Venus. *J. Geophys. Res.*, 112(E04S06).

Fischer, D., Marcy, G., Butler, R., Vogt, S., Laughlin, G., Henry, G., Abouav, D., Peek, K., Wright, J., Johnson, J., McCarthy, C., and Isaacson, H. (2008). Five planets orbiting 55 cancri. *The Astrophysical Journal*, 675:790.

Foley, B., Bercovici, D., and Landuyt, W. (2012). The conditions for plate tectonics on super-earths: Inferences from convection models with damage. *Earth and Planetary Science Letters*, 331-332:281–290.

Gelman, S., Elkins-Tanton, L., and Seager, S. (2011). Effects of stellar flux on tidally locked terrestrial planets: Degree-1 mantle convection and local magma ponds. *The Astrophysical Journal*, 735:72.

Gillmann, C. and Tackley, P. (2014). Atmosphere/mantle coupling and feedbacks on venus. *J. Geophys. Res. Planets*, 119:1189–1217.

Grott, M., Breuer, D., and Laneuville, M. (2011a). Thermo-chemical Evolution and Global Contraction of Mercury. *Earth and Planetary Science Letters*, 397(1-2):135–146.

Grott, M., Morschhauser, A., Breuer, D., and Hauber, E. (2011b). Volcanic Outgassing of CO2 and H2O on Mars. *Earth and Planetary Science Letters*, 308(3-4):391–400.

Haberle, R., McKay, C., Schaeffer, J., Cabrol, N., Grin, E., Zent, A., and Quinn, R. (2001). On the possibility of liquid water on present-day mars. *J. Geophys. Res.*, 106(E10):23'317–23'326.

Hart, M. H. (1979). Habitable Zones about Main Sequence Stars. *Icarus*, 37:351–357.

Hatzes, A. P., Fridlund, M., Nachmani, G., Mazeh, T., Valencia, D., Hebrard, G., Carone, L., Paetzold, M., Udry, S., Bouchy, F., Borde, P., Deeg, H., Tingley, B., Dvorak, R., Gandolfi, D., Ferraz-Mello, S., Wuchterl, G., Guenther, E., Rauer, H., Erikson, A., Cabrera, J., Csizmadia, S., Leger, A., Lammer, H., Weingrill, J., Queloz, D., Alonso, R., and Schneider, J. (2011). The Mass of CoRoT-7b. *The Astrophysical Journal*, 743:75.

Hevelius, J. (1647). Selenographia sive lunae descriptio, historical map.

Hirschmann, M. and Withers, A. (2008). Ventilation of CO2 from a reduced mantle and consequences for the early Martian greenhouse. *Earth and Planetary Science Letters*, 270(1-2):147–155.

Hirth, G. and Kohlstedt, D. L. (2003). Rheology of the upper mantle and the mantle wedge: A view from the experimentalists. In Eiler, J., editor, *Inside the Subduction Factory*, volume 138, pages 83–105. Geophysical Monograph American Geophysical Union, Washington, D.C.

Höning, D., Hansen-Goos, H., Airo, A., and Spohn, T. (2014). Biotic vs. abiotic earth: A model for mantle hydration and continental coverage. *Planetary and Space Science*, 98:5–13.

Hu, Y. and Ding, F. (2011). Radiative constraints on the habitability of exoplanets Gliese 581c and Gliese 581d. *A&A*, 526:A135.

Hüttig, C. and Breuer, D. (2011). Regime classification and planform scaling for internally heated mantle convection. *Physics of the Earth and Planetary Interiors*, 186(3-4):111–124.

Hüttig, C. and Stemmer, K. (2008). Finite volume discretization for dynamic viscosities on voronoi grids. *Physics of the Earth and Planetary Interiors*, 171(1-4):137–146.

Kaltenegger, L., Segura, A., and Mohanty, S. (2011). Model Spectra of the First Potentially Habitable Super-Earth Gl581d. *The Astrophysical Journal*, 733:35.

Karato, S. and Wu, P. (1993). Rheology of the upper mantle: A synthesis. *Science*, 260:771–778.

Karato, S.-i. (2008). *Deformation of Earth Materials: An Introduction to the Rheology of Solid Earth*. Cambridge University Press.

Karato, S.-i. (2011). Rheological structure of the mantle of a super-earth: Some insights from mineral physics. *Icarus*, 212(1):14–23.

Kasting, J. F., Whitmire, D. P., and Reynolds, R. T. (1993). Habitable Zones around Main Sequence Stars. *Icarus*, 101:108–128.

Katz, R., Spiegelman, M., and Langmuir, C. (2003). A new parameterization of hydrous mantle melting. *Geochem. Geophys. Geosyst.*, 4(9):1073.

Keller, T. and Tackley, P. J. (2009). Towards self-consistent modelling of the martian dichotomy: The influence of low-degree convection on crustal thickness distribution. *Icarus*, 202(2):429–443.

Kereszturi, A. and Noack, L. (2016). Review on the role of planetary factors on habitability. *Origins of Life and Evolution of Biospheres*, in press.

King, S. D., Lee, C., van Keken, P. E., Leng, W., Zhong, S., Tan, E., Tosi, N., and Kameyama, M. C. (2010). A Community Benchmark for 2D Cartesian Compressible Convection in the Earth's Mantle. *Geophys. J. Int.*, 180(1):73–87.

Kite, E., Manga, M., and Gaidos, E. (2009). Geodynamics and Rate of Volcanism on Massive Earth-like Planets. *The Astrophysical Journal*, 700:1732.

Kohlstedt, D., Evans, B., and Mackwell, S. (1995). Strength of the lithosphere: Constraints imposed by laboratory experiments. *J. Geophys. Res.*, 100(B9):17,587–17,602.

Kopparapu, R. K., Ramirez, R., Kasting, J. F., Eymet, V., Robinson, T. D., Mahadevan, S., Terrien, R. C., Domagal-Goldman, S., Meadows, V., and Deshpande, R. (2013). Habitable Zones around Main-sequence Stars: New Estimates. *The Astrophysical Journal*, 765:131.

Kopparapu, R. K., Ramirez, R. M., SchottelKotte, J., Kasting, J. F., Domagal-Goldman, S., and Eymet, V. (2014). Habitable zones around main-sequence stars: Dependence on planetary mass. *The Astrophysical Journal Letters*, 787(2):L29.

Korenaga, J. (2007). Thermal cracking and the deep hydration of oceanic lithosphere: A key to the generation of plate tectonics? *J. Geophys. Res.*, 112(B05408).

Korenaga, J. (2010). On the likelihood of plate tectonics on super-earths: Does size matter? *The Astrophysical Journal Letters*, 725:L43–L46.

Landuyt, W. and Bercovici, D. (2009). Variations in planetary convection via the effect of climate on damage. *Earth and Planetary Science Letters*, 277:29–37.

Leblanc, F., Chassefiere, E., Gillmann, C., and Breuer, D. (2012). Mars' atmospheric 40ar: A tracer for past crustal erosion. *Icarus*, 218(1):561–570.

Léger, A. and 160 co-authors (2009). Transiting exoplanets from the CoRoT space mission. VIII. CoRoT-7b: the first super-Earth with measured radius. *A&A*, 506:287–302.

Lenardic, A. and Crowley, J. (2012). On the notion of well defined tectonic regimes for terrestrial planets in this solar system and in others. *The Astrophysical Journal*, 755(132).

Lenardic, A., Jellinek, A., and Moresi, L.-N. (2008). A climate induced transition in the tectonic style of a terrestrial planet. *Earth and Planetary Science Letters*, 271:34–42.

Lovelock, J. and Margulis, L. (1974). Atmospheric homeostasis by and for the biosphere: the gaia hypothesis. *Tellus*, 26(1-2):2–10.

Martin, W. and Russell, M. (2003). On the origins of cells: a hypothesis for the evolutionary transitions from abiotic geochemistry to chemoautotrophic prokaryotes, and from prokaryotes to nucleated cells. *Phil. Trans. R. Soc. Lond. B*, 358:59–85.

Mayor, M., Bonfils, X., Forveille, T., Delfosse, X., Udry, S., Bertaux, J., Beust, H., Bouchy, F., Lovis, C., Pepe, F., Perrier, C., Queloz, D., and Santos, N. C. (2009). The HARPS search for southern extra-solar planets. XVIII. An Earth-mass planet in the GJ 581 planetary system. *A&A*, 507:487–494.

Mayor, M. and Queloz, D. (1995). A Jupiter-Mass Companion to a Solar-Type Star. *Nature*, 378:355–359.

McDonough, W. F. and Sun, S.-S. (1995). The composition of the earth. *Chemical Geology*, 120(3):223–253.

McGovern, P. and Schubert, G. (1989). Thermal evolution of the Earth: effects of volatile exchange between atmosphere and interior. *Earth and Planetary Science Letters*, 96(1-2):27–37.

Morschhauser, A., Grott, M., and Breuer, D. (2011). Crustal recycling, mantle dehydration, and the thermal evolution of Mars. *Icarus*, 212(2):541–558.

Mosenfelder, J. L., Asimow, P. D., Forst, D. J., and Rubie, D. C. (2009). The $MgSiO_3$ system at high pressure: Thermodynamic properties of perovskite, postperovskite, and melt from global inversion of shock and static compression data. *J. Geophys. Res.*, 114(B01203):B01203.

Mumford, N. (1909). Intelligence on mars or venus. *Popular Astronomy*, 17:497–504.

Murray, S. (1965). The effect of triaxial stress systems on the strength of rocks at atmospheric temperatures. *Geophys. J. R. astr. Soc.*, 10:231–281.

Nimmo, F. and McKenzie, D. (1998). Volcanism and tectonics on Venus. *Annu. Rev. Earth Planet. Sci.*, 26:23–51.

Noack, L. (2012). *Resurfacing Mechanisms on Earth-like Planets: Plate Tectonics and Convective Surface Mobilization*. PhD thesis, Westfälische Wilhelms-Universität Münster, Germany.

Noack, L. and Breuer, D. (2013). Interior and surface dynamics of terrestrial bodies and their implications for the habitability. In de Vera, J.-P. and Seckbach, F., editors, *Habitability on other planets and satellites: The quest for extraterrestrial life*, pages 203–233. Springer, Dordrecht.

Noack, L. and Breuer, D. (2014). Plate tectonics on rocky exoplanets: Influence of initial conditions and rheology. *Planetary and Space Science*, 98:41–49.

Noack, L., Breuer, D., and Spohn, T. (2012). Coupling the atmosphere with interior dynamics: Implications for the resurfacing of Venus. *Icarus*, 217(2):484–498.

Noack, L. et al. (2014). Constraints for planetary habitability from interior modeling. *Planetary and Space Science*, 98:14–29.

Noack, L., Rivoldini, A., and Van Hoolst, T. (2015). CHIC - Coupling Habitability, Interior and Crust. *INFOCOMP 2015, Brussels, Belgium*, ISBN: 978-1-61208-416-9:84–90.

Noack, L. and Tosi, N. (2013). High-performance modelling in geodynamics. In Rückemann, C., editor, *Integrated Information and Computing Systems for Natural, Spatial, and Social Sciences*, pages 324–352. IGI Global.

Ohtani, E., Nagata, Y., Suzuki, A., and Kato, T. (1995). Melting relations of peridotite and the density crossover in planetary mantles. *Chemical Geology*, 120(3-4):207–221.

Ojha, L., McEwen, A., Dundas, C., Byrne, S., Mattson, S., Wray, J., Masse, M., and Schaefer, E. (2014). Hirise observations of recurring slope lineae (rsl) during southern summer on mars. *Icarus*, 231:365–376.

O'Neill, C., Jellinek, A. M., and Lenardic, A. (2007). Conditions for the onset of plate tectonics on terrestrial planets and moons. *Earth and Planetary Science Letters*, 261:20–32.

O'Neill, C. and Lenardic, A. (2007). Geological consequences of super-sized Earths. *Geophysical Research Letters*, 34(L19204):L19204.

O'Neill, C. and Nimmo, F. (2010). The role of episodic overturn in generating the surface geology and heat flow on Enceladus. *Nature Geoscience*, 3:88–91.

Papuc, A. and Davies, G. (2008). The internal activity and thermal evolution of earth-like planets. *Icarus*, 195:447–45.

Parai, R. and Mukhopadhyay, S. (2012). How large is the subducted water flux? New constraints on mantle regassing rates. *Earth and Planetary Science Letters*, 317-318:396–406.

Parnell, J. (2004). Plate tectonics, surface mineralogy, and the early evolution of life. *Int. J. Astrobio.*, 3(2):131–137.

Pepe, F., Lovis, C., Ségransan, D., Benz, W., Bouchy, F., Dumusque, X., Mayor, M., Queloz, D., Santos, N. C., and Udry, S. (2011). The HARPS search for Earth-like planets in the habitable zone. I. Very low-mass planets around HD 20794, HD 85512, and HD 192310. *A&A*, 534:A58.

Phillips, R., Bullock, M., and S.A. Hauck, I. (2001). Climate and Interior Coupled Evolution on Venus. *Geophysical Research Letters*, 28(9):1779–1782.

Pickering, W. (1926). Report on mars. *Popular Astronomy*, 37(34):482–491.

Plesa, A.-C. and Breuer, D. (2014). Partial melting in one-plate planets: Implications for thermo-chemical and atmospheric evolution. *Planetary and Space Science*, 98:50–65.

Plesa, A.-C. and Spohn, T. (2012). The influence of partial melt on mantle convection. In *High performance computing in science and engineering '11: Transactions of the High Performance Computing Center Stuttgart (HLRS) 2011*, pages 551–565. Springer.

Plesa, A.-C., Tosi, N., and Hüttig, C. (2013). Thermo-chemical convection in planetary mantles: advection methods and magma ocean overturn simulations. In Rückemann, C.P., editor, *Integrated Information and Computing Systems for Natural, Spatial, and Social Sciences*, pages 302–323. IGI Global.

Rauer, H. and 154 co-authors (2014). The PLATO 2.0 mission. *Experimental Astronomy*, 38(1-2):249–330.

Reddy, S. and Evans, D. (2009). Palaeoproterozoic supercontinents and global evolution: correlations from core to atmosphere. In Reddy, S., Mazumder, R., Evans, D., and Collins, A., editors, *Palaeoproterozoic supercontinents and global evolution*, volume 323, pages 1–26. Geological Society, London, Special Publications.

Rolf, T. and Tackley, P. (2011). Focussing of stress by continents in 3d spherical mantle convection with self-consistent plate tectonics. *Geophysical Research Letters*, 38(L18301).

Rosing, M. T., Bird, D. K., Sleep, N. H., Glassley, W., and Albarede, F. (2006). The rise of continents - an essay on the geologic consequences of photosynthesis. *Palaeogeography, Palaeoclimatology, Palaeoecology*, 232:99–113.

Sautter, V., Toplis, M. J., Wiens, R. C., Cousin, A., Fabre, C., Gasnault, O., Maurice, S., Forni, O., Lasue, J., Ollila, A., Bridges, J. C., Mangold, N., Le Mouelic, S., Fisk, M., Meslin, P.-Y., Beck, P., Pinet, P., Le Deit, L., Rapin, W., Stolper, E. M., Newsom, H., Dyar, D., Lanza, N., Vaniman, D., Clegg, S., and Wray, J. J. (2015). In situ evidence for continental crust on early mars. *Nature Geoscience*.

Schiaparelli, G. (1893). Il pianeta marte. *Natura ed Arte, Casa Editrice Dottor Francesco Vallardi, Milano*, 5-6(1).

Schubert, G., Turcotte, D., and Olson, P. (2001). *Mantle convection in the Earth and planets*. Cambridge University Press.

Schulze-Makuch, D., Grinspoon, D., Abbas, O., Irwin, L., and Bullock, M. (2004). A Sulfur-Based Survival Strategy for Putative Phototrophic Life in the Venusian Atmosphere. *Astrobiology*, 4(1):11–18.

Selsis, F., Kasting, J. F., Levrard, B., Paillet, J., Ribas, I., and Delfosse, X. (2007). Habitable planets around the star Gliese 581? *A&A*, 476:1373–1387.

Smith, D., Zuber, M., Phillips, R., Solomon, S., Hauck II, S., Lemoine, F., Mazarico, E., Neumann, G., Peale, S., Margot, J.-L., Johnson, C., Torrence, M., Perry, M., Rowlands, D., Goossens, S., Head, J., and Taylor, A. (2012). Gravity Field and Internal Structure of Mercury from MESSENGER. *Science*, 336(6078):214–217.

Sotin, C., Grasset, O., and Mocquet, A. (2007). Mass-radius curve for extrasolar earth-like planets and ocean planets. *Icarus*, 191(1):337–351.

Spohn, T., Konrad, W., Breuer, D., and Ziethe, R. (2001). The longevity of lunar volcanism: Implications of thermal evolution calculations with 2d and 3d mantle convection models. *Icarus*, 149:54–65.

Sramek, O. and Zhong, S. (2012). Martian crustal dichotomy formation tharsis formation by partial melting coupled to early plume migration. *J. Geophys. Res.*, 117, E01005(E01005).

Stamenkovic, V., Breuer, D., and Spohn, T. (2011). Thermal and transport properties of mantle rock at high pressure: Applications to super-earths. *Icarus*, 216(2):572–596.

Stamenkovic, V., Noack, L., Breuer, D., and Spohn, T. (2012). The influence of pressure-dependent viscosity on the thermal evolution of super-earths. *The Astrophysical Journal*, 748:41–64.

Steele, A., Beaty, D., Amend, J., Anderson, R., Beegle, L., Benning, L., Bhattacharya, J., Blake, D., Brinckerhoff, W., Biddle, J., Cady, S., Conrad, P., Lindsay, J., Mancinelli, R., Mungas, G., Mustard, J., Oxnevad, K., Toporski, J., and Waite, H. (2006). The astrobiology field laboratory. *By the Mars Exploration Program Analysis Group (MEPAG) at http://mepag.jpl.nasa.gov/reports/index.html*.

Stein, C., Finnenkötter, A., Lowman, J. P., and Hansen, U. (2011). The pressure-weakening effect in super-earths: Consequences of a decrease in lower mantle viscosity on surface dynamics. *Geophysical Research Letters*, 38(L21201):L21201.

Stein, C. and Hansen, U. (2008). Plate motions and the viscosity structure of the mantle - insights from numerical modelling. *Earth and Planetary Science Letters*, 272:29–40.

Stein, C., Lowman, J. P., and Hansen, U. (2013). The influence of mantle internal heating on lithospheric mobility: Implications for super-earths. *Earth and Planetary Science Letters*, 361:448–459.

Stevenson, D. (2003). Planetary magnetic fields. *EPSL Frontiers*, 208:1–11.

Sundquist, E. (1993). The global carbon dioxide budget. *Sci New Ser*, 259(5097):934–941.

Tackley, P. (1998). Self-consistent generation of tectonic plates in three-dimensional mantle convection. *Earth and Planetary Science Letters*, 157:9–22.

Tackley, P. (2000). Self-consistent generation of tectonic plates in time-dependent, three-dimensional mantle convection simulations. 1. pseudoplastic yielding. *Geochem. Geophys. Geosyst.*, 1(2000GC000036).

Tackley, P. J., Ammann, M., Brodholt, J. P., Dobson, D. P., and Valencia, D. (2013). Mantle dynamics in super-earths: Post-perovskite rheology and self-regulation of viscosity. *Icarus*, 225:50–61.

Taylor, F. and Grinspoon, D. (2009). Climate evolution of venus. *J. Geophys. Res.*, 114(E00B40).

Tosi, N., Yuen, D. A., de Koker, N., and Wentzcovitch, R. M. (2013). Mantle dynamics with pressure- and temperature-dependent thermal expansivity and conductivity. *Physics of the Earth and Planetary Interiors*, 217:48–58.

Trompert, R. and Hansen, U. (1998). Mantle convection simulations with rheologies that generate plate-like behaviour. *Nature*, 395:686–689.

Tuomi, M., Anglada-Escude, G., Gerlach, E., Jones, H. R. R., Reiners, A., Rivera, E. J., Vogt, S. S., and Butler, R. P. (2013). Habitable-zone super-Earth candidate in a six-planet system around the K2.5V star HD 40307. *A&A*, 549:A48.

Turcotte, D. L. and Schubert, G. (2002). *Geodynamics*. 2nd edition, Cambridge University Press, New York.

Udry, S., Bonfils, X., Delfosse, X., Forveille, T., Mayor, M., Perrier, C., Bouchy, F., Lovis, C., Pepe, F., Queloz, D., and Bertaux, J.-L. (2007). The HARPS search for southern extra-solar planets. XI. Super-Earths (5 and 8 M_{earth}) in a 3-planet system. *A&A*, 469:L43–L47.

Valencia, D., O'Connell, R., and Sasselov, D. (2006). Internal structure of massive terrestrial planets. *Icarus*, 181:545–554.

Valencia, D., O'Connell, R., and Sasselov, D. (2007). Inevitability of Plate Tectonics on Super-Earths. *The Astrophysical Journal*, 670:L45–L48.

van Heck, H. J. and Tackley, P. J. (2008). Planforms of self-consistently generated plates in 3d spherical geometry. *Geophysical Research Letters*, 35:L19312.

van Heck, H. J. and Tackley, P. J. (2011). Plate tectonics on super-earths: Equally or more likely than on earth. *Earth and Planetary Science Letters*, 310:252–261.

van Summeren, J., Conrad, C., and Gaidos, E. (2011). Mantle Convection, Plate Tectonics, and Volcanism on Hot Exo-earths. *The Astrophysical Journal Letters*, 736:L15 (6pp).

van Thienen, P., Benzerara, K., Breuer, D., Gillmann, C., Labrosse, S., Lognonne, P., and Spohn, T. (2007). Water, life, and planetary geodynamical evolution. *Space Sci. Rev.*, 129(1-3):167–203.

von Paris, P., Gebauer, S., Godolt, M., Grenfell, J. L., Hedelt, P., Kitzmann, D., Patzer, A. B. C., Rauer, H., and Stracke, B. (2010). The extrasolar planet GL 581 d: A potentially habitable planet? *A&A*, 522:A23.

von Paris, P., Grenfell, J. L., Hedelt, P., Rauer, H., Selsis, F., and Stracke, B. (2013). Atmospheric constraints for the CO2 partial pressure on terrestrial planets near the outer edge of the habitable zone. *A&A*, 549:A94.

Wada, I., Behn, M., and Shaw, A. (2012). Effects of heterogeneous hydration in the incoming plate, slab rehydration, and mantle wedge hydration on slab-derived H2O flux in subduction zones. *Earth and Planetary Science Letters*, 353-354:60–71.

Wagner, F., Sohl, F., Hussmann, H., Grott, M., and Rauer, H. (2011). Interior structure models of solid exoplanets using material laws in the infinite pressure limit. *Icarus*, 214(2):366–376.

Wagner, F., Tosi, N., Sohl, F., Rauer, H., and Spohn, T. (2012). Rocky super-Earth interiors structure and internal dynamics of CoRoT-7b and Kepler-10b. *A&A*, 541:A103.

Walker, J., Hays, P., and Kasting, J. (1981). A negative feedback mechanism for the long-term stabilization of the earth's surface temperature. *J. Geophys. Res.*, 86:9776–9782.

Ward, P. and Brownlee, D. (2000). *Rare Earth: Why Complex Life is Uncommon in the Universe*. New York: Springer.

Weber, R., Lin, P.-Y., Garnero, E., Williams, Q., and Lognonné, P. (2011). Seismic detection of the lunar core. *Science*, 331(6015):309–312.

Weller, M. and Lenardic, A. (2012). Hysteresis in mantle convection-plate tectonic systems. *Geophysical Research Letters*, 39(L10202):L10202.

Winn, J. N., Matthews, J. M., Dawson, R. I., Fabrycky, D., Holman, M. J., Kallinger, T., Kuschnig, R., Sasselov, D., Dragomir, D., Guenther, D. B., Moffat, A. F. J., Rowe, J. F., Rucinski, S., and Weiss, W. W. (2011). A Super-Earth Transiting a Naked-eye Star. *The Astrophysical Journal Letters*, 737:L18.

Wolszczan, A. and Frail, D. (1992). A planetary system around the millisecond pulsar psr1257 + 12. *Nature*, 355:145–147.

Wood, A., Wattson, R., and Pollack, J. (1968). Venus: Estimates of the surface temperature and pressure from radio and radar measurements. *Science*, 162(3849):114–116.

Wordsworth, R., Forget, F., Selsis, F., Madeleine, J., Millour, E., and Eymet, V. (2010). Is Gliese 581d habitable? Some constraints from radiative-convective climate modeling. *A&A*, 522:A22.

Wordsworth, R. D., Forget, F., Selsis, F., Millour, E., Charnay, B., and Madeleine, J.-B. (2011). Gliese 581d is the First Discovered Terrestrial-mass Exoplanet in the Habitable Zone. *The Astrophysical Journal Letters*, 733:L48.

Zerr, A., Diegeler, A., and Boehler, R. (1998). Solidus of earth's deep mantle. *Science*, 281(5374):243–246.